

Imaging activity-dependent structural and functional plasticity of hippocampal CA3-CA1 synapses

Dissertation zur Erlangung des Doktorgrades der Naturwissenschaften
der Fakultät für Biologie der Ludwig-Maximilians-Universität München

Vorgelegt von

Nadine Becker

München, 27. März 2008

Erstgutachter: Prof. Tobias Bonhoeffer
Zweitgutachter: Prof. Gerd Schuller
Tag der mündlichen Prüfung: 09. Mai 2008

Ehrenwörtliche Versicherung:

Ich versichere hiermit ehrenwörtlich, dass ich die Dissertation mit dem Titel “Imaging activity-dependent structural and functional plasticity of hippocampal CA3-CA1 synapses“ selbständig und ohne unerlaubte Beihilfe angefertigt habe. Ich habe mich dabei keiner anderen als der von mir ausdrücklich bezeichneten Hilfen und Quellen bedient.

Erklärung:

Hiermit erkläre ich, dass ich mich nicht anderweitig einer Doktorprüfung ohne Erfolg unterzogen habe. Die Dissertation wurde in ihrer jetzigen oder ähnlichen Form bei keiner anderen Hochschule eingereicht und hat noch keinen sonstigen Prüfungszwecken gedient.

München, 27. März 2008

Nadine Becker

Contents

Contents	vii
List of Figures	xi
Abbreviations	xiii
1 Summary	1
2 Introduction	3
2.1 The hippocampus – a model system for synaptic plasticity	4
2.2 The mechanisms and significance of hippocampal LTD	6
2.2.1 Induction and expression of LTD	8
2.2.2 Physiological significance of hippocampal LTD	9
2.3 Structural synaptic plasticity	10
2.3.1 Structural plasticity of dendritic spines	12
2.3.2 Structural plasticity of axonal boutons	14
2.4 Assembly and disassembly of synapses	16
2.5 Objectives of this study	18
3 Material & Methods	21
3.1 Material	21
3.1.1 Chemicals	21
3.1.2 Media	22
3.1.3 Dyes	23
3.1.4 Antibodies	23
3.1.5 Equipment	24
3.2 Methods	25
3.2.1 Organotypic hippocampal slice cultures	25

3.2.2	Two-photon laser-scanning microscopy	27
3.2.3	Electrophysiology	30
3.2.4	Image Analysis.....	31
3.2.5	Statistics	34
3.2.6	Spatial resolution of optical system	35
3.2.7	Immunohistochemistry	39
4	Results	41
4.1	Imaging activity-dependent structural plasticity of boutons and spines .	41
4.1.1	LTD induction enhances bouton turnover	43
4.1.2	Enhanced bouton turnover affects the number of boutons in contact with spines.....	48
4.1.3	LTD inductions leads to a net loss of spines and their contacts with boutons.....	48
4.1.4	Quantification of structural plasticity of bouton-spine pairs	51
4.1.5	The size of synaptic structures affects the plasticity of their partners.....	52
4.2	Detection of evoked Ca ²⁺ transients in preexisting and new boutons	56
4.2.1	Boutons reliably show activity-dependent local Ca ²⁺ transients	57
4.2.2	Newly grown boutons rapidly show activity-dependent Ca ²⁺ transients.....	62
4.2.3	Reliability, spatial restriction and size of Ca ²⁺ transients in newly grown boutons compared to preexisting boutons.....	64
4.2.4	Bouton turnover	66
5	Discussion	69
5.1	LTD induces structural plasticity of presynaptic boutons	70
5.2	LTD-induced reduction of contacts between Schaffer collaterals and CA1 pyramidal neurons	75
5.2.1	Identity of contacts between boutons and spines.....	76

5.3	New and preexisting boutons show activity-dependent Ca^{2+} transients	78
5.3.1	The generation of Ca^{2+} transients in new boutons	80
5.3.2	The significance of Ca^{2+} for LTD and structural plasticity	82
6	Conclusions & Outlook	85
	Bibliography	87
	Acknowledgements	103
	Curriculum vitae	105
	Publications	107

List of Figures

Introduction

2.1	Basic anatomy of the hippocampus.....	5
2.2	Example of LTD and LTP evoked in the Schaffer collateral-CA1 pathway.....	7
2.3	Models for the formation of synapses.....	11
2.4	Changes in actin polymerization and spine morphology with LTP and LTD.....	12
2.5	Remodeling synapses by modulating vesicle sharing.....	15

Material & Methods

3.1	Schematic overview of the two-photon setup.....	26
3.2	Experimental approach.....	28
3.3	Example of an individual bouton-spine pair, illustrating how the structural changes were quantified by Matlab-based image analysis.....	32
3.4	Point spread function of the two-photon microscope.....	36
3.5	Fluorescent beads of various sizes are distinguishable in diameter and volume.....	38

Result

4.1	Putative synaptic contacts and presynaptic identity.....	42
4.2	Electrophysiological recordings.....	43
4.3	Presynaptic structural plasticity after LTD induction.....	45
4.4	Size and localization of plastic boutons.....	46

4.5	LTD-induced presynaptic structural plasticity in identified bouton-spine pairs.....	47
4.6	Postsynaptic structural plasticity after LTD induction.....	49
4.7	LTD-induced postsynaptic structural plasticity in identified bouton-spine pairs.....	50
4.8	LTD induction leads to a net loss of bouton-spine pairs.....	51
4.9	Characterization of the volume and volume changes of boutons and spines associated with plastic synaptic partners.....	53
4.10	Ca ²⁺ imaging in boutons of single CA3 pyramidal cell axons.....	56
4.11	Stability of Ca ²⁺ responses over several hours.....	58
4.12	Example traces of Ca ²⁺ responses of preexisting boutons.....	59
4.13	Spatial restriction of the Ca ²⁺ signal.....	61
4.14	New boutons display Ca ²⁺ responses.....	63
4.15	Reliability and amplitudes of Ca ²⁺ responses.....	65
4.16	Comparison of bouton turnover between CA3 neurons patched and labeled with Fluo-5F and those bolus-loaded with Calcein red-orange AM.....	67

Discussion

5.1	Trafficking of vesicle clusters respectively boutons along the axon.	73
-----	--	----

Abbreviations

3D	three dimensions
4D	four dimensions
A.U.	arbitrary unit
ACSF	artificial cerebrospinal fluid
AM	acetoxymethyl
AMPA	α -amino-3-hydroxy-5-methyl-4-isoxazolepropionic receptor
AP	action potential
ATP	adenosine triphosphate
BME	basal medium Eagle
BSA	bovine serum albumine
BP	bandpass
CA	Cornus ammonis
CAM	Cell adhesion molecule
CaMKII	Ca ²⁺ /Calmodulin-dependent kinase II
cAMP	cyclic adenosine monophosphate
CNS	central nervous system
DG	dentate gyrus
DM	dichroic mirror
DMSO	dimethyl sulfoxide
EM	electron microscopy
EPSC	excitatory postsynaptic current
EPSP	excitatory postsynaptic potential
F	fluorescence
fEPSC	field excitatory postsynaptic potential

FWHM	full width half maximum
GBSS	Grey's balanced salt solution
GFP	green fluorescent protein
HBSS	Hank's balanced salt solution
HFS	high-frequency stimulation
LFS	low-frequency stimulation
LTD	long-term depression
LTP	long-term potentiation
MIP	maximum intensity projection
n	number
NA	numerical aperture
NMDA	N-methyl-D-aspartate
PBS	phosphate buffered saline
PFA	paraformaldehyde
PMT	photomultiplier tube
PSF	point spread function
RMS	root mean square
ROI	region of interest
SD	standard deviation
SEM	standard error of the mean
sER	smooth endoplasmatic reticulum
TBS	theta-burst stimulation
Ti:Sa	Titanium:Sapphire
TPLSM	two-photon laser-scanning microscopy
VGCC	voltage-gated calcium channel
VGlut1	vesicular glutamate transporter 1

1 Summary

Activity-dependent plasticity of synaptic networks is thought to provide the cellular basis for learning and memory. Stimulus-induced long-term potentiation (LTP) and long-term depression (LTD) of synaptic transmission are well-established models for activity-dependent plasticity in the hippocampus. A central question in neuroscience is how changes in the strength of synaptic transmission are represented in the structural organization of a neuronal network. Many studies over the last decade have indicated that morphological changes at the level of single synapses play a key role in activity-dependent synaptic plasticity. While most of these studies have examined structural synaptic plasticity at the postsynaptic level of dendritic spines, little is known about how synaptic plasticity affects the presynaptic structures of axonal boutons. Moreover, it is unclear how structural changes of spines affect associated boutons and *vice versa*.

The aim of this thesis was to study the structural dynamics of presynaptic boutons and contacting postsynaptic spines in the classic plasticity paradigm of LTD in organotypic hippocampal slice cultures, which was shown to lead to the retraction of spines in a previous study of this laboratory. While the main focus was to characterize the plasticity of boutons, I also examined how they interacted with spines they were in contact with. In addition to the structural characterization, I set out to assess functional aspects of plastic boutons using Ca^{2+} imaging.

In the first part of my thesis, I used two-color time-lapse two-photon laser scanning microscopy and extracellular field potential recordings to monitor simultaneously synaptic morphology and activity. While electrically stimulating the CA3 neurons, field recordings and time-lapse imaging were performed in the target region of the CA3 axons labeled in red overlapping with CA1 dendrites labeled in green. My data show that the effect of LTD on the structural dynamics

of boutons is at least as large as the effect on postsynaptic spines, resulting in a net loss of contacts between labeled boutons and spines. Structural plasticity at individual pairs of boutons and spines occurred more frequently due to the bouton rather than the spine undergoing plasticity. While the loss of a bouton was not associated with a change in spine volume, spine loss correlated strongly with a volume decrease of the associated bouton. Moreover, newly grown boutons preferentially formed contacts with small spines.

In the second part of my thesis, I followed up on the finding that LTD enhanced bouton turnover and determined whether and when newly formed boutons become functional. To this end, I established Ca^{2+} imaging in individual boutons and characterized action potential-driven Ca^{2+} transients in preexisting and newly formed boutons. I found that preexisting boutons reliably respond even to single evoked action potentials, and that new boutons showed voltage-dependent Ca^{2+} transients shortly after their first morphological appearance.

In conclusion, the data of this thesis reveal a significant, potentially even larger, contribution by the presynaptic axon terminals to activity-dependent plasticity of synaptic connections beyond the well-established role of dendritic spines. My studies indicate that the link between structural and functional changes at the level of synapses is close and important for the activity-dependent remodeling of synaptic circuits in the brain. Moreover, these studies open up interesting opportunities to dissect the molecular mechanisms that underlie the important neurophysiological phenomenologies I have explored.

2 Introduction

Synaptic plasticity refers to the ability of the brain to modify its synaptic connectivity in an activity-dependent way. Its most prominent form was discovered in 1973 by Bliss and Lomo and is called long-term potentiation (LTP). Many of its properties make it ideally suited to serve as a cellular mechanism of learning and memory. In fact, a large body of data indicates that synaptic plasticity plays an important role in learning and memory formation. While much is known about the cell biological mechanisms of how changes in the strength of synaptic transmission are initiated, it remains unclear how these functional changes are laid down more permanently. A long-standing hypothesis in neuroscience posits that changes in neuronal morphology are a key mechanism for how information can be maintained in a synaptic network in an enduring way. In recent years, novel labeling and microscopic techniques have made it possible to image neuronal structure at the level of single synapses in time-lapse experiments. This approach has uncovered a wealth of information on how neuronal structure can change in response to synaptic activation. While many studies have focused on dendritic spines, which represent the postsynaptic structural part of most excitatory synapses in the brain, surprisingly little effort has gone into examining the structural plasticity of the presynaptic axon terminals that provide the synaptic input onto the dendritic spines. It is important not to leave out the presynaptic side, because presynaptic structural changes would be expected to have qualitatively very different consequences for the functional connectivity of the synaptic network. Moreover, examining both sides of the synapse at the same time is expected to yield important insights into how these critical compartments interact during plasticity.

For my thesis, I set out to understand the roles that both sides of a synapse play in synaptic plasticity by investigating presynaptic axon terminals (or

`boutons') in contact with postsynaptic spines at the same time. To this end, I chose the hippocampal organotypic slice preparation as a model system and used a combination of two-photon live-cell imaging and electrophysiology.

2.1 The hippocampus – a model system to study learning and memory

The hippocampus forms a part of the medial temporal lobe memory system, together with the adjacent entorhinal, perirhinal and parahippocampal cortices (Squire and Zola-Morgan, 1991). Classically, the hippocampal formation was described as a trisynaptic pathway: the entorhinal cortex projects onto the dentate gyrus (DG), the DG granule cells give rise to the mossy fibers, which project onto CA3 pyramidal neurons, whose Schaffer collateral axons in turn form synapses with CA1 pyramidal neurons. Today, the connectivity is known to be much more complex, since the entorhinal inputs in fact project to all hippocampal regions (Fig.1), and the Schaffer collaterals do not form a uniform path, but synapse onto CA1 neurons in a highly branched pattern (Amaral, 1993). Nevertheless, the hippocampus reveals a strictly laminar organization, which makes it particularly suitable for extracellular recording techniques *in vitro* and *in vivo*. In addition, hippocampal neurons can be cultured as transversely cut organotypic slice cultures (Gähwiler, 1981; Stoppini *et al.*, 1991). The cultures develop with the same time course as in the *in situ* situation (Muller *et al.*, 1993) and the connectivity and the expression profiles of synaptic proteins are comparable to that of acute slices (De Simoni *et al.*, 2003; Buckby *et al.*, 2004). After a few days of incubation, organotypic slices become a thinned, stabilized *in vitro* system unaffected by degradative processes associated with acute brain slices. These features make organotypic slices a system well-suited for long-term manipulations and imaging studies.

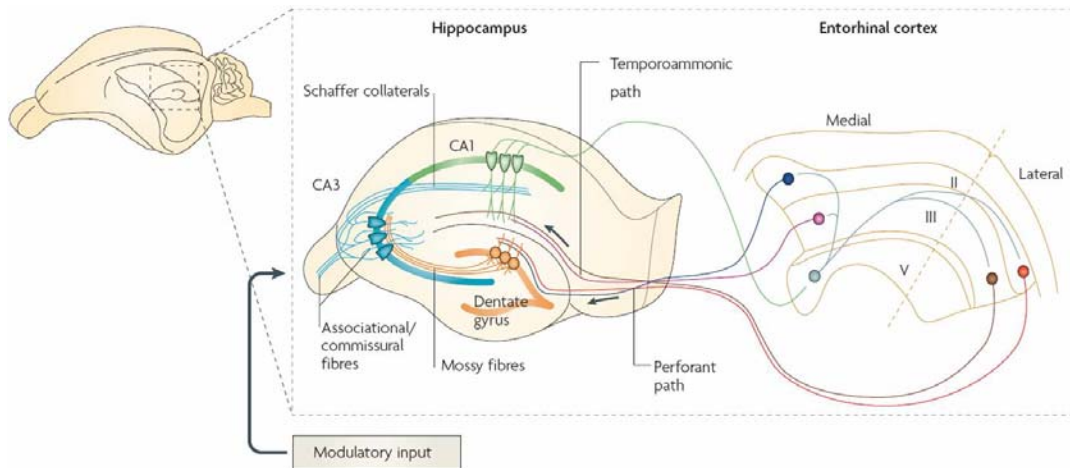


Figure 2.1 Basic anatomy of the hippocampus. The schematic shows a transversally cut section of the hippocampus, its major inputs from the entorhinal cortices, and the basic intrahippocampal connectivity. Modified from Neves et al. (2008).

Studying the hippocampus on the organismic level, a large number of lesion studies in different hippocampal regions in animals and humans indicated an essential role in episodic memory and learning, especially spatial learning (Milner and Penfield, 1955; Milner, 1972; Moser *et al.*, 1993; Rogers *et al.*, 2006; Kesner and Hopkins, 2006). Moreover, the hippocampus seems to be involved in spatial memory in humans, i.e. it was found to reveal larger volumes in human subjects with extensive spatial navigation experience (Maguire *et al.*, 2000).

On the cellular level, the hippocampus was shown to be a highly plastic brain region throughout development and even adulthood. The best known and most prominent form of synaptic plasticity in the hippocampus is activity-dependent long-term potentiation (LTP, Fig. 2.2) (Bliss and Lomo, 1973; Bliss *et al.*, 1983; Bliss and Collingridge, 1993). Its functional counterpart, long-term depression (LTD), was discovered later (Fig. 2.2) (Dudek and Bear, 1992; Mulkey and Malenka, 1992) and is still not as well understood. However, morphological changes of the hippocampus have been correlated with both forms of synaptic plasticity in *in vitro* systems on the subcellular level (Maletic-Savatic *et al.*, 1999; Engert and Bonhoeffer, 1999; Matsuzaki *et al.*, 2004; Nägerl *et al.*, 2004).

Furthermore, the underlying molecular pathways of long-term plasticity are successively being explored (Fukunaga *et al.*, 1993; Malleret *et al.*, 2001; Lisman *et al.*, 2002).

Although hippocampal function in an organism and its cellular plasticity have been extensively studied, cellular processes could not be linked to learning for a long time. However, from the many correlative findings of the past decades, Martin *et al.* (2000) have postulated the *Synaptic Plasticity and Memory* (SPM) hypothesis: “*Activity-dependent synaptic plasticity is induced at appropriate synapses during memory formation, and is both necessary and sufficient for the information storage underlying the type of memory mediated by the brain area in which that plasticity is observed*”. This concept has proven to be valid in other brain regions earlier, i.e. in the amygdala (Rogan and Ledoux, 1995; McKernan and Shinnick-Gallagher, 1997; Tsvetkov *et al.*, 2002). More recently, some studies eventually have provided exciting evidence for a direct mutual dependence between learning and synaptic plasticity in the hippocampus as well (Rutishauser *et al.*, 2006; Whitlock *et al.*, 2006; Gruart *et al.*, 2006). Whitlock *et al.* showed that one-trial inhibitory avoidance learning caused an increase of evoked synaptic transmission *in vivo*, while Rutishauser *et al.* found increased firing after single-trial learning in a novelty detection task. Those findings strongly support the long-standing hypothesis that synaptic plasticity underlies learning, demonstrating that the hippocampus is a favorable model system to study synaptic plasticity on cellular and behavioral expression levels.

2.2 The mechanisms and significance of hippocampal LTD

LTD is an activity-dependent decrease in synaptic transmission, which exists in heterosynaptic and homosynaptic forms. Homosynaptic LTD refers to a depression of the synaptic pathway at which plasticity was induced, whereas heterosynaptic LTD occurs at a separate pathway, at which the presynaptic input is

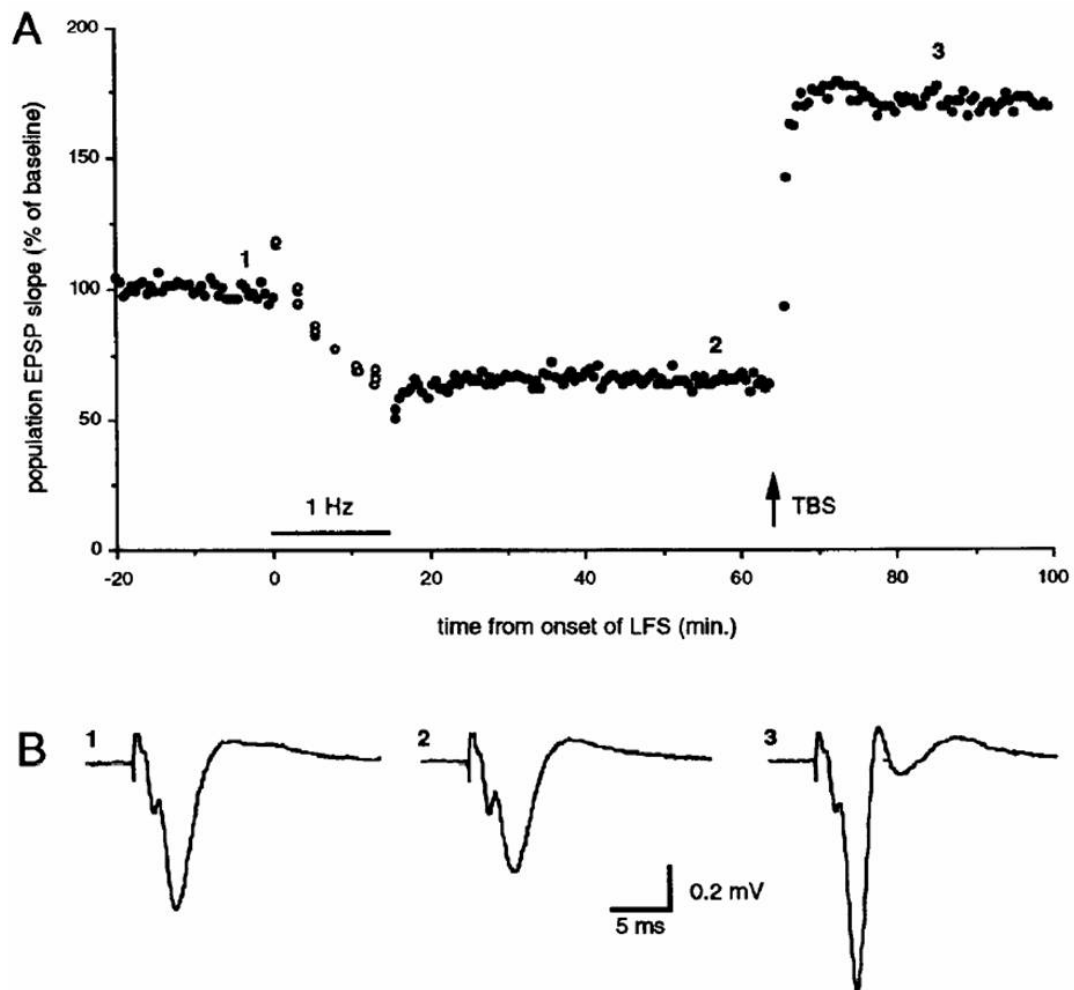


Figure 2.2 Example of LTD and LTP evoked in the Schaffer collateral-CA1 pathway. **A** Plot of fEPSPs initial slope measured every 30 sec. At time zero, 1 Hz stimulation was applied for 15 min (900 pulses). Open circles show selected responses measured during the conditioning stimulation. At the completion of the 1 Hz conditioning, baseline measurements were resumed at 0.03 Hz. Note the persistent depression of the response to baseline stimulation. At the arrow, theta burst stimulation (TBS) was applied, and LTP resulted. **B** Field potentials (averages of 10 consecutive sweeps) taken before 1 Hz stimulation (1), after 1 Hz stimulation (2) and after the TBS (3). The times at which the illustrated sweeps were taken are indicated in A. Taken from Dudek and Bear (1992).

inactive. The first study describing activity-dependent depression had discovered heterosynaptic LTD, which occurred at a non-tetanized pathway in the CA1 region, in parallel to another pathway expressing LTP after tetanic stimulation

(Lynch *et al.*, 1977). Subsequently, this form of LTD was also found in the dentate gyrus (Levy and Steward, 1979). Homosynaptic depression was first discovered in the form of depotentiation, i.e. as a reversal of LTP in response to low-frequency stimulation (LFS) (Barrionuevo *et al.*, 1980). Independent homosynaptic LTD following LFS, without the necessity of preceding potentiation, was first described a decade later in the CA1 region (Dudek and Bear, 1992; Mulkey and Malenka, 1992). The fact that LTD has been established in various other brain regions since then (Kirkwood and Bear, 1994; Hedberg and Stanton, 1995; Ziakopoulos *et al.*, 1999), suggests that it represents a similarly universal principle of synaptic plasticity as LTP (Martin *et al.*, 2000) or homeostatic plasticity (Turrigiano and Nelson, 2004). However, it seems to be more dependent on very particular conditions during the induction, e.g. frequency and place of stimulation, than LTP (Kemp and Bashir, 2001). Nevertheless, LTD has been found to play a role *in vivo* as well, in the hippocampus (Doyere *et al.*, 1996; Manahan-Vaughan, 1997), but also in other brain regions (Takita *et al.*, 1999; Froc *et al.*, 2000; Heynen *et al.*, 2003), supporting its physiological significance.

2.2.1 Induction and expression of LTD

In the following section about induction and expression mechanisms, only LTD at the CA3-CA1 synapse will be considered, being the relevant type of LTD for this thesis. Typically, hippocampal LTD is induced by LFS of 1 - 5 Hz, consisting of 500 – 900 stimuli (Debanne and Thompson, 1996; Kemp and Bashir, 2001), but also can be a parallel effect of high-frequency stimulation (HFS) if expressed heterosynaptically. Induction and expression mechanisms seem to differ for homosynaptic and heterosynaptic LTD. While the induction of homosynaptic LTD requires pre- and postsynaptic activity, postsynaptic depolarization alone is sufficient for heterosynaptic LTD (Bear and Abraham, 1996). Although the expression of both forms of LTD requires postsynaptic Ca^{2+} influx during the induction, Ca^{2+} is provided by NMDA receptor activation in homosynaptic LTD (Dudek and Bear, 1992; Mulkey and Malenka, 1992), and by voltage-gated

calcium channels (VGCCs) in heterosynaptic LTD (Wickens and Abraham, 1991; Bear and Abraham, 1996). Moreover, metabotropic glutamate receptors and endocannabinoid receptors can play a role in the induction of homosynaptic LTD (Manahan-Vaughan, 1997; Gerdeman *et al.*, 2002). Beyond the Ca^{2+} influx, homosynaptic and heterosynaptic LTD seem to share the same pathways (Bear and Abraham, 1996), involving CaMKII (Mulkey *et al.*, 1993), protein phosphatase PP1 (Thiels *et al.*, 1998), and protein synthesis (Huber *et al.*, 2000). Although the expression mechanisms are only incompletely explored, the interplay of inactivated CaMKII and upregulated activity of PP1 have been suggested to lead to an enhanced removal of AMPA receptors from the postsynaptic membrane (Luscher *et al.*, 1999; Carroll *et al.*, 1999; Snyder *et al.*, 2001; Kemp and Bashir, 2001; Huang *et al.*, 2004), leading to decreased postsynaptic responses. Moreover, a large body of evidence indicates a presynaptic expression site for homosynaptic and heterosynaptic LTD (Bolshakov and Siegelbaum, 1994; Oliet *et al.*, 1997; Fitzjohn *et al.*, 2001; Zakharenko *et al.*, 2001; Xiao *et al.*, 2001; Faas *et al.*, 2002; Zhang *et al.*, 2006), for review see Anwyl (2006); yet, the underlying mechanisms for those effects remain unclear. Interestingly, for both, pre- and postsynaptic expression, modifications of the synapse structure have been suggested early in the debate about mechanisms (Desmond and Levy, 1983; Bear and Abraham, 1996; Kemp and Bashir, 2001), see also section 2.3 below and section 5.1 of the Discussion.

2.2.2 Physiological significance of hippocampal LTD

Unlike for LTP, which was shown to be directly involved in some learning processes (see section 2.1), a role of LTD in learning and memory seems to be more elusive. However, some studies do support a physiological role for LTD, although the experimental evidence in support of it is more circumstantial. For instance, LTD was suggested to be involved in the processing of object-place configurations during spatial learning tasks. When LFS was applied during exploration of a novel, object-enriched environment, LTD was facilitated in the

CA1 region (Manahan-Vaughan and Braunewell, 1999). This facilitation was specific for novel objects, whereas a novel environment alone impaired LTD, while facilitating LTP (Kemp and Manahan-Vaughan, 2004). In contrast, exposure to stress facilitates LTD, but impairs LTP (Xu *et al.*, 1997; Diamond *et al.*, 2005; Artola *et al.*, 2006). The facilitation of LTD seems to result from the blockade of glutamate uptake mechanisms (Yang *et al.*, 2005), which is in line with the finding that stress-induced glucocorticoids elevate extracellular glutamate levels in the hippocampus (Moghaddam *et al.*, 1994). Apart from the hippocampus, LTD was shown to occur in the visual cortex after monocular deprivation (Heynen *et al.*, 2003), as well as after chronic cocaine administration in the *nucleus accumbens* (Thomas *et al.*, 2001).

Although LTD that usually is induced by lengthy induction protocols appears unlikely to represent a physiological process, some particular protocols exist that may be of more physiological relevance. For instance, a brief burst of 40 ms can induce LTD if coinciding with the negative peak in a theta frequency oscillation (Huerta and Lisman, 1995). Therefore, the methods used today to explore synaptic plasticity may not be sensitive enough to detect the subtle synaptic modifications that underlie learning and memory. In general, LTD can be regarded as a proof that synaptic depression can occur in an activity-dependent manner. Certainly, LTD-like modifications are important to maintain flexibility in an information storage system.

2.3 Structural synaptic plasticity

Activity-dependent changes in synaptic connections are thought to be important for learning and memory as well as for setting up and refining neural circuits during postnatal development. Synaptic strength at a given synapse can be adjusted by changing the transmitter release probability or the postsynaptic receptor composition. In addition to the mere scaling of the synaptic strength of existing synapses, profound structural changes such as the removal or formation of

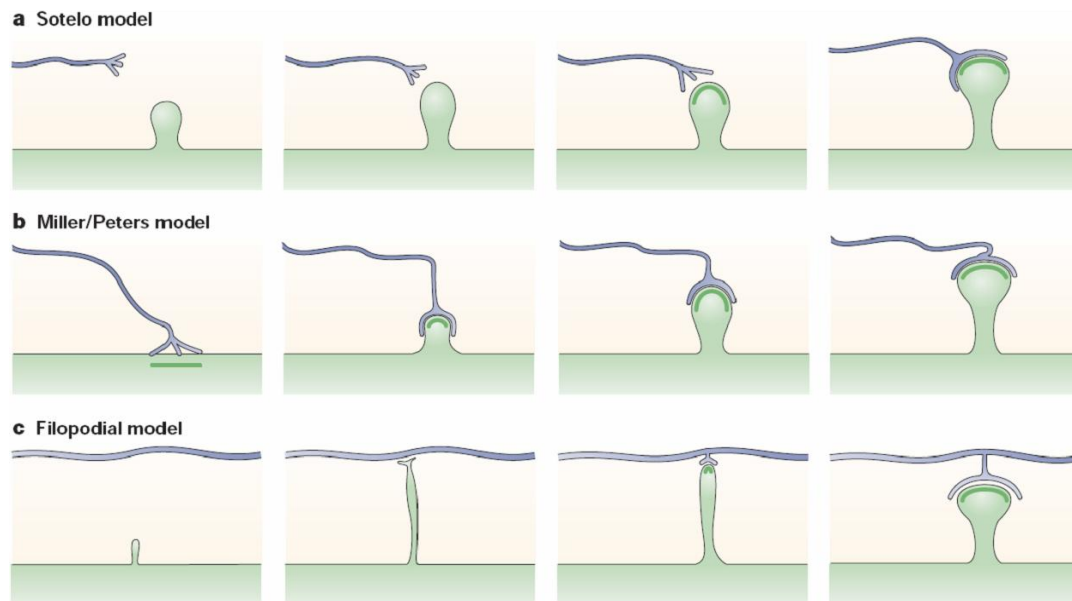


Figure 2.3 Models for the formation of synapses. **A** Sotelo model: spine and axon terminal emerging independently. **B** Miller/Peters model: synapse formation induced by axon terminal. **C** Filopodial model: synapse formation induced by dendritic filopodium. Modified from Yuste and Bonhoeffer (2004).

a synapse, were already postulated a century ago (Cajal, 1892). While synapse formation and elimination are known to shape a neuronal network during development, they have been suggested also for adult experience-dependent plasticity. Three principle models were suggested how synapses could form, differing in the modes of pre- and postsynaptic contribution (Fig. 2.2) (Yuste and Bonhoeffer, 2004). While the “online” detection of synaptic changes for decades was mostly limited to electrophysiological recordings of populations of synapses, the relatively recent utilization of two-photon laser scanning microscopy (TPLSM) for biological purposes now allows for monitoring of individual synaptic structures. A number of imaging studies in recent years have revealed a close

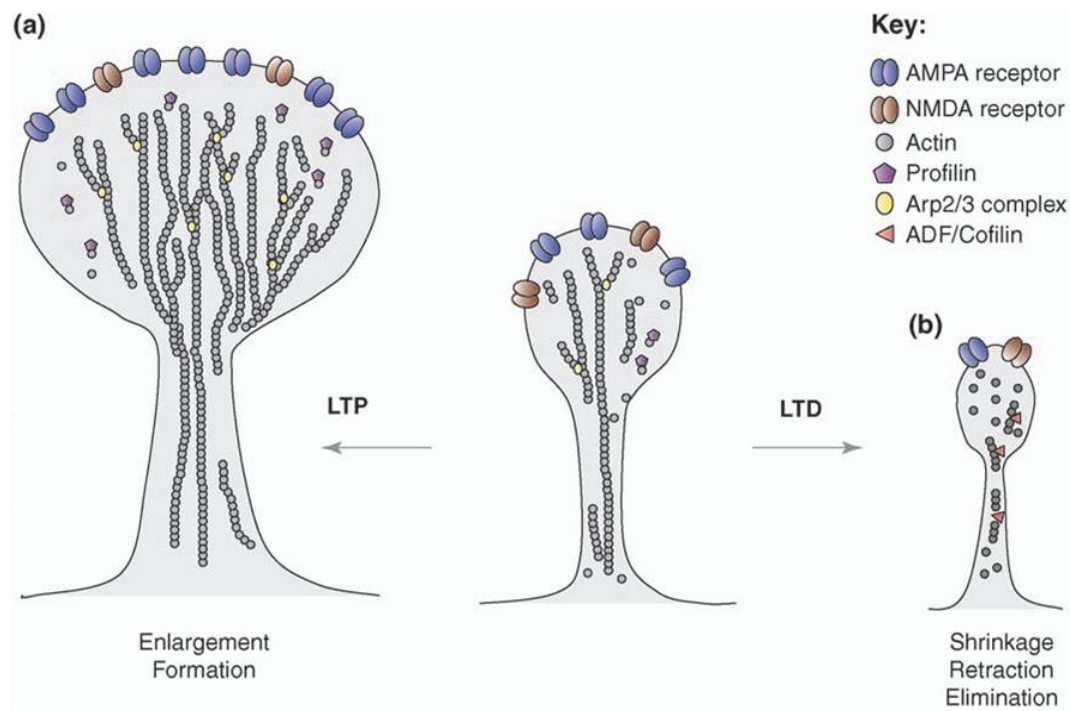


Figure 2.4 Changes in actin polymerization and spine morphology with LTP and LTD. A LTP is associated with a shift of actin equilibrium toward filamentous F-actin in spines, enlargement of the spine head, and recruitment of more AMPA receptors to the postsynaptic membrane. Profilin promotes actin filament assembly; the Arp2/3 complex stimulates nucleation of new actin filaments and formation of branches. **B** LTD shifts the equilibrium toward actin depolymerization, resulting in shrinkage or loss of spines. The actin severing protein ADF/cofilin might be involved in spine shrinkage. Modified from Tada and Sheng (2006).

association between activity-dependent synaptic plasticity, such as LTP or LTD, and structural plasticity at individual synapses (Yuste and Bonhoeffer, 2001; 2004; Alvarez and Sabatini, 2007). However, most of these studies focused exclusively on the postsynaptic site, while the presynaptic site and the synapse as a whole remain relatively poorly explored.

2.3.1 Structural plasticity of dendritic spines

In the past decade, numerous studies have indicated that spine plasticity frequently occurs in activity- and experience-dependent experimental paradigms. It

was shown, for instance, that the induction of LTP in hippocampal slices leads to the growth of new spines (Maletic-Savatic *et al.*, 1999; Engert and Bonhoeffer, 1999; Toni *et al.*, 1999), and ultimately to the formation of new synapses (Nägerl *et al.*, 2007). LTP induction was also shown to cause dendritic spines of potentiated synapses to increase in size (Lang *et al.*, 2004; Matsuzaki *et al.*, 2004). In parallel, *in vivo* studies of cortical regions provided evidence for experience-dependent formation of spines (Trachtenberg *et al.*, 2002; Holtmaat *et al.*, 2006), which would eventually form synapses (Knott *et al.*, 2006). These and other studies support the idea that morphological changes at the level of dendritic spines provide a potential structural basis of how transient changes in synaptic strength are made long-lasting. A number of studies aimed at elucidating the underlying mechanisms of structural plasticity. While it was already known that an important expression mechanism of LTP is the insertion of AMPA receptors into the postsynaptic membrane (Lu *et al.*, 2001), recent studies suggest that activity-induced spine enlargement is accompanied by exocytosis-mediated insertion of AMPA receptors (Kopec *et al.*, 2006; Park *et al.*, 2006; Matsuo *et al.*, 2008). Furthermore, activity-regulated actin dynamics are involved in the structural plasticity of spines (Fig. 2.3) (Fischer *et al.*, 2000; Fukazawa *et al.*, 2003; Okamoto *et al.*, 2004).

Importantly, it was also demonstrated that a decrease in synaptic strength affects synaptic structure, since the induction of LTD causes spines on CA1 pyramidal neurons in hippocampal slices to retract and/or shrink (Zhou *et al.*, 2004; Nägerl *et al.*, 2004). However, beyond the involvement of actin (Fig. 2.3) (Okamoto *et al.*, 2004) and AMPA receptor removal (Snyder *et al.*, 2001; Xiao *et al.*, 2001; Huang *et al.*, 2004; Nosyreva and Huber, 2005), little is known about the cellular mechanisms that lead to the removal of a spine and the associated disassembly of the synapse. In the light of those and several developmental studies, which suggest that spine turnover reflects an ongoing adjustment of the neuronal network (Katz and Shatz, 1996; Holtmaat *et al.*, 2005), it seems crucial to elucidate the mechanisms of synapse formation as well as of synapse degradation.

2.3.2 Structural plasticity of axonal boutons

In contrast to the plasticity of dendritic spines, activity-dependent structural plasticity at the presynaptic site has not been studied in great detail. Some recent studies have looked at the spontaneous plasticity of presynaptic boutons in adult and developing hippocampal and cortical tissue *in vitro* (Toni *et al.*, 1999; Krueger *et al.*, 2003; Konur and Yuste, 2004; Deng and Dunaevsky, 2005) and *in vivo* (De Paola *et al.*, 2006; Stettler *et al.*, 2006; Majewska *et al.*, 2006). All of those studies concur that boutons reveal some degree of spontaneous structural plasticity, similar to spines. Whether experience affects bouton plasticity is completely unknown. However, a few studies have examined activity-dependent bouton plasticity in hippocampal slices and dissociated hippocampal neurons (Nikonenko *et al.*, 2003; De Paola *et al.*, 2003; Umeda *et al.*, 2005; Ninan *et al.*, 2006). These studies exclusively used LTP-inducing stimulation, employing either theta burst stimulation (TBS), HFS or chemical LTP induction. They observed differing effects on bouton plasticity, ranging from no effect over increased motility to the formation of new release sites. So far, no study has looked at bouton plasticity resulting from LTD-inducing stimulation. Altogether, the behavior of boutons under the conditions of classic plasticity paradigms known to induce synaptic plasticity is still largely unknown. However, it is well-established that many forms of synaptic plasticity are expressed at the presynaptic site. Therefore, many speculations were made about how the observed functional changes, e.g. altered transmitter release probability, could be reflected in presynaptic cellular mechanisms. Today, a large body of evidence resulting from cellular and molecular studies supports the idea that a substantial part of presynaptic plasticity is accounted for by sharing of presynaptic elements between boutons (Krueger and Fitzsimonds, 2006; Staras, 2007). The constitutive sharing of vesicle pools (Fig. 2.4) has been shown by a number of studies (Matteoli *et al.*, 1992; Kraszewski *et al.*, 1995; Lemke and Klingauf, 2005; Darcy *et al.*, 2006), some of which have found activity-regulated trafficking of vesicles between release sites (Waters and Smith, 2002; Vanden Berghe and Klingauf, 2006). Moreover, activity-dependent

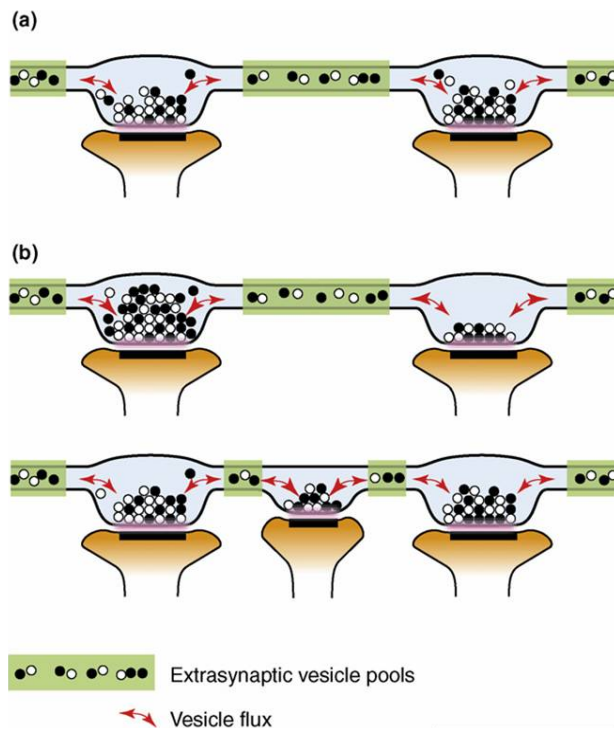


Figure 2.5 Remodeling synapses by modulating vesicle sharing. **A** Relationship between stable synaptic release sites and extrasynaptic mobile vesicle pools. **B** Mechanism for remodeling of vesicle pools. Top: biasing of vesicle exchange towards vesicle accumulation or disassembly leading to rescaling of synaptic vesicle pools. Bottom: recruitment of mobile vesicles to nascent sites. Closed circles, recycling vesicles; open circles, nonreleasable vesicles; pink lines, active zone; blue, presynaptic, brown, postsynaptic. Modified from Staras (2007).

scaling of presynaptic vesicle pools is associated with an enlargement of the bouton, as well as with an increased release probability (Murthy *et al.*, 2001; Thiagarajan *et al.*, 2005). In addition, BDNF, which is required for the presynaptic expression of LTP at the CA3-CA1 synapse (Zakharenko *et al.*, 2003), can increase the number of mobile vesicle clusters and promote the formation of new synapses (Tyler *et al.*, 2006; Bamji *et al.*, 2006).

It has been shown that AMPA receptors, protein kinase A, CaMKII and MAP kinase are critically involved in mediating activity-induced vesicle dynamics (De Paola *et al.*, 2003; Chi *et al.*, 2003). In contrast, protein synthesis or proteasome-mediated protein degradation were not required for presynaptic scaling (Tsuruel *et al.*, 2006), indicating a dominant role of the local exchange and redistribution of presynaptic constituents. Notably, not only vesicles are shared between boutons; additionally, a number of presynaptic proteins including VAMP, synapsins, syntaxin, and SNAP-25 have been found to be transported along the axon (Garcia *et al.*, 1995; Ahmari *et al.*, 2000; Tsuruel *et al.*, 2006), presumably in transport packets that contribute to the assembly of new boutons (Ahmari *et al.*,

2000). While microtubule-based axonal transport was shown to be critical for the trafficking of active zone components (Cai *et al.*, 2007), synaptic matrix molecules such as neuroligins seem to be involved in the targeting of those components (Sabo *et al.*, 2006).

Altogether, those data indicate that the molecular composition of presynaptic terminals can be dynamically regulated and is associated with synaptic performance (Atwood and Karunanithi, 2002). In addition, the high mobility of presynaptic components may form the basis for the rapid assembly or disassembly of functional boutons.

2.4 Assembly and disassembly of synapses

Today, it is generally assumed that synapses are formed and removed not only during development, but also in an experience-dependent fashion during adulthood. Although many studies found numerous molecular players involved in the assembly and disassembly of synapses, their precise functions and interplay are not fully understood.

Filopodia have been suggested to play an inductive role in synapse assembly (Fiala *et al.*, 1998; Jontes and Smith, 2000). Yet, it is unclear whether filopodial contacts occur at random, or are directed by diffusional messengers, such as neurotransmitters or neurotrophins. Some evidence for glutamate increasing the chances of making contact comes from studies that examined the motility of axonal and dendritic filopodia (Dailey and Smith, 1996; Tashiro *et al.*, 2003), reporting enhanced motility upon glutamate or presynaptic electrical stimulation. Once a physical contact is made, cell adhesion molecules (CAMs) from the pre- and postsynaptic membrane can interact and possibly trigger signaling cascades that lead to the molecular assembly of the respective pre- and postsynaptic structures (Brose, 1999; Benson *et al.*, 2000; Garner *et al.*, 2002). A number of cell adhesion molecules have been found to be implicated in synaptogenesis, being involved in contact recognition and synapse assembly. For instance, the

heterophilic interaction between presynaptically expressed β -neurexins and postsynaptically expressed neuroligins revealed a strong synaptogenic potential (Rao *et al.*, 2000). Neuroligins have been reported to induce presynaptic assembly (Scheiffele *et al.*, 2000) by inducing the clustering of neurexins in the presynaptic membrane, which in turn recruit synaptic vesicles to their cytoplasmic domains (Dean *et al.*, 2003). While heterophilic interactions represent a means to implement the asymmetric nature of a synapse, also homophilic CAMs are known to be crucial for synaptogenesis. For instance, SynCAM mediates homophilic binding across the synaptic cleft, and is associated with postsynaptic PDZ-domain proteins, but at the same time is responsible for presynaptic assembly (Biederer *et al.*, 2002), indicating that homophilic interactions can still convey asymmetric effects.

How interaction of CAMs leads to the recruitment of receptors, release machinery or postsynaptic density remains largely unclear. However, similarly as it has been discussed above (section 2.3.2) for the assembly of presynaptic sites, postsynaptic sites can also recruit preassembled transport packets, as shown for NMDA receptor and PSD-95 clusters (Prange and Murphy, 2001; Washbourne *et al.*, 2002; Park *et al.*, 2006). In contrast, AMPA receptors are recruited from the diffuse plasma membrane pool by lateral diffusion (Borgdorff and Choquet, 2002; Ehlers *et al.*, 2007). Altogether, the coordination of synapse assembly seems complex and requires further studies.

Even less is known about synapse disassembly, although a number of studies strongly suggest that the removal of synapses is a regular mode of refining neuronal circuits (Shatz and Stryker, 1978; Trachtenberg *et al.*, 2002; Zhou *et al.*, 2004; Nägerl *et al.*, 2004). Nevertheless, information about the underlying processes is rare and fragmental, especially at vertebrate central synapses. Some evidence about signaling cascades leading to synapse disassembly comes from cerebellar and visual cortex studies, suggesting an involvement of mGluR1, NMDA receptors, CaMKII and CREB signaling (Goda and Davis, 2003). Moreover, it was shown at the neuromuscular junction that receptor removal precedes the removal of a presynaptic terminal (Akaaboune *et al.*, 1999). In

summary, it remains elusive how synapse assembly and disassembly are coordinated, and how neuronal activity influences these processes.

2.5 Objectives of this study

Activity-dependent changes in the synaptic connections of the brain are thought to be important for learning and memory. The hippocampus has been shown to be involved in those processes and is a well-established model system for synaptic plasticity; in particular for LTP and LTD. Although LTD is considered to be critical to maintain flexibility in a memory system, it is less well explored than LTP. Recently, novel imaging techniques have enabled the examination of structural rearrangements during activity-dependent processes at individual synapses. Many morphological studies suggest that spine turnover reflects an ongoing adjustment of the neuronal network. However, most of these studies focused exclusively on the postsynaptic site, while the presynaptic site and the synapse as a whole remain relatively poorly explored.

I therefore set out to study whether and how presynaptic boutons change in an activity-dependent plasticity paradigm. In addition, I was interested in the behavior of boutons in contact with spines that underwent plasticity. I performed two-color two-photon time-lapse imaging to visualize the structural dynamics of Schaffer collateral boutons and associated spines of CA1 pyramidal neurons in hippocampal organotypic slice cultures. Since LTD-inducing low-frequency stimulation is known to lead to the retraction of spines of CA1 pyramidal neurons, I examined how boutons of Schaffer collateral axons, which provide the presynaptic input to those spines, are affected by this paradigm. Moreover, I monitored pairs of boutons and spines to examine the fate of the synapses of which a spine or a bouton reveals structural plasticity. Furthermore, I aimed at examining the functionality of plastic presynaptic boutons. For this purpose, I established Ca^{2+} imaging of individual boutons in our laboratory and assessed whether and when plastic boutons show voltage-gated entry of Ca^{2+} ions.

This study is the first to report presynaptic structural plasticity associated with the induction of LTD. It adds to the understanding of the role of structural plasticity for a neuronal network and opens up interesting opportunities to study the molecular mechanisms of activity-dependent structural plasticity.

3 Material & Methods

3.1 Material

Chemicals, dyes, antibodies and media were purchased from Merck/VWR (Darmstadt, Germany), Sigma (Munich, Germany), Invitrogen / Molecular Probes / Gibco (Karlsruhe, Germany), Chemicon (Temecula, CA), Synaptic Systems (Göttingen, Germany), and Jackson ImmunoResearch (Newmarket, UK). Deionized water from a Millipore filter system (Schwalbach/Ts., Germany) was used to prepare all solutions.

3.1.1 Chemicals

Chemical	Supplier
ACSF/intracellular solution	
CaCl ₂ *2H ₂ O	Merck/VWR
Glucose	Merck/VWR
HEPES	Sigma
KCl	Merck/VWR
K-Gluconate	Sigma
Mg ²⁺ -ATP	Sigma
MgCl ₂	Merck/VWR
NaCl	Merck/VWR
NaH ₂ OPO ₄	Merck/VWR
NaHCO ₃	Merck/VWR
Pyruvate	Sigma
Trolox (6-Hydroxy-2,5,7,8-tetramethylchroman-2-carbon acid)	Sigma

Culture media

5-Fluorodeoxyuridine	Sigma
BME (basal medium + Earle's)	Gibco
Cytosine β -D-arabino-furaoside hydrochloride	Sigma
HBSS (Hanks balanced salt solution 10x) + MgCl ₂ , + CaCl ₂	Gibco
Horse serum	Invitrogen
KH ₂ PO ₄	Merck/VWR
Kynurenic acid	Sigma
L-glutamine	Invitrogen
MgSO ₄ *7H ₂ O	Merck/VWR
Uridine	Sigma

Other

Beads (fluorescent, diameters 0.2, 0.5, 1.0, 2.5 μ m)	Invitrogen
Bovine serum albumine	Sigma
Chicken plasma	Sigma
DMSO	Sigma
NaOH	Merck/VWR
Paraformaldehyde (PFA)	Merck/VWR
Triton X-100	Sigma

3.1.2 Media

- **ACSF (artificial cerebrospinal fluid)**

126 mM NaCl, 2.5 mM KCl, 2.5 mM CaCl₂, 1.3 mM MgCl₂, 10 mM glucose, 1.25 mM NaH₂PO₄, 26 mM NaHCO₃, 1 mM pyruvate, 1 mM Trolox, 310 mosm, pH 7.4

- **Intracellular solution for patch pipettes**

120 mM K-Gluconate, 10 mM KCl, 20 mM HEPES, 5 mM NaCl, 12 mM Mg²⁺-ATP, 295 mosm, pH 7.25, sterile filtered

- **Preparation medium for organotypic slice cultures**

Gey's balanced salt solution (GBSS; 2.5 mM CaCl₂ *2H₂O, 4.96 mM KCl, 0.22 mM KH₂PO₄, 1.03 mM MgCl₂ *6 H₂O, 0.28 mM MgSO₄ *7H₂O, 136.89 mM NaCl, 2.7 mM NaHCO₃, 0.87 mM Na₂HPO₄), 5.05 mM D-glucose, 1 mM kynurenic acid, pH 7.2, sterile filtered

- **Gähwiler culture medium**

50 % (v/v) BME, 25 % (v/v) horse serum, 25 % (v/v) HBSS, 1 mM L-glutamine, 5 mg/ml D-glucose, sterile filtered

- **PBS**

137 mM NaCl, 2.7 mM KCl, 4.3 mM Na₂HPO₄, 1.4 mM KH₂PO₄, pH 7.4

- **PFA 4 %**

20 g PFA (w/v), 500 ml PBS, 200 µl 5N NaOH, pH 7.4

3.1.3 Dyes

Dye	Concentration [mM]	Supplier
Alexa Fluor 568 hydrazide	0.2	Invitrogen
Calcein green	4	Invitrogen
Calcein red-orange AM	0.5	Invitrogen
Fluo-5F	0.1	Invitrogen

3.1.4 Antibodies

Antibody	Dilution	Supplier
Primary antibodies		
α-GFP (rabbit)	1:1000	Chemicon
α-synapsin (rabbit)	1:500	Chemicon
α-VGlut1 (rabbit)	1:400	Synaptic Systems

Secondary antibodies

α -chicken-Alexa488	1:500	Invitrogen
α -rabbit-Alexa633	1:500	Invitrogen
α -rabbit-Cy3	1:500	Jackson ImmunoResearch

3.1.5 Equipment

Instrument	Supplier
Two-Photon Laser-Scanning Microscope	
Electro-optical modulator	Polytec, Waldbronn, Germany
Bandpass filter HQ525/50 (green)	LOT Oriel, Darmstadt, Germany
Bandpass filter HQ590/55 (red)	LOT Oriel, Darmstadt, Germany
Dichroic mirror CH-700DCXR2638	LOT Oriel, Darmstadt, Germany
Dichroic mirror HQ572LP	LOT Oriel, Darmstadt, Germany
Inverted microscope IX70	Olympus, Hamburg, Germany
Mira-Verdi laser system (5 W)	Coherent, Santa Clara, CA
Photomultiplier tubes R6357	Hamamatsu, Herrsching, Germany
Scanhead Yanus II	TILL Photonics, Gräfelfing, Germany
Water-immersion objective, 40x, NA 1.2	Zeiss, Oberkochen, Germany
Electrophysiology	
A/D converter PCI-6052 (16 bit)	National Instruments, Austin, TX
Axopatch 200B amplifier	Axon Instruments, Foster City, CA
Glass capillaries (thin-wall, 4", with filament, outer diameter 1.5 mm)	WPI (World Precision Instruments), Sarasota, FL
Stimulus Isolator A360	WPI, Sarasota, FL

Software

ImageJ	NIH, Bethesda, MD
Imaris 5.1	Bitplane, Zürich, Switzerland
LabVIEW software 7.2	National Instruments, Austin, TX
LabVIEW software 8.2	National Instruments, Austin, TX
Matlab 7.1	MathWorks, Natick, MA
Statistica 7	StatSoft, Tulsa, OK

Other

Confocal microscope Leica SP2UV	Leica, Wetzlar, Germany
Minipuls peristaltic perfusion pump	Gilson, Middleton, WI
Picospritzer	Parker Hannifin Corp., Fairfield, NJ
Tissue Chopper (McIlwain)	Campden Instruments, Loughborough, UK

3.2 Methods

3.2.1 Organotypic hippocampal slice cultures

Organotypic hippocampal slices were prepared from postnatal day 5-7 mice of both sexes according to the Gähwiler method (Gähwiler, 1981). C57 BL/6 mice were used for all experiments, except for immunohistochemistry experiments, where transgenic GFP-mice (Thy-1 promoter, GFP-M mouse line, courtesy of J. Sanes, Harvard University, Cambridge, MA) were used.

In brief, after decapitation, the hippocampi of both hemispheres were dissected in ice-cold GBSS. Transversal slices of 400 μm thickness were cut using a tissue chopper, then placed back into the preparation medium and separated with fine forceps. The sections were stored at 4°C for 30 min to allow regeneration and removal of debris. Subsequently, the slices were placed on a drop of plasma solution on a glass coverslip and thrombin was added to induce coagulation. After

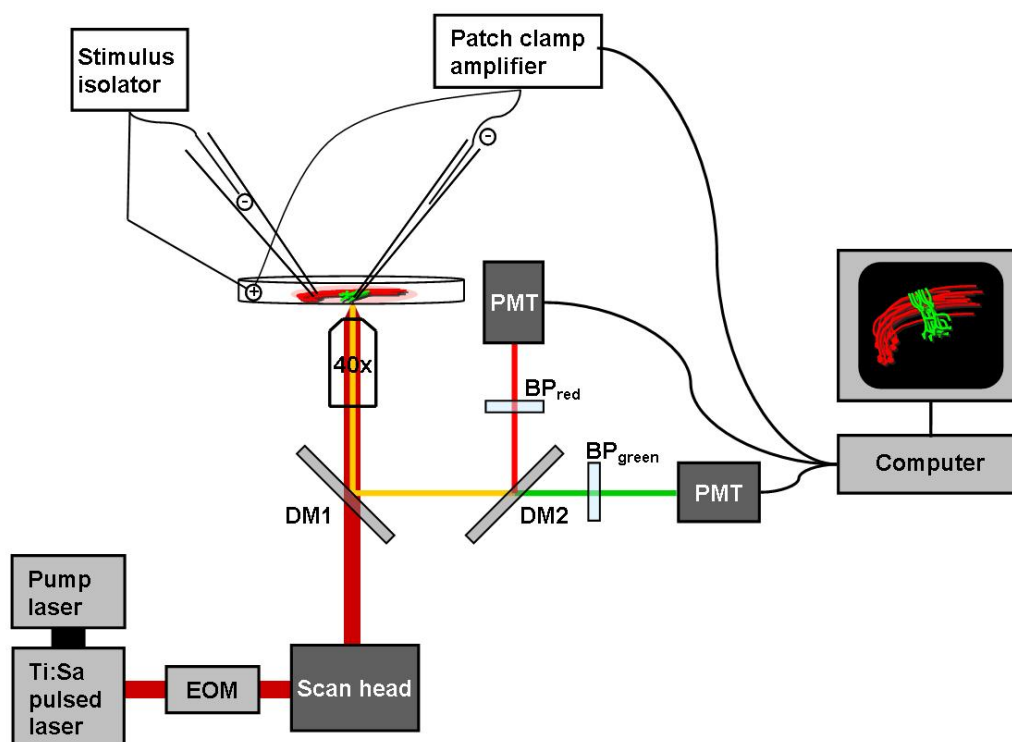


Figure 3.1 Schematic overview of the two-photon setup. Excitation light path: pump laser, Ti:Sa pulsed laser, electro-optical modulator (EOM), scan head, first dichroic mirror (DM1), objective, and specimen. Emission light path: specimen, objective, DM1, DM2, band pass filter green/red (BP), photomultiplier tubes (PMTs), and computer. The electrophysiological circuit consists of stimulus isolator, stimulation electrode, recording electrode, and patch clamp amplifier.

a drying period of 30 min, the coverslips were incubated in Gähwiler medium in a roller incubator at 35°C. After three days *in vitro*, a mitosis inhibiting solution was added to stop glia proliferation.

The slice cultures used in the experiments were maintained 10 to 20 days *in vitro* after the preparation. For the experiments, slice cultures were transferred into a heated recording chamber (35°C), where they were continuously perfused with carbogenated (95 % O₂, 5 % CO₂) ACSF.

3.2.2 Two-photon laser-scanning microscopy

Two-color time-lapse two-photon laser-scanning microscopy (TPLSM) was used to monitor the morphology of Schaffer collateral axons and dendrites of CA1 pyramidal neurons over time, and to detect Ca^{2+} transients in preexisting and newly formed boutons. The red excitation light ($\lambda = 790$ nm for the structural plasticity experiments, $\lambda = 810$ nm for the Ca^{2+} imaging experiments) from a femtosecond pulsed laser system (5 W pump laser) was routed through a laser scanhead, a dichroic mirror (CH-700DCXR2638) separating excitation and emission fluorescence, and a 40x, 1.2 NA water-immersion objective mounted on an inverted microscope (Fig. 3.1). For all experiments, the power of the excitation light was adjusted to 2 mW after the objective by an electro-optical modulator. The emitted fluorescence was split by a suitable dichroic mirror (HQ572LP) into red and green fluorescence, filtered by adequate bandpass filters (red channel: HQ590/55; green channel: HQ525/50l), and detected by two external photomultiplier tubes. Image acquisition was performed by custom-programmed software (LabVIEW 8.2).

Structural imaging of Schaffer collateral axons and CA1 pyramidal cell dendrites

A glass micropipette filled with 0.5 mM Calcein red-orange AM diluted in HEPES-buffered ACSF, connected to a pressurized-air microinjection device, was placed in the middle of the cell body layer of the CA3 area (Fig. 3.2 A). The dye was injected into the tissue by applying brief positive pressure pulses of 5 to 15 ms every 20 s. After 1 h, about 30 to 40 CA3 neurons were labeled. TPLSM was used to localize the projection area of the labeled axons of the CA3 neurons in the CA1 region. Two to four CA1 pyramidal neurons in this area were loaded for 2-3 min using a patch pipette filled with intracellular solution containing 4 mM Calcein green. The field of view was chosen in the region with optimal overlap of the CA3 pyramidal cell axons and the CA1 pyramidal cell dendrites (Fig. 3.2 B), which was always located within the *stratum oriens*. 3D image stacks (spanning 140 μm in x,

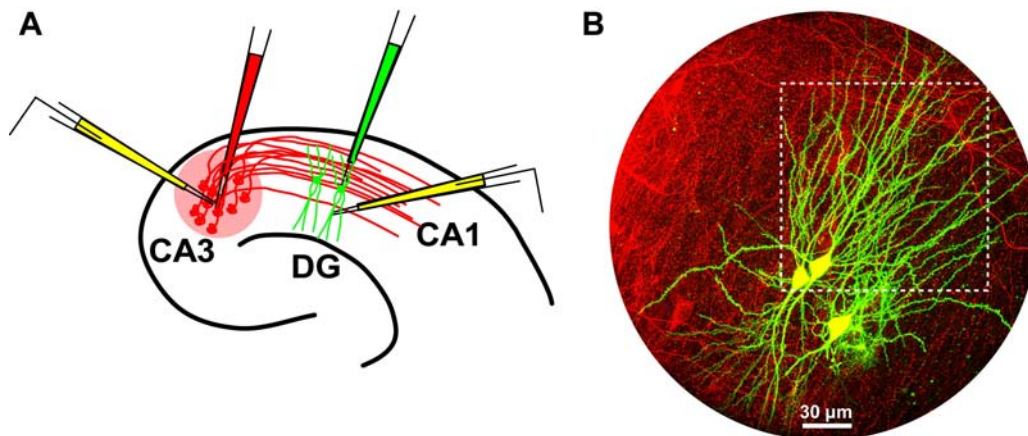


Figure 3.2 Experimental approach. **A** The red pipette is used for extracellular pressure injection of Calcein red-orange AM in the CA3 area, the green pipette contains Calcein green for labeling individual CA1 pyramidal neurons by whole-cell patching. The yellow pipettes indicate the positions of the stimulation (left) and recording (right) electrodes after the labeling procedure. **B** Overview of labeled CA3 axons (red) and CA1 pyramidal cells (green) displayed in a maximum intensity projection (MIP). White rectangle marks a typical field of view for imaging.

140 μm in y and 25-40 μm in z using 1024 x 1024 pixels in xy, corresponding to a nominal pixel resolution of 731 nm, and 0.5 μm steps in z) were acquired every 30 min. The labeling of both sets of neurons remained constant for the duration of the experiment.

Structural and functional Ca^{2+} imaging of single Schaffer collateral axons

Single CA3 pyramidal neurons were patched to fill and monitor them over 4 - 8 h. The intracellular solution contained 0.2 mM Alexa Fluor 568 hydrazide to label neuronal morphology, and 0.1 mM Fluo-5F, a Ca^{2+} indicator with an intermediate affinity for Ca^{2+} ($K_d = 2.3 \mu\text{M}$) to detect small and fast changes in Ca^{2+} concentrations in the small volumes of presynaptic boutons (Brenowitz and Regehr, 2007). The labeling was equilibrated after 30 min of patching. Out of 25 cells, 20 cells were patched for the entire duration of the experiment. In the cases

of the other five cells, the patch pipette was retracted after at least 45 min of patching. However, Ca^{2+} transients could not be detected about 2 h after retraction of the pipette, suggesting that continued supply of Fluo-5F is necessary for Ca^{2+} imaging.

Overview 3D image stacks (spanning 200 μm in x, 200 μm in y and 30-40 μm in z using 1024 x 1024 pixels in xy and 1 μm steps in z) were acquired to find the axon. The field of view was chosen in the region that contained the most axon branches, which was usually located within the *stratum oriens*. 3D image stacks for monitoring axonal structural plasticity were acquired with the same parameters as described above for the previous experiments in section 3.2.2. Two baseline image stacks were taken within 20 min before the induction of LTD. Thereafter, image stacks were taken every 30 min and immediately analyzed for the growth of new boutons.

Ca^{2+} imaging was performed in preexisting and newly formed boutons. 75 boutons were imaged from 25 cells, 15 of them had newly formed. For the Ca^{2+} imaging, the field of view was chosen to include either two preexisting boutons on the same stretch of axon, or the new bouton and its next neighboring preexisting bouton. Three types of Ca^{2+} imaging experiments were performed. At first, Ca^{2+} transients were recorded in preexisting boutons to determine their dependence on the number of action potentials (APs; 1, 3 or 10). Then, LTD experiments were performed in which after baseline imaging, cells were stimulated with the LTD protocol described above. Bouton turnover was monitored during the experiment, and preexisting and new boutons were tested for induced Ca^{2+} transients subsequently. In a subset of two LTD experiments, the Ca^{2+} transients of some preexisting boutons were monitored at several time points before and after LTD induction. In three control experiments, bouton turnover was monitored over 4 h without LTD induction, and preexisting and new boutons were subsequently tested for AP-induced Ca^{2+} transients.

The field of view typically spanned 5 x 5 μm^2 in the xy plane, with a resolution of 64 x 64 Pixels. All images were taken in a single z-plane, chosen by

the centre of the boutons. Ca^{2+} imaging was performed with a frame rate of 15 ms while evoking 1, 3 or 10 APs. APs were evoked after 20 imaging frames, corresponding to 300 ms of baseline imaging. Total imaging time per trial was 80 frames corresponding to 1.2 s. For practical reasons, only the green channel displaying the Fluo-5F fluorescence was recorded during Ca^{2+} imaging. Immediately before Ca^{2+} imaging, a single picture was taken in the red channel to define the regions of interest for the subsequent analysis of the Ca^{2+} transients.

3.2.3 Electrophysiology

CA3 pyramidal neurons were stimulated extracellularly by brief (0.2 ms) current pulses from a stimulus isolator using a glass micropipette filled with 3 M NaCl, immobilized at the tip by agar, or filled with ACSF. Stimulus strength ranged between 12 and 25 μA . fEPSPs or APs were recorded using a patch clamp amplifier, an A/D converter and custom-programmed acquisition software (LabVIEW 7.2). The stimulus protocol used for induction of long-term depression (LTD) consisted of 900 pulses delivered at 1 Hz (Dudek and Bear, 1992).

fEPSP recording and LTD induction during structural plasticity experiments

Field excitatory postsynaptic potentials (fEPSPs) were recorded from the cell body layer near the labeled CA1 pyramidal neurons, using a glass micropipette filled with ACSF. To ensure a high degree of overlap between the fibers that underwent LTD and the fibers that were imaged, the tip of the stimulating electrode was placed at the same location as the pipette used to apply the presynaptic label (Fig. 3.2 A, left yellow pipette). Stimulus strength was adjusted to elicit fEPSPs of half-maximal amplitude, ranging from 0.2 to 1.4 mV. Bouton and spine turnover was measured in recordings where electrical stimulation was performed once every 15 s (0.067 Hz) and started with the acquisition of the first image stack and continued throughout the control and LTD experiments. The LTD

induction protocol started after recording a baseline of 35 min during which two image stacks were taken. In an additional set of control experiments bouton turnover was measured during and after 1400 pulses were applied at a frequency of once every 6 sec (0.17 Hz) for a period of 2 hours and 20 min, exactly matching the number of pulses (LFS plus subsequent test pulsing) that were applied in the LTD experiments over the same time window. The initial slopes of fEPSPs were determined with custom-made analysis software (LabVIEW 7.2).

Evoking APs and LTD induction in the Ca²⁺ imaging experiments

22 out of 25 CA3 pyramidal neurons were patched within a maximum distance of 40 μm to an extracellular stimulation electrode. Stimulus strength was adjusted to reliably evoke APs in the patched cell. In three cells of the LTD experiments, APs were evoked directly by injecting current through the patch pipette, because no stimulation electrode was placed. A current injection of 0.7 to 1.4 nA for 1 ms was necessary to reliably evoke APs. After breaking into the cell, the neurons were held in voltage clamp at -70 mV for about 5 min to stabilize. Then the recording mode was changed to current clamp to allow action potential firing. AP firing was measured via the patch pipette and displayed on an oscilloscope. The membrane potential was -60 to -68 mV and monitored throughout the experiment.

3.2.4 Image Analysis

4D (x, y, z, t) image stacks were processed and analyzed using ImageJ, Imaris 5.1, and custom-programmed MATLAB software to determine turnover of boutons and spines, measure axon and dendrite length, volumes of boutons and spines and determine the size of Ca²⁺ transients.

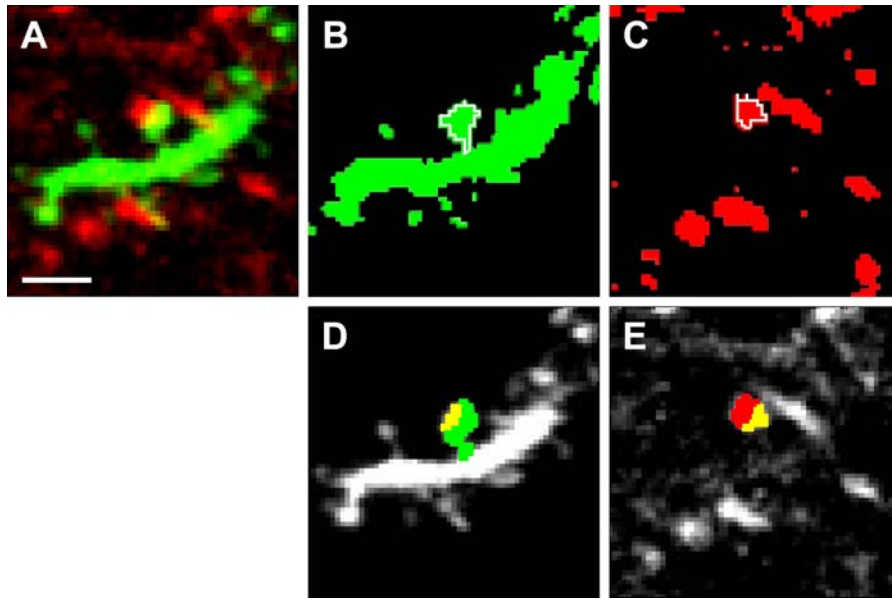


Figure 3.3 Example of an individual bouton-spine pair, illustrating how the structural changes were quantified by Matlab-based image analysis. **A** Single-section image of a bouton-spine pair selected for volume and motility measurements. **B**, **C** MIPs of the separate channels with the outline of the spine (**B**) and the bouton (**C**) in white. **D**, **E** Single sections showing the individual pixels assigned to the spine and bouton. The pixel overlap (in yellow) indicates sites of putative synaptic contact, the pixels in red and green indicating non-overlapping areas of the bouton and spines, respectively. Scale bar 2 μm .

Image analysis of the structural plasticity experiments

Bouton turnover was analyzed blindly with respect to control and LTD experiments. Individual stacks of the red channel were visualized and filtered with a Gaussian algorithm in ImageJ. For each experiment, two to four axons were analyzed over lengths ranging from 55 to 130 μm . The selected axons were displayed and analyzed as maximum intensity projections. The presence of every bouton was assessed on the basis of intensity plots, which were calculated as the average intensity over every line of pixels from a rectangle drawn along short stretches of axon (Fig. 4.3 C, D). Boutons were defined by a peak intensity >30 % larger than the intensity level of the axonal shaft. Spine turnover analysis was

carried out on volume-rendered images of the green channel, which was spatially filtered by an edge-preserving algorithm using the Imaris software. In addition, individual sections were analyzed to confirm if a spine was lost or gained. All spines visible in the field of view were included in the analysis.

For the analysis of bouton-spine pairs, contacting boutons and spines were detected visually in single planes of image stacks with both channels overlaid and filtered by an edge-preserving algorithm in Imaris. All bouton-spine pairs undergoing structural changes, and a random sample of stable pairs were analyzed. Only those pairs were analyzed for which both bouton and spine were centered in the same z-section. In total, 908 pairs of boutons and spines were analyzed, of those 223 came from five slices in control experiments and 685 came from eleven slices in LTD experiments. The volumes of both partners of bouton-spine pairs were determined by a MATLAB program in the following manner. Stacks of raw images of both channels were read in as time series, filtered with an adaptive Wiener algorithm and drift-corrected in all dimensions. Data were binarized in each channel separately by an intensity threshold. Thresholds were empirically defined by a semi-automatic two-step procedure. In the first step, background was distinguished from neuronal structures such as dendrites and axons (threshold = mean + 3 SD of intensity values of a local 200×200 pixel area). In the second step, boutons were distinguished from axonal shafts (threshold = mean + 1.5 SD of axon pixel intensities). In this way, thresholds were objective and they were kept constant over all time points. Outlines of boutons and spines of putative contacts were determined semi-automatically in the individual z-sections of the thresholded images of the separate channels (Fig. 3.3). From these, the volumes of the individual structures were calculated.

Image analysis of the Ca²⁺ imaging experiments

Bouton turnover needed to be analyzed while the experiment was in progress. As a consequence, it was not blindly assessed. Raw image stacks of each time point were visualized in ImageJ, converted into maximum intensity projections

immediately after acquisition, corrected for drift compared to the first time point using the StackReg plugin in ImageJ, and screened for newly grown boutons. As soon as a new bouton was detected, it was zoomed-in under the two-photon microscope and tested for AP-induced Ca^{2+} transients. Ca^{2+} transients were determined measuring the Fluo-5F fluorescence intensity in a region of interest, which was either the bouton area or a stretch of axon shaft. The regions of interest were determined with the help of the morphology image (Alexa Fluor 568, red channel) taken before the Ca^{2+} imaging (Fig. 4.10 C). The Fluo-5F fluorescence intensity values (F_i) of each frame of each region of interest were exported to MS Excel. All frames recorded before triggering the action potentials, usually 19 frames, were considered baseline values. In Excel, the average fluorescence intensity of all baseline frames (F_0) was calculated and subtracted from the values of all frames ($F_i - F_0 = \Delta F$). Then, those values were divided by the average baseline fluorescence to normalize them to the baseline ($\Delta F / F_0$). All traces are displayed as single traces or averages of two to ten traces, which is always explicitly stated in the figure legends. Single traces and averaged traces are processed by calculating a moving average of three consecutive values. All further analysis was done on the basis of these processed traces. The peak amplitude was taken as the size of the signal. To determine the noise level, the standard deviation of the baseline fluorescence was calculated, which equals the root mean square (RMS) for the $\Delta F / F_0$ values, a measure of noise. Two times the standard deviation was set as the threshold for signal detection for all Ca^{2+} transients recorded. All Ca^{2+} transients measured in boutons had at least seven times the size of the standard deviation, indicating a very good signal-to-noise ratio. In contrast, Ca^{2+} transients recorded in the shaft hardly ever crossed the threshold in an activity-correlated manner.

3.2.5 Statistics

Data are reported as means \pm SEM unless stated otherwise. Statistical significance of the effects of LTD was calculated using two-tailed, unpaired t-tests.

Statistical significance of the effect of changing boutons or spines on their synaptic partner was determined using two-tailed, paired t-tests. For the comparison of the amplitudes of Ca^{2+} transients depending on the number of APs, single-factor ANOVAs were calculated for preexisting and new boutons. In cases of multiple comparisons, p-values were post-hoc Bonferroni-corrected. The following levels of significance (p, error probabilities) were applied: * $p < 0.5$, ** $p < 0.01$, *** $p < 0.001$.

A MATLAB code was used to simulate the random insertion of boutons into and their deletion from the axonal segments that were analyzed. To this end, the distribution of boutons along each individual axon was determined. The random insertion of a single bouton was simulated 100 times for each axon; the removal of one randomly chosen bouton was simulated 10 times per axon.

3.2.6 Spatial resolution of optical system

To assess the spatial resolution of our optical system a realistic point spread function (PSF) was determined of the two-photon microscope by imaging sub-resolution beads *in situ* i.e. after depositing them in a hippocampal slice (0.17 μm diameter). The full width at half maximum (FWHM) values in the lateral and axial dimensions (Fig. 3.4 A, B) were computed based on Gaussian fits to the pixel intensities as a function of the respective spatial coordinate.

In addition, the ability of the optical system to discriminate beads with diameters near the nominal resolution limit was checked. Beads of varying diameters (0.2, 0.5, 1.0, 2.5 μm) were imaged, and the nominal diameters and volumes were compared with the measured ones (Fig. 3.5 A, Table 3.1). The pictures show that the beads can be reliably discriminated, also after the thresholding performed by the MATLAB program for volume calculation. The measured diameters closely approximate the nominal ones (Table 3.1). For the small beads (0.2 and 0.5 μm diameters) the measured volumes were markedly larger than the nominal volumes. This volume overestimation is easily explained by the relatively poor axial resolution of a two-photon microscope. However, importantly, the systematic error

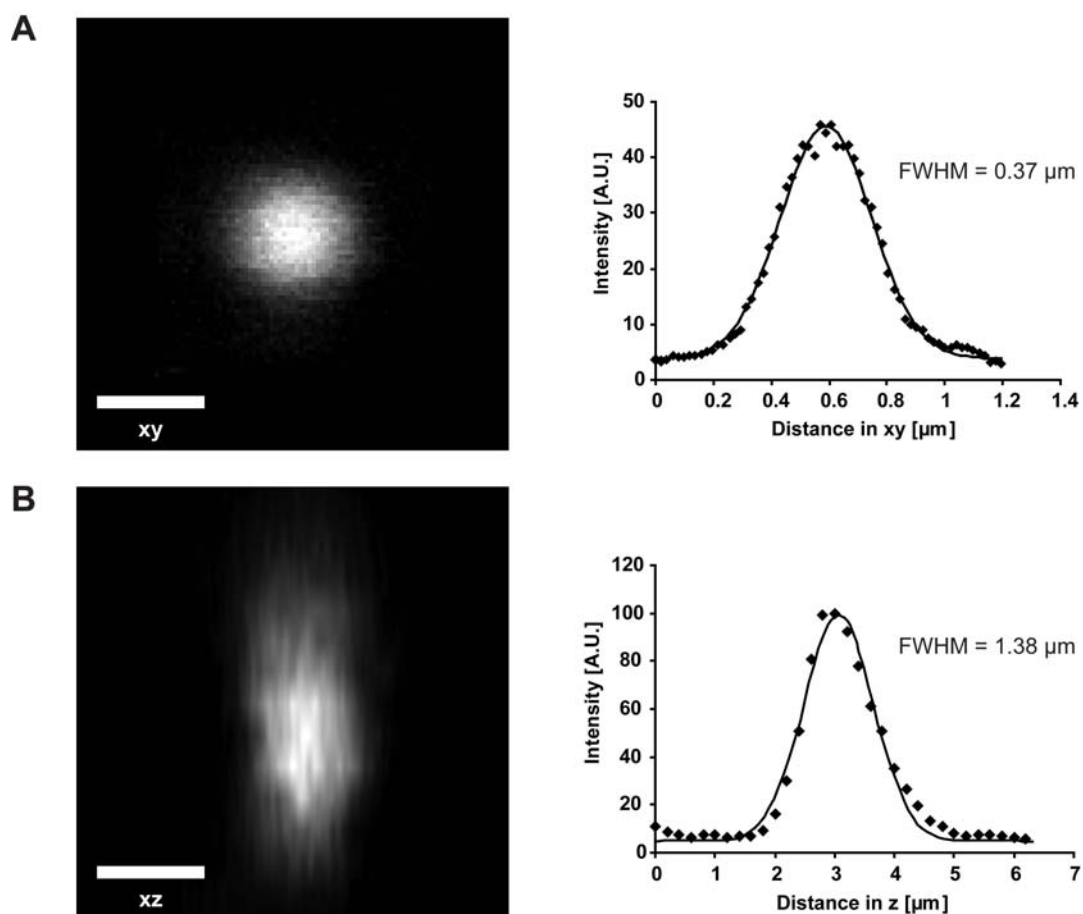


Figure 3.4 Point spread function of the two-photon microscope. **A** Left panel: Intensity plot of the averaged maximum intensity projections of ten measurements of single fluorescent sub-resolution ($0.17 \mu\text{m}$ diameter) beads. Right panel: Averaged point spread function in the xy-plane of ten measurements of single beads (black symbols), fitted by a Gaussian curve (black line). The full width at half maximum (FWHM) value was computed from the standard deviation of the Gaussian fit. **B** Left panel: Intensity plot of the averaged maximum intensity projection of three measurements of single beads in the xz-plane. Right panel: Averaged point spread function of the z-plane of three measurements of single beads (black symbols), fitted by a Gaussian curve (black line). Both scale bars are $0.5 \mu\text{m}$.

that was introduced in this way did not compromise our ability to detect differences in size reliably. If one compares the measured volumes for 0.2 and $0.5 \mu\text{m}$ beads, the standard deviations show (1) that the measurement is highly reproducible and (2) that differences between these beads are highly significant.

Since all bouton and spine volumes fall within the range of the bead volumes used here, one can be confident that the volume changes reported are genuine. The absolute numbers will be affected by the limited axial resolution of the two-photon microscope. Therefore, a rough correction of the absolute values based was performed on a power law fit of the relationship between the measured and nominal bead dimensions (Fig. 3.5 B). All values in the figures are percent changes of the measured values. The measured and corrected absolute values are shown in Table 3.1. Spine sizes measured by two-photon microscopy (without correction) were about six-fold larger in volume than spines measured by EM-based volumetry ($0.92 \pm 0.10 \mu\text{m}^3$, $n = 15$, vs. $0.14 \pm 0.02 \mu\text{m}^3$, $n = 14$). This is in line with the overestimation of the volume described above for TPLSM, and a presumed underestimation of the volume from EM data, resulting from shrinkage of the tissue during the fixation process.

The bead experiments also confirmed the usefulness of pixel overlap to assess physical contact of synaptic structures. As illustrated in Fig. 3.5 C, when structures such as beads are just abutting the pixel overlap comprises only one or very few pixels indicating that pixel overlap is indeed a stringent criterion for physical contact.

Table 3.1 Nominal diameters and volumes compared with the measured diameters and volumes.

Diameter [μm]			Volume [μm^3]		
Nominal	Measured \pm SD	Factor	Nominal	Measured \pm SD	Factor
0.2	0.30 ± 0.04	1.50	0.004	0.04 ± 0.01	10.00
0.5	0.57 ± 0.04	1.14	0.065	0.28 ± 0.04	4.31
1.0	1.09 ± 0.03	1.09	0.524	1.45 ± 0.14	2.77
2.5	2.44 ± 0.05	0.98	8.177	8.29 ± 0.85	1.01

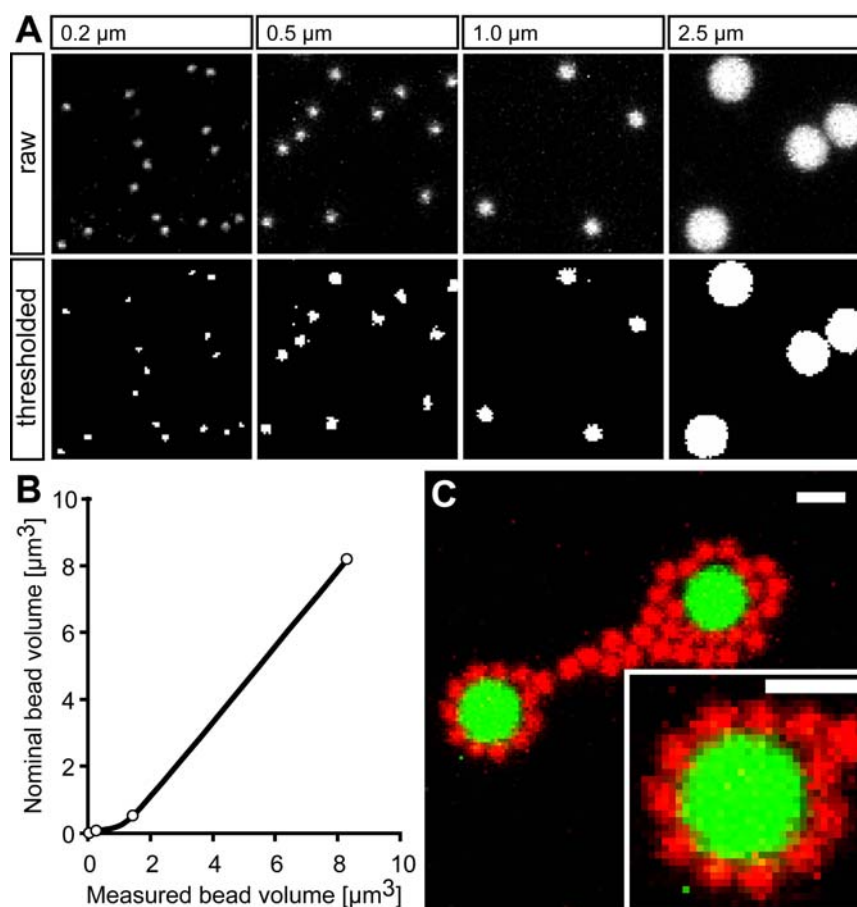


Figure 3.5 Fluorescent beads of various sizes are distinguishable in diameter and volume. A Upper row: Maximum intensity projections of raw images of fluorescent beads of nominal diameters of 0.2, 0.5, 1.0, and 2.5 μm . Lower row: Images of upper row processed with the same paradigm as used for the volume measurements of boutons and spines. **B** Plot of nominal *versus* measured bead volumes, the data points were fitted ($R^2 = 0.9985$) by a power law function ($f(x) = 0.3712x^{1.4144}$) **C** Maximum intensity projection of clustering red (1 μm diameter) and green (2.5 μm diameter) beads. Inset shows a magnification of the right green bead. Note that there is only a very small pixel overlap between the green and red channels, indicating that pixel overlap (yellow pixels) only occurs when structures are truly touching each other. Scale bars, 2 μm .

3.2.7 Immunohistochemistry

Hippocampal slice cultures from transgenic GFP-mice (Thy-1 promoter, GFP-M mouse line, courtesy of J. Sanes, Harvard University, Cambridge, MA) prepared as described above were used for immunostainings. Synapsin (rabbit α -synapsin, 1:500), a presynaptic marker for synaptic vesicles, the vesicular glutamate transporter VGlut1 (rabbit α -VGlut1, 1:400), and enhanced GFP (chicken α -GFP, 1:1000) to visualize the neuronal structure were immunohistochemically labeled. Cultures were fixed overnight in 4 % paraformaldehyde at 4°C, washed in 0.1 M phosphate buffer (PBS) and removed from their coverslips. Permeabilization and blocking was achieved by overnight incubation in 0.1 M PBS, 0.4 % Triton, 1.5 % horse serum and 0.1 % bovine serum albumin. Primary antibodies were applied overnight at 4°C; secondary antibodies (α -rabbit-alexa633, α -chicken-alexa488, α -rabbit-Cy3, each at 1:500) were applied overnight after extensive wash in PBS. Images were taken with a confocal microscope and analyzed on the basis of individual sections.

4 Results

In the first part of my thesis, I studied pre- and postsynaptic structural plasticity following the induction of long-term depression (LTD). The most interesting finding of this part was an enhanced bouton loss and growth after LTD induction, accompanied by a net loss of contacts between boutons and spines. In the second part, I examined whether newly grown boutons show voltage-gated Ca^{2+} entry. A transient rise in Ca^{2+} concentration inside the axonal terminal normally triggers vesicular release of neurotransmitters and thus, gives an indication of the functionality of the bouton.

4.1 Imaging activity-dependent structural plasticity of boutons and spines

Two-photon microscopy was combined with electrophysiological recordings to study the structural dynamics of axonal boutons of Schaffer collateral axons and dendritic spines of CA1 pyramidal neurons subjected to the classic plasticity paradigm of LTD. Axons and dendrites were labeled by dyes of two different colors (Fig. 3.2, Fig. 4.1 A), allowing to characterize and distinguish activity-dependent pre- and postsynaptic structural plasticity.

Axons and dendrites could be readily discerned and sites where the axonal varicosities came into close physical contact with dendritic spines were clearly identifiable (Fig. 4.1 A). About 50 pairs of boutons and spines were detected in each experiment. Contacts between boutons and spines mostly occurred on spine heads, as would be expected for synaptic connections (Harris and Stevens, 1989). Immunohistochemical labeling of axons showed that the vast majority of

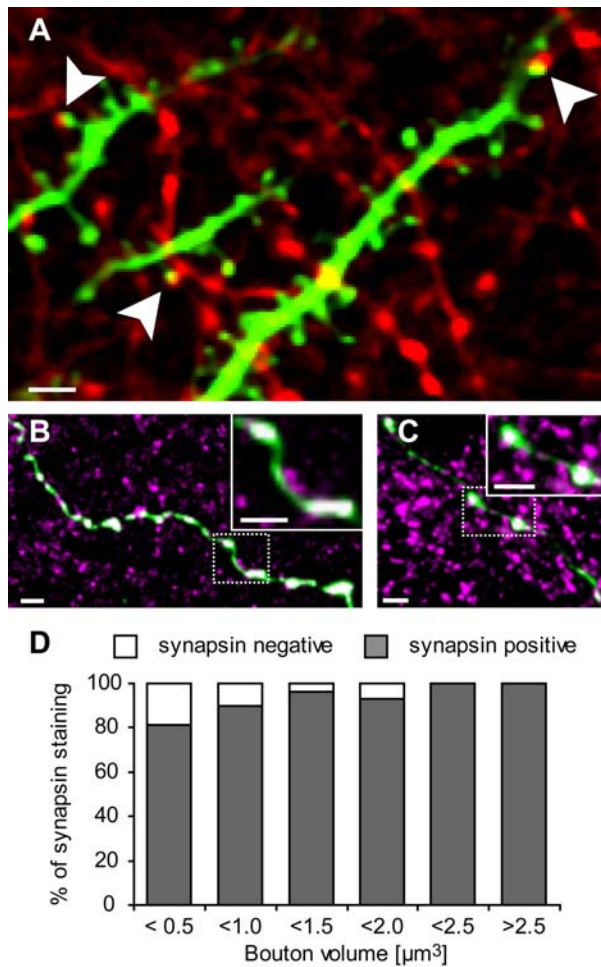


Figure 4.1 Putative synaptic contacts and presynaptic identity. **A** Single section displaying boutons on axons and spiny dendrites. White arrows indicate putative synaptic contacts. **B** MIP of three subsequent confocal sections ($\Delta z = 0.5 \mu\text{m}$) of a Gähwiler slice culture, immunostained for α -synapsin (magenta) and for eGFP (green; overlapping pixels are white). **C** MIP of six confocal sections ($\Delta z = 0.5 \mu\text{m}$) of a Gähwiler slice culture, immunostained for VGlut1 and eGFP. Insets shows zoom-in on axonal stretch. **D** Bar graph illustrating the fractions of boutons that are synapsin-positive dependent of their size. Note that even boutons smaller than $0.5 \mu\text{m}^3$ colocalize with synapsin in 81 % of the cases. All scalebars $2 \mu\text{m}$.

varicosities was positive for the presynaptic marker protein synapsin ($89 \pm 3 \%$, $n = 191$ varicosities in 6 slices), confirming that in our preparation most varicosities represent actual presynaptic boutons (Fig. 4.1 B). Immunohistochemical labeling of the vesicular glutamate transporter 1 (VGlut1) also revealed a high degree of colocalization with boutons ($80 \pm 3 \%$, $n = 248$ varicosities in 7 slices; Fig. 4.1 C), providing additional evidence for the synaptic nature of the varicosities. This conclusion also holds for small varicosities ($< 0.5 \mu\text{m}^3$), since most of them (81 %) were also synapsin-positive (Fig. 4.1 D).

Low-frequency stimulation (LFS) was used to induce LTD at Schaffer collateral-CA1 synapses (Fig. 3.1 A), which was monitored by field potential recordings in the CA1 area throughout all experiments. As expected, LFS resulted in robust LTD evidenced by a significant reduction of normalized fEPSP slopes

compared to baseline (LTD: $66 \pm 2\%$, $n = 11$; $p < 0.001$; Fig. 4.2). In an additional set of control experiments, overall activity was matched with the experiments experiencing LFS (for the exact protocol, see Methods section 3.2.3). As expected, this protocol did not result in any significant changes of the fEPSPs compared to control conditions with a test pulse frequency of once every 15 s (Fig. 4.2).

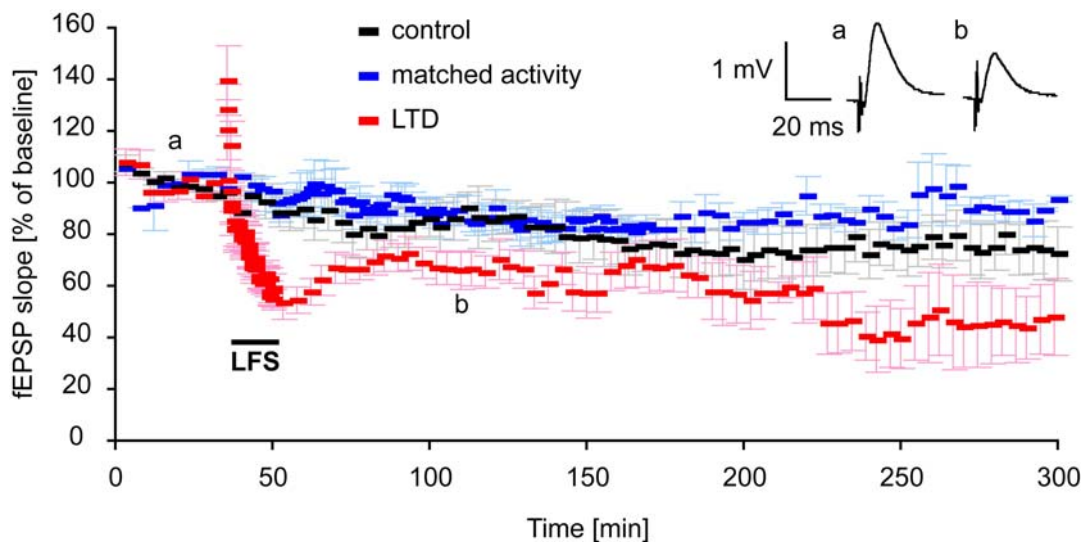


Figure 4.2 Electrophysiological recordings. Normalized and averaged fEPSP slopes for control (black symbols), matched-activity (blue symbols) and LTD experiments (red symbols). Inset shows raw data traces before (a) and after (b) induction of LTD.

4.1.1 LTD induction enhances bouton turnover

To study the effects of LTD on the structural dynamics of presynaptic boutons, bouton turnover was analyzed along defined stretches of the axons of CA3 pyramidal neurons counting fluorescence intensity peaks (Fig. 4.3 A-D, for details see Methods section 3.2.4). The number of appearing and disappearing boutons on was quantified under baseline and LTD conditions. LTD significantly increased the number of boutons that disappeared over 4 h of time-lapse imaging after the induction compared with control conditions (boutons lost per 100 μm ;

LTD: 0.9 ± 0.3 ; $n = 26$ axons; control: 0.2 ± 0.1 ; $n = 16$ axons; $p < 0.05$). At the same time the rate at which new boutons appeared after LTD was also increased almost two-fold over control conditions (boutons gained per $100 \mu\text{m}$; LTD: 2.2 ± 0.3 ; $n = 26$ axons; control: 1.1 ± 0.2 ; $n = 16$ axons; $p < 0.01$; Fig. 4.3 E). Therefore, under LTD as well as under control conditions there was a small net gain of boutons over the imaging period. The main result, however, was that LTD induction significantly increased the rate at which boutons appeared and disappeared.

To test whether this morphological plasticity is specific for the LTD-inducing stimulation (LFS) or is associated more generally with elevated levels of neuronal activity, slices with matched overall activity (see Methods) as well as unstimulated slices were also investigated. First, it was confirmed that the activity-matched stimulation did not induce LTD (Fig. 4.2). Then the turnover rates of boutons in activity-matched, control and no-stimulus conditions were determined and found to be statistically indistinguishable. Thus, of the stimulus paradigms tested only LFS reliably induces presynaptic morphological plasticity (boutons lost per $100 \mu\text{m}$; no-stimulus: 0.4 ± 0.1 ; $n = 14$ axons; $p = 0.15$ compared to control; matched-activity: 0.4 ± 0.2 ; $n = 21$ axons; $p = 0.36$ compared to control; control: 0.2 ± 0.1 ; $n = 16$ axons; boutons gained per $100 \mu\text{m}$; no-stimulus: 0.5 ± 0.2 ; $n = 14$ axons; $p = 0.19$ compared to control; matched-activity: 0.7 ± 0.2 ; $n = 21$ axons; $p = 0.21$ compared to control; control: 1.1 ± 0.2 ; $n = 16$ axons; Fig. 4.3 E).

To examine the temporal dynamics of bouton turnover the time course of the number of boutons gained or lost was plotted. The time course reveals that the onset of the increase in bouton turnover was delayed by about 2 h with respect to the start of the stimulation (Fig. 4.3. 2F). The positive (respectively, negative) slope in the control cases result from the fact that integrals of positive numbers (bouton gain) or negative numbers (bouton loss) are plotted, necessarily leading to a slope of greater (respectively, smaller) than zero.

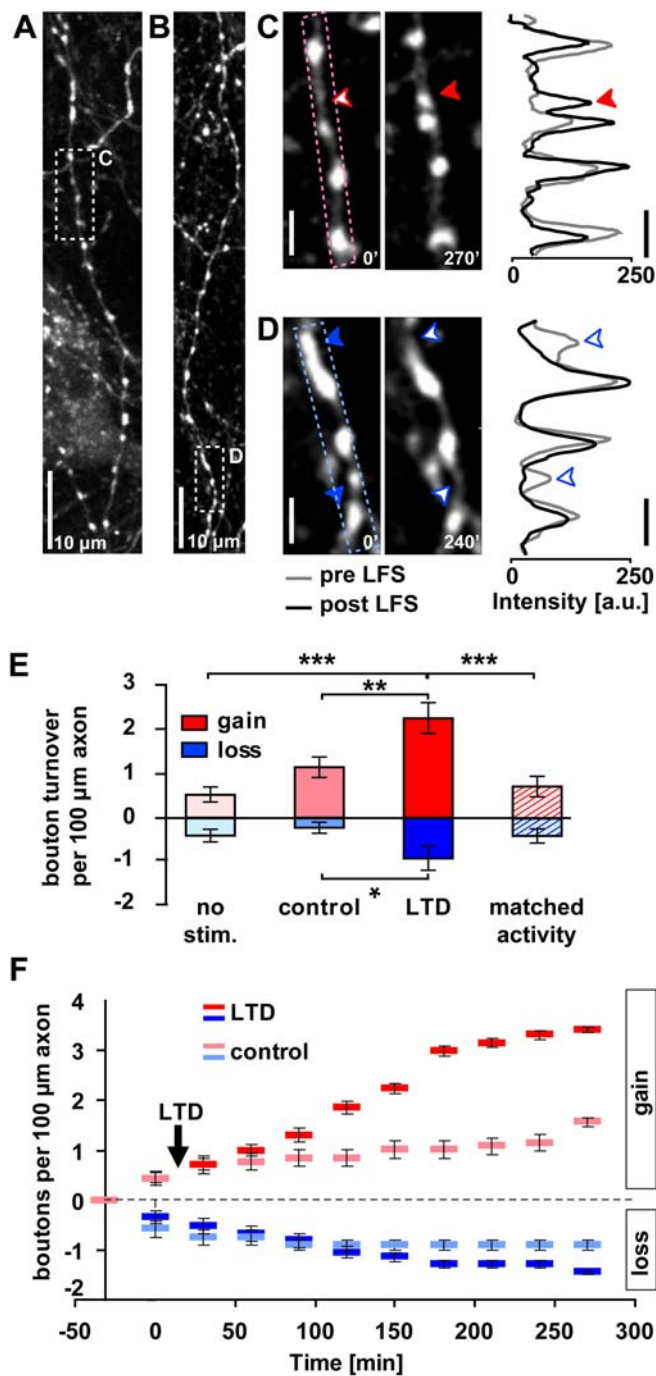


Figure 4.3 Presynaptic structural plasticity after LTD induction. **A, B** Maximum intensity projections of labeled Schaffer collateral axons. **C** Higher magnification of the box marked in panel **A** showing the emergence of a bouton, **D** Higher magnification of the box marked in panel **B** showing the loss of a bouton after LTD induction. Arrows indicate the boutons of interest. The graphs next to each example show the corresponding intensity plots along the parent axon before (gray) and after (black) LTD induction. Arrows point at the intensity peaks of the respective boutons. Eleven sections were used for the MIPs in panels **A** and **C**, and nine sections in panels **B** and **D**, the Δz spacing was 0.5 μm. **E** Summary of bouton turnover for the various experimental conditions (red bars, bouton gain; blue bars, bouton loss). **F** Time course of bouton turnover (red symbols, bouton gain; blue symbols, bouton loss). In all panels and following figures: asterisks indicate significant differences: * p<0.05; ** p<0.01; *** p<0.001.

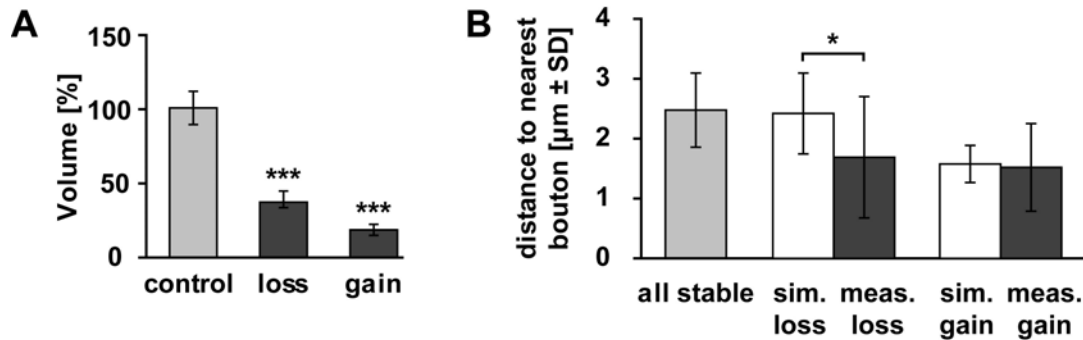


Figure 4.4 Size and localization of plastic boutons. **A** Volume of stable control boutons (gray bar), lost and gained boutons after LTD (black bars). **B** Distance to the nearest neighboring bouton (median \pm SD) for all (gray bar), simulated lost and gained (sim; white bars), and measured lost and gained (meas.; black bars) boutons after LTD.

Size and location of plastic boutons

In order to characterize this presynaptic structural plasticity in more detail, the volume of the newly gained or lost boutons was measured and their location along the axon examined. Boutons that appeared or disappeared after LTD (termed 'plastic' boutons) were significantly smaller than stable control boutons (Fig. 4.4 A and Table 4.1), suggesting a higher stability for larger boutons.

Additionally, for each bouton the distance to its nearest neighboring bouton (nearest-neighbor distance) was determined. When these values were compared for plastic boutons and stable boutons, nearest-neighbor distances were significantly shorter for plastic boutons (median \pm SD; gained: $1.5 \pm 0.8 \mu\text{m}$, $n = 24$ axons, $p < 0.001$; lost: $1.7 \pm 1.1 \mu\text{m}$, $n = 11$ axons, $p < 0.05$; all stable: $2.5 \pm 0.7 \mu\text{m}$, $n = 26$ axons; Mann-Whitney U test; Fig. 4.4 B). However, if new boutons are inserted randomly between existing boutons, they are expected to have shorter nearest-neighbor distances than the existing boutons on a given axon. Therefore, simulated random insertion and removal of boutons between the stable boutons was tested on each axon. Based on the nearest-neighbor distance, gained boutons could not be distinguished from randomly inserted boutons (median \pm SD; simulated gained: $1.6 \pm 0.3 \mu\text{m}$, $n = 2600$, $p = 0.84$). Lost boutons were closer to

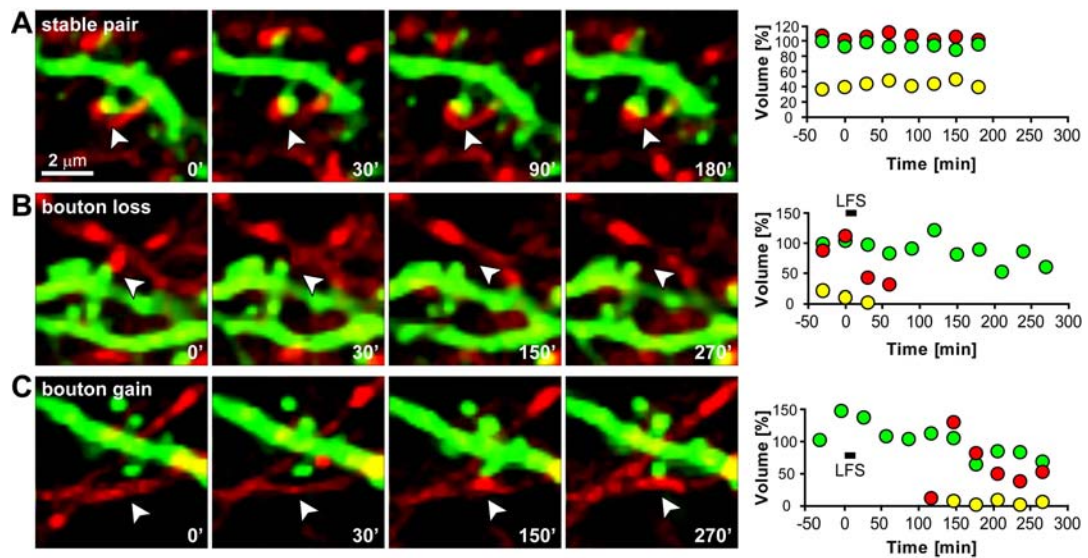


Figure 4.5 LTD-induced presynaptic structural plasticity in identified bouton-spine pairs. All images are single sections, chosen for best focal plane. White arrows indicate the bouton-spine pair of interest. **A** Stable bouton-spine pair under unstimulated control conditions. **B, C** Illustrative examples of bouton loss (**B**) and bouton gain (**C**) in bouton-spine pairs after LTD induction. The graphs on the right plot the time courses of the volume of the respective bouton (red dots), spine (green dots) and their overlap (yellow dots), normalized to initial spine volume. LTD induction starts at $t=0$ (indicated by black bars).

their neighbors than expected from simulated random removal (simulated lost: $2.4 \pm 0.7 \mu\text{m}$, $n = 260$, $p < 0.05$). This suggests that boutons disappeared preferentially if they were close to other boutons.

LTD increasing bouton turnover raised the question whether bouton loss and gain were restricted to separate axons or whether they occurred within the same axon. Therefore the numbers of gained and lost boutons were compared for a given stretch of axon (26 axons in total). While in 13 axons only bouton growth was detected (on average 2.2 ± 0.4 boutons), and in one axon only bouton loss (1 bouton), 12 axonal stretches showed both loss and gain of boutons, which was roughly balanced. These numbers show that growth and loss of boutons can occur in parallel within the same axon.

4.1.2 Enhanced bouton turnover affects the number of boutons in contact with spines

The simultaneous imaging of pre- and postsynaptic structures made it possible to monitor the structural dynamics of putative CA3-CA1 synapses at bouton-spine pairs after LTD induction. To assess the effect of newly formed or disappearing boutons on the network, boutons that were in close physical contact with spines were detected and these contacts were inspected for changes after LTD induction. Eighty-five percent of all bouton-spine contacts monitored (579 of 685 in total under LTD conditions) were stably associated throughout the duration of the experiment (Fig. 4.5 A). For the pairs showing plasticity, a significant fraction of plastic boutons caused the break-up or formation of contacts. Two kinds of bouton plasticity in contacting pairs of boutons and spines were observed: a bouton disappearing from a spine, with the spine persisting (Fig. 4.5 B) and a new bouton forming a contact with an existing spine after LTD induction (Fig. 4.5 C). These structural changes were quantified (Fig. 4.5, right panels) by measuring the volumes of the boutons and spines and their pixel overlap (see also Fig. 3.3). This analysis shows that boutons can undergo plasticity (i.e. appear or disappear) irrespective of the fate of the associated spine. It was never observed that a spine disappeared after the loss of the corresponding bouton.

4.1.3 LTD inductions leads to a net loss of spines and their contacts with boutons

The turnover of spines on the labeled CA1 pyramidal neurons within the field of view were analyzed in order to compare the rate of spine formation and spine loss under LTD and control conditions (Fig. 4.6 A, B). While LTD increased the rate of spine loss considerably, the rate of spine gain was modestly increased over control conditions (spines lost per 100 μm ; LTD: 0.84 ± 0.09 ; $n = 11$ experiments; control: 0.15 ± 0.04 ; $n = 5$ experiments; $p < 0.001$; spines gained per 100 μm ; LTD: 0.30 ± 0.04 ; $n = 11$ experiments; control: 0.11 ± 0.03 ; $n = 5$ experiments;

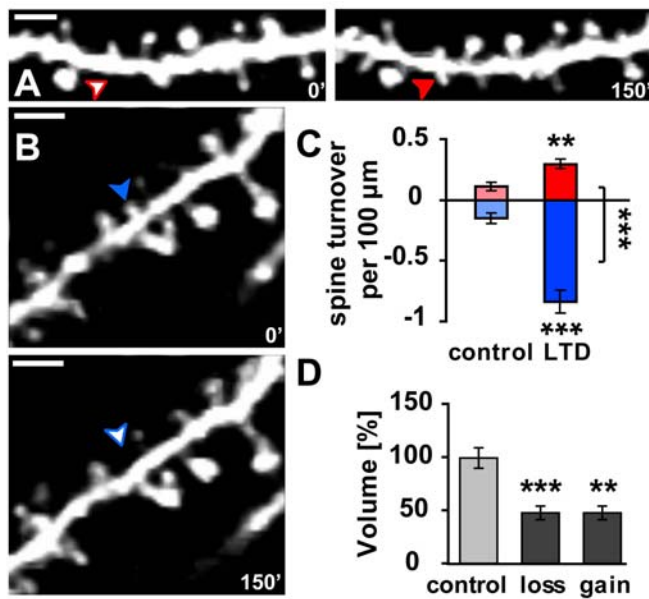


Figure 4.6 Postsynaptic structural plasticity after LTD induction. **A, B** Maximum intensity projections of dendrites showing the growth of a new spine (A) and the loss of a spine (B), indicated by the arrows. Eight sections were used in both panels and the Δz spacing was $0.5 \mu\text{m}$. **C** Summary of spine turnover (red bars, spine gain; blue bars, spine loss). **D** Volume of stable control spines (gray bar), lost gained spines after LTD (black bars). All scale bars, $2 \mu\text{m}$.

$p < 0.01$; Fig. 4.6 C). As a result there was a pronounced net loss of spines following LTD, in line with previous results (Nägerl *et al.*, 2004). Moreover, similar to the observations for boutons, highly plastic spines were smaller than stable control spines (Fig. 4.6 D and Table 4.1), suggesting an inverse correlation between the size of spines and boutons and their plasticity.

Plasticity of spines in contact with boutons

Since spine loss has never been proven to go along with the loss of the synapse, the fate of spines and their association with boutons after LTD induction was analyzed. Spines in contacts with boutons were observed to disappear after LTD induction, while the associated boutons appeared unaffected (Fig. 4.7 A). In a single case, however, the corresponding bouton disappeared after the disappearance of the spine. In five cases, spines forming newly after LTD induction contacted existing boutons (Fig. 4.7 B). In addition to the striking structural changes associated with the formation or retraction of boutons and/or spines, movements and changes in size of existing structures were observed. Such changes in volume and position of boutons and/or spines also led to the

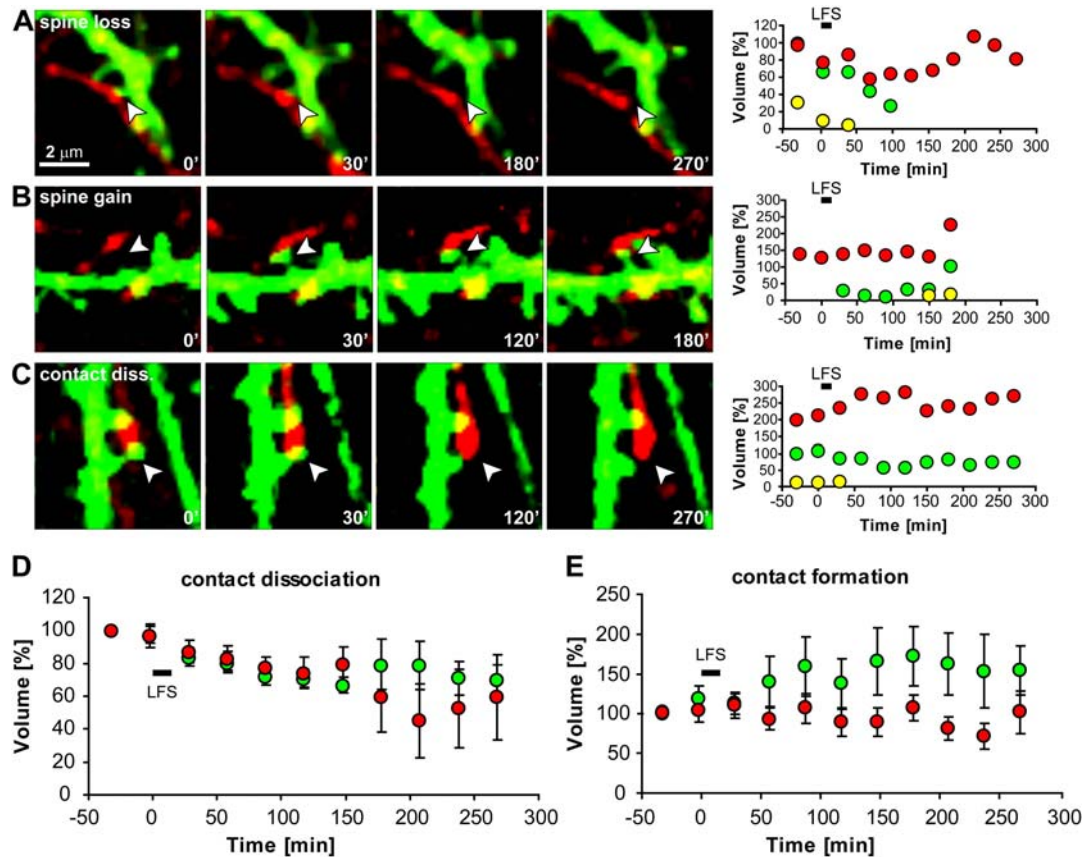


Figure 4.7 LTD-induced postsynaptic structural plasticity in identified bouton-spine pairs. A-D Illustrative examples of the types of structural plasticity in bouton-spine pairs after LTD induction. **A** Spine loss. **B** Spine gain. **C** Contact dissociation. Volume graphs as in Fig. 4.5, normalized to final spine volume in **B**. **D** Average time-course of all cases of contact dissociations. **E** Average time-course of all cases of contact formations. LTD induction is indicated by black bar.

dissociation (Fig. 4.7 C) or the association (data not shown) of bouton-spine pairs. Volume decreases of boutons and spines after LTD induction are on average equally responsible for the dissociation of contacts (Fig. 4.7 D). In contrast, only increases in spine volume seemed to be responsible for the association of contacts, while bouton volume remained stable (Fig. 4.7 E).

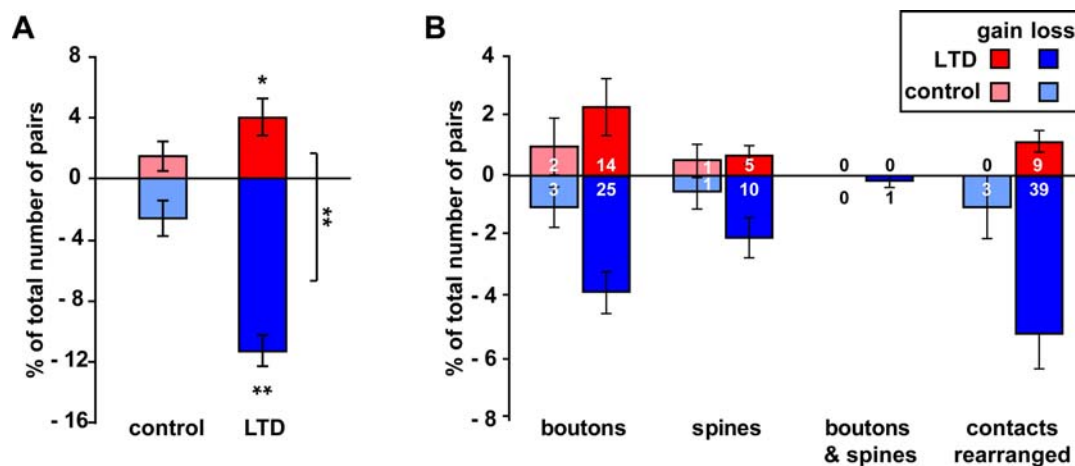


Figure 4.8 LTD induction leads to a net loss of bouton-spine pairs. **A** Percentage of the total number of contacts lost (blue bars) or gained (red bars) under LTD and control conditions. **B** Frequency histogram for the different types of structural changes contributing to contact formation or severing in all bouton-spine pairs in LTD and control experiments. The numbers indicate the numbers of observed pairs in each category.

4.1.4 Quantification of structural plasticity of bouton-spine pairs

In order to quantify the effects of LTD induction on contacting bouton-spine pairs, all structural changes causing the break-up or the formation of contacts were counted under LTD and control conditions. There was a highly significant increase in the number of bouton-spine pairs that disconnected under LTD compared to control conditions (LTD: $11 \pm 1\%$; $n = 11$ experiments; control: $3 \pm 1\%$; $n = 5$ experiments; $p < 0.01$; Fig. 4.8 A). In addition, there was a significant - but more modest - increase in the number of new pairs under LTD conditions (LTD: $4 \pm 1\%$; $n = 11$ experiments; control: $1 \pm 1\%$; $n = 5$ experiments; $p < 0.05$; Fig. 4.8 A). As a result, there was a significant net loss of contacting pairs of boutons and spines under LTD ($p < 0.01$), but not under control conditions ($p = 0.17$). It was quantified how often either bouton or spine plasticity was responsible for the break-up or the formation of contacts. The loss and gain of boutons seemed to be more frequently responsible for structural plasticity

compared to spine loss and gain (Fig. 4.8 B). In addition, changes in volume and position of boutons and/or spines contributed considerably to the break-up and formation of contacts (Fig. 4.8 B). Although the percentages for each particular type of plasticity are relatively low, taken together they reveal a significant level of structural plasticity caused by boutons as well as spines. This shows that contact severing and formation are attributable to structural changes on both sides of the synapse and that bouton plasticity actually appears to be more frequent than postsynaptic plasticity of dendritic spines.

Only once it was observed that both the bouton and the spine of a pair disappeared. This low incidence of simultaneous loss of boutons and spines during the imaging period is consistent with them disappearing independently. Similarly, the formation of a new contact between a new bouton and a new spine was never observed. Importantly, also the retraction of a spine while ‘pulling’ the partner bouton along to the dendritic shaft was never detected, suggesting that LTD does not lead to the conversion of spine synapses to shaft synapses.

4.1.5 The size of synaptic structures affects the plasticity of their partners

The fact that synaptic structures with a high degree of plasticity tended to be smaller than their stable neighbors raised the question whether the size of the associated partner also exerts an influence on plasticity. To this end, the initial volume of boutons and spines in pairs that showed structural plasticity and in pairs that remained stable was measured. This analysis revealed that boutons and spines whose associated partner was plastic tended to have smaller initial volumes compared to stable pairs (Fig. 4.9 A and Table 4.1). Due to the low number of observations, this effect only reached significance for spines that made contact with new boutons (Fig. 4.9 B and Table 4.1). This indicates that smaller spines were preferred partners of newly forming boutons.

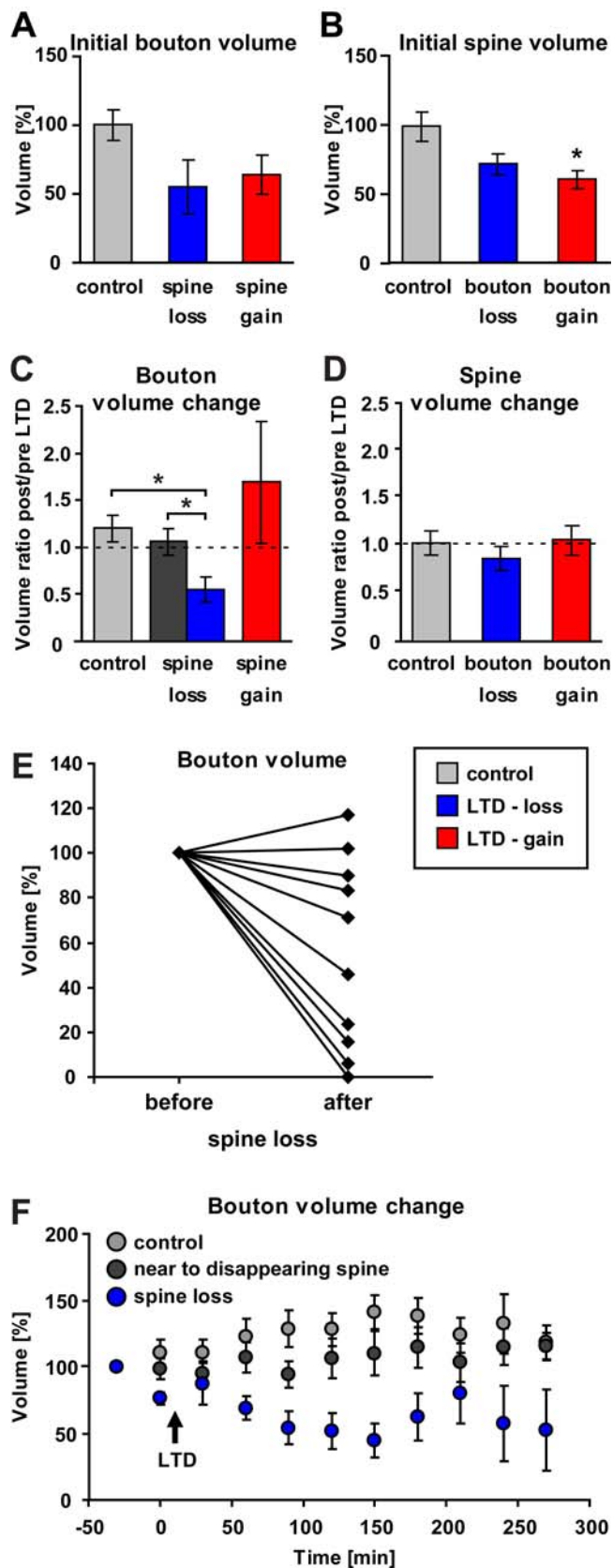


Figure 4.9 Characterization of the volume and volume changes of boutons and spines associated with plastic synaptic partners. **A, B** Initial normalized volumes of boutons and spines whose synaptic partner disappeared or was gained during the experiment. **C, D** Volume changes of the boutons and spines that lost or gained a synaptic partner compared to volume changes of synaptic structures engaged in stable pairs. Note that the volumes of boutons decreased significantly (blue bar) if their partner spine retracted after LTD. Neighboring boutons that were close to but not in physical contact with the retracting spines did not undergo any significant change in volume (black bar). **E** Bouton volume before and after spine loss for all boutons, normalized to initial bouton volume. **F** Time-course of the average bouton volume of boutons in stable pairs (grey symbols), boutons near disappearing spines (black symbols), and boutons contacting a disappearing spine (blue symbols).

Finally, it was examined whether pre- and postsynaptic structures are affected if their partner disappears or a new one is formed. The volumes of boutons and spines were measured whose associated partner was stable, lost or gained before and after LTD. Interestingly, the volume of almost all boutons decreased significantly after their associated spines were lost (Fig. 4.9 C, E, F and Table 4.1), while the volumes were unaffected in boutons contacting stable spines or boutons right next to (but not contacting) spines which disappeared after LTD. The converse effect, namely that the volume of a bouton increases after a new spine comes into contact with it, was only observed in three out of five cases and thus not significant. The volume of spines was not affected by the appearance or disappearance of an associated bouton (Fig. 4.9 D and Table 4.1). Spines in stable association with a bouton also did not reveal any significant volume changes.

The fact that the retraction of spines is clearly associated with a reduction in bouton volume is a further argument that those bouton-spine pairs where the spine disappeared had in fact been functionally connected. Moreover, these results indicate that boutons are more affected by plastic changes of their associated partners than spines.

Table 4.1 Statistics of bouton and spine volumes. Absolute values of the measured volumes and the percentage corresponding to the measured volume changes. Corrected values (see Methods, Fig. 3.5) are shown in parentheses. The statistical comparisons are either unpaired between groups of changing and control stable synaptic structures or paired within synaptic structures before and after LTD.

Boutons			Spines	
	volume (μm^3) measured \pm SEM (corrected)	n p	volume (μm^3) measured \pm SEM (corrected)	n p
Initial volume				
volume of stable control	1.37 \pm 0.15 (0.58)	n = 15	0.92 \pm 0.10 (0.33)	n = 15
volume of new structure	0.27 \pm 0.04 (0.06)	n = 48 p < 0.001	0.46 \pm 0.06 (0.12)	n = 14 p < 0.001
volume of disappearing structure	0.52 \pm 0.08 (0.15)	n = 18 p < 0.001	0.46 \pm 0.06 (0.12)	n = 20 p < 0.01
initial volume with retracting partner	0.76 \pm 0.37 (0.25)	n=10 p = 0.09	0.66 \pm 0.07 (0.21)	n = 25 p = 0.12
initial volume with new partner	0.88 \pm 0.37 (0.31)	n = 5 p = 0.32	0.56 \pm 0.06 (0.16)	n = 14 p < 0.05
Volume changes				
Δ with stable partner (% change)	+0.20 \pm 0.19 (+20 \pm 14 %)	n = 15	+0.03 \pm 0.12 (+3 \pm 13%)	n = 15
Δ with new partner	+0.14 \pm 0.26 (+69 \pm 65%)	n = 5 p = 0.78	+0.04 \pm 0.07 (+6 \pm 15%)	n = 14 p = 0.94
Δ with retracting partner (% change)	-0.27 \pm 0.09 (-45 \pm 13 %)	n = 10 p < 0.05	-0.12 \pm 0.06 (-13 \pm 12%)	n = 25 p = 0.27
Δ bouton with near retracting spine	+0.05 \pm 0.07	n = 15 p = 0.46	--	--

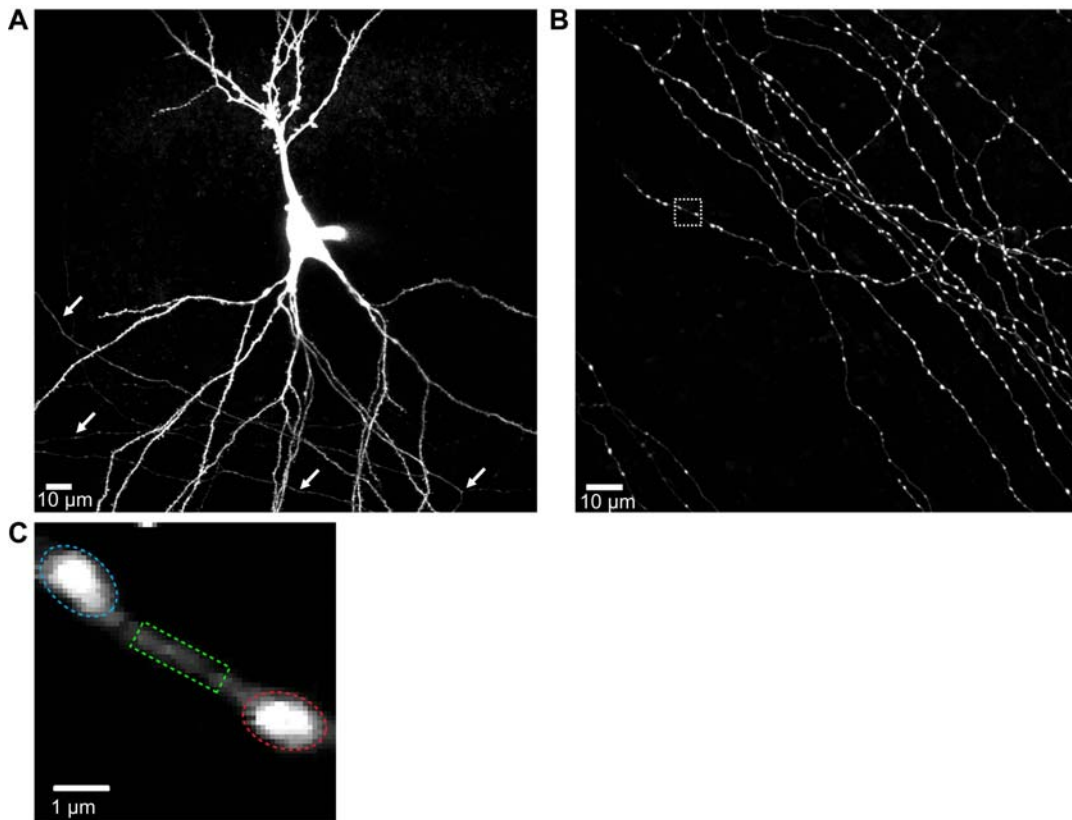


Figure 4.10 Ca^{2+} imaging in boutons of single CA3 pyramidal cell axons. **A** Overview of a single Alexa Fluor 568 labeled CA3 neuron displayed in a MIP over 35 μm . The white arrow indicates axon branches. Note the tip of the patch pipette at the right side of the soma. **B** MIP over 53 μm of a bundle of branches of a single CA3 axon. White rectangle indicates a typical field of view for Ca^{2+} imaging. **C** Magnification of the rectangle displayed in B. Dotted lines mark the regions of interest (ROIs) selected for the analysis of the Ca^{2+} -dependent Fluo-5F intensity.

4.2 Detection of evoked Ca^{2+} transients in preexisting and new boutons

In order to assess the functionality of newly formed boutons, imaging of Ca^{2+} transients in individual boutons was established in response to evoked firing of action potentials (APs). Single CA3 pyramidal cells were patched to label the morphology with Alexa Fluor 568, and to image changes in Ca^{2+} concentration

with the indicator Fluo-5F. Moreover, patching the cells allowed for monitoring the cells' membrane potential and evoking APs at purpose. Overview images were taken in the region of the soma to locate the axon and to identify the patched cell as a CA3 pyramidal neuron (Fig. 4.10 A). CA3 neurons are characterized by a large cell body of about 30 μm length and a characteristic type of large, arborescent spines at their proximal apical dendrites. After localization of the axon, it was followed for some hundreds of micrometers into an area where many branches appeared in the same field of view (Fig. 4.10 B). Data acquisition began at least 30 min after patching the cell to ensure that the concentration of the dye had equilibrated throughout the cell. Recording of evoked Ca^{2+} transients in single boutons was performed in parallel with or subsequent to time-lapse imaging of this region. For Ca^{2+} imaging, fields of view were usually chosen to include two neighboring boutons (Fig. 4.10 C). Ca^{2+} transients were analyzed separately for the two boutons and the stretch of axon shaft between them (Fig. 4.10 C).

4.2.1 Boutons reliably show activity-dependent local Ca^{2+} transients

In order to test Ca^{2+} responsiveness of individual boutons and response stability over time, labeled CA3 neurons were repeatedly stimulated extracellularly evoking 3 APs at 100 Hz at several time points over up to 7h. Boutons consistently showed Ca^{2+} transients in response to the stimulation (Fig. 4.11 A, B). Signals were reliably detected over several hours in all eight boutons tested in two cells patched for the entire duration of the imaging period. The example in Fig. 4.11 A shows two neighboring boutons that both showed Ca^{2+} transients without fail, with the response of the larger bouton 1 decreasing over time, while the response of the smaller bouton 2 remained stable. Thus, although both boutons experienced exactly the same stimulation, their Ca^{2+} transients could show variations. Moreover, in this example the two boutons are of very different size, yet show Ca^{2+} transients of comparable amplitudes, indicating that the amplitude of Ca^{2+} transients does not necessarily scale with the size of the bouton. On average, the

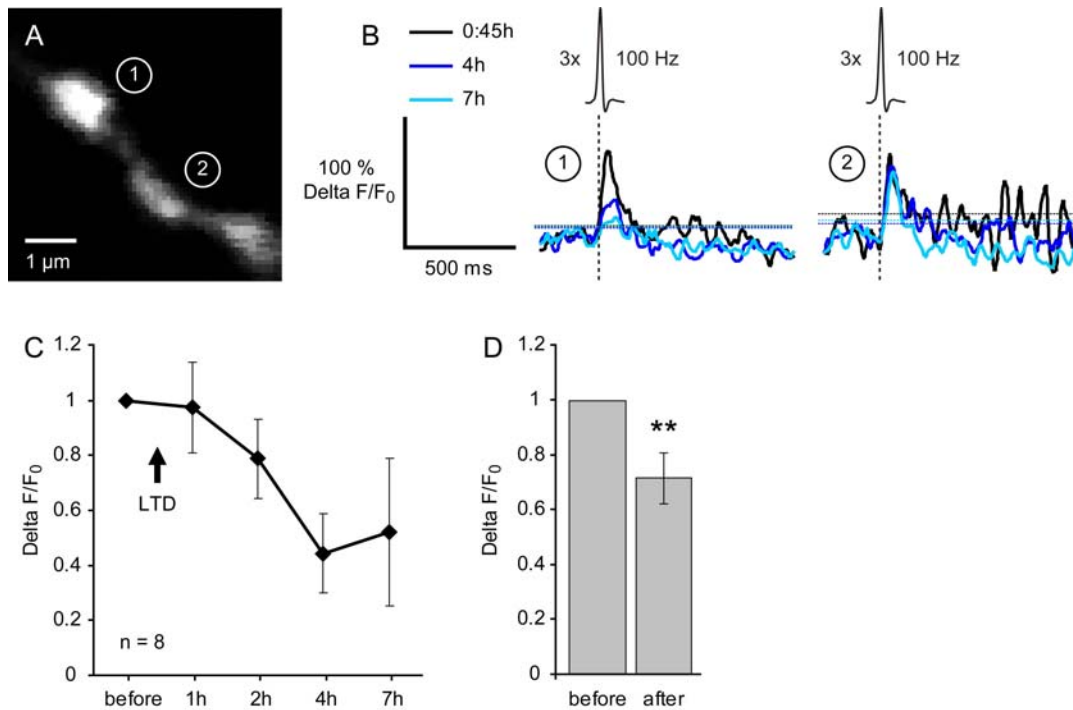


Figure 4.11 Stability of Ca²⁺ responses over several hours. **A** Field of view that was repeatedly imaged. **B** Ca²⁺ responses to 3 APs of the two neighboring boutons at three different imaging time points. Each trace is an average of two recordings. Note that Ca²⁺ responses decrease over time for bouton 1, but remain stable for the neighboring bouton 2. **C** Time course of average amplitudes of Ca²⁺ responses. **D** Bar graph showing a significant decrease of Ca²⁺ response amplitudes of all later recordings compared to the first.

Ca²⁺ transients significantly decreased over time (Fig. 4.11 C, D). Since the repeated imaging was only done in LTD experiments, it is unclear, whether this decrease in amplitude is due to an unspecific rundown or a specific effect of LTD induction. Control experiments to distinguish between these possibilities will need to be carried out. In three cells, in which the patch pipette containing the Ca²⁺ indicator was retracted after 45 min, no Ca²⁺ transients could be detected 2 h later (data not shown), although they were present before retraction of the pipette, suggesting that the intracellular functionality of the dye is not stable over time. Alternatively, the cells did not survive the retraction of the pipette. In summary, Ca²⁺ transients can be detected in boutons over extended periods of time, as long as constant supply of Fluo-5F is provided.

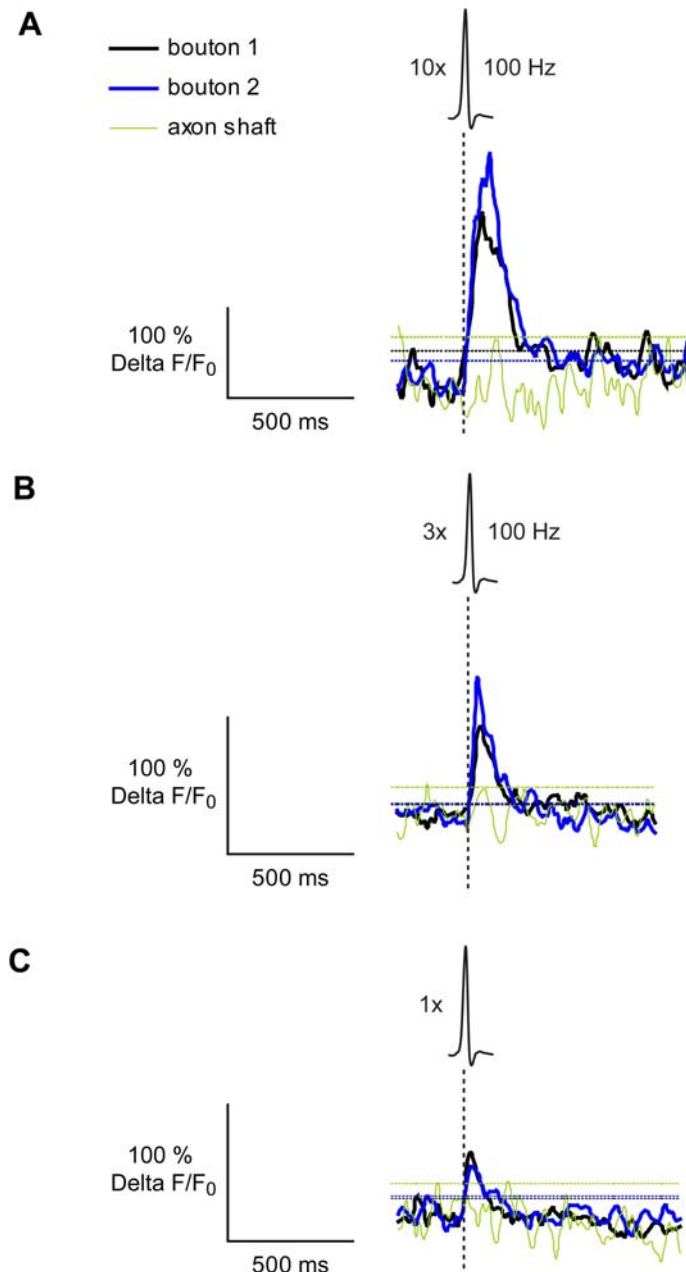


Figure 4.12 Example traces of Ca^{2+} responses of preexisting boutons. For each example, two boutons in the same field of view, and a stretch of axon shaft between them were tested for Ca^{2+} responses. Dashed lines indicate the threshold for signal detection at twice the standard deviation of the baseline fluorescence before triggering of APs. **A** Ca^{2+} signals in response to 10 APs (average of two recordings). **B** Ca^{2+} signals in response to 3 APs (average of seven recordings). **C** Ca^{2+} signals in response to 1 AP (average of two recordings).

To characterize the properties of AP-driven Ca^{2+} transients of boutons in more detail, Ca^{2+} transients were recorded in response to different numbers of APs (10, 3, or 1 APs). Ca^{2+} transients were consistently detected in boutons independent of the number of evoked APs (Fig. 4.12 A-C). Electrophysiological recordings with the patch pipette showed that the cells could follow the stimulation frequency of 100 Hz (data not shown). However, the imaging speed of 15 ms per

frame was not sufficient to resolve single peaks in the Ca^{2+} transients associated with single APs every 10 ms (Fig. 4.12 A, B). Yet, the imaging paradigm was sensitive enough to reliably resolve Ca^{2+} transients in response to single APs (Fig. 4.12 C). The amplitude of the Ca^{2+} transients, and thus, Ca^{2+} influx, increased with the number of APs (for quantification, see Fig. 4.15, section 4.2.3). Although in most cases Ca^{2+} transients were restricted to the bouton, occasionally a Ca^{2+} transient could be detected in the nearby axon shaft. Any signals detected in the axon shaft were significantly smaller than in the boutons and may be explained by diffusion of Ca^{2+} ions into the shaft after prolonged Ca^{2+} entry at the site of the boutons. Taken together, bouton-specific Ca^{2+} transients can be detected with sufficient sensitivity to resolve single APs.

To examine the propagation of the Ca^{2+} transient into the shaft, relatively long stretches of axon shafts devoid of boutons were imaged (Fig. 4.13 A-C). Fig. 4.13 A shows an example of a field of view that was imaged at a speed of 8 ms per frame while evoking a single AP. To analyze the spatial extent of the Ca^{2+} transient, several regions of interest (ROIs) were evenly distributed along the length of the axon shaft in the field of view (Fig. 4.13 A, left panel). The Ca^{2+} transients of each single ROI were plotted together with the signal of the bouton (Fig. 4.13 A, right four panels). The shaft signal of the ROI directly adjacent to the bouton reveals a Ca^{2+} transient, whose onset is delayed by about 100 ms compared to the AP and the Ca^{2+} transient of the bouton, which is inconsistent with it being a direct response to the AP. The two following ROIs do not reveal Ca^{2+} transients, indicating that the rise in Ca^{2+} is spatially restricted to the boutons. To investigate whether a single AP is possibly below the detection limit for Ca^{2+} transients of the axon shaft, a similar experiment was repeated with three APs (one image frame per 15 ms), (Fig. 4.13 B). Again, a Ca^{2+} transient could be detected in the two ROIs directly next to a bouton (red and grey traces in Fig. 4.13 B), but not in the two ROIs that were about 1 μm away from the next bouton (blue and green traces in Fig. 4.13 B). However, it is important to rule out the possibility that axonal shaft Ca^{2+} transients were obscured for reasons of higher noise levels inherent in

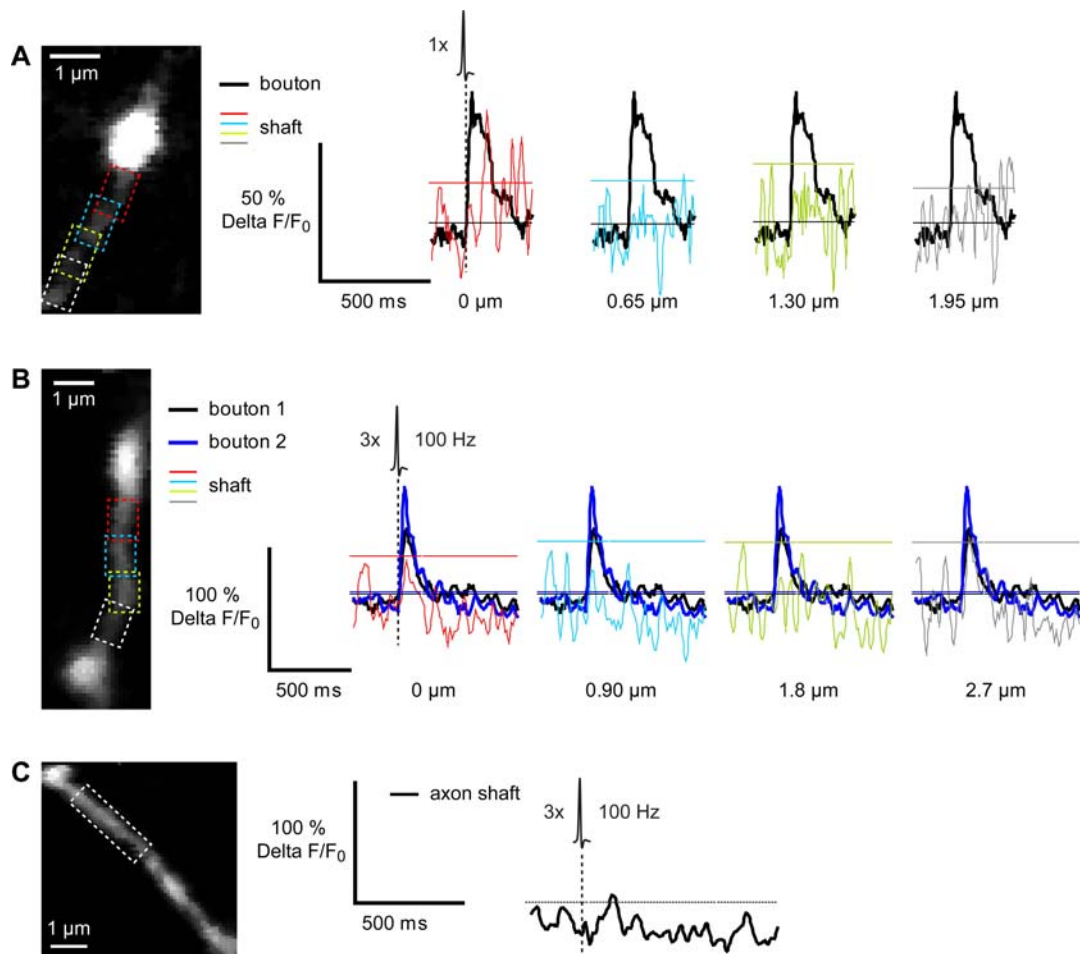


Figure 4.13 Spatial restriction of the Ca^{2+} signal. **A** Picture on the left showing the imaged stretch of axon with different ROIs of the axon shaft in four different distances to the bouton. Traces on the right display Ca^{2+} responses recorded at 8 ms/frame: Ca^{2+} signal in the bouton (black traces), Ca^{2+} signal in the axon shaft (colored traces) in the respective distance of the bouton specified below the trace (each trace represents an average of seven recordings). Distances are measured from the upper rim of the ROI to the edge of the bouton. Dashed lines indicate the threshold for signal detection at twice the standard deviation of the baseline fluorescence. **B** ROIs depicted as in A. Traces show bouton and axon shaft signals as in A, in response to 3 APs, recorded at 15 ms/frame (each trace is an average of seven recordings). **C** The picture on the left shows a stretch of axon with sparse distribution of boutons. The ROI was chosen in a region that was devoid of boutons. Ca^{2+} responses were recorded at 15 ms/frame (each trace represents an average of ten recordings). Note that the small signal crossing the threshold occurs with large delay to the evoked APs.

fluorescence signals generated from smaller volumes. To this end, the noise in

the fluorescence signals obtained from the axonal shafts was reduced by averaging over ten repeated trials to levels that were comparable to the noise levels associated with signals recorded from the boutons. Ten recordings were the maximal number of times a stretch of axon could be imaged before producing obvious photo damage within the field of view. It turned out that even then Ca^{2+} transients associated with AP firing failed to be detected from axonal shafts (Fig. 4.13.C). Only a very small signal was detected above threshold with about 100 ms delay compared to the last AP. Altogether, it can be concluded that the axon shaft shows little voltage-gated Ca^{2+} entry. Therefore, the Ca^{2+} transients that were recorded in individual boutons are most likely sourced by local Ca^{2+} entry, and cannot be accounted for by diffusion from neighboring sites.

4.2.2 Newly grown boutons rapidly show activity-dependent Ca^{2+} transients

In order to investigate whether and when newly grown boutons respond to evoked APs, CA3 neurons were stimulated with the same LTD-inducing paradigm as for the structural plasticity experiments that were shown in this study to enhance the turnover of presynaptic boutons. The CA3 axons were checked for newly growing boutons during the time-lapse experiment. As soon as a newly grown bouton was clearly identified (Fig. 4.14 A), it was tested for activity-dependent Ca^{2+} transients (Fig. 4.14 B, left panel) by evoking 10, 3 or 1 APs. At the same time, its nearest neighboring preexisting bouton and the stretch of axon shaft between them were also analyzed for Ca^{2+} transients (Fig. 4.14 B-D). Also in the newly grown boutons, Ca^{2+} transients could be clearly detected irrespective of the number of evoked APs. In most cases the Ca^{2+} transient was restricted to the new and the preexisting bouton, and no Ca^{2+} transients were detected in the axonal shafts between them (Fig. 4.14 B-D). Thus, the Ca^{2+} transients detected in the new boutons are unlikely to be sourced by diffusion of Ca^{2+} ions from neighboring boutons, but rather reflect the presence of functional voltage-gated Ca^{2+} channels in the membrane of new boutons.

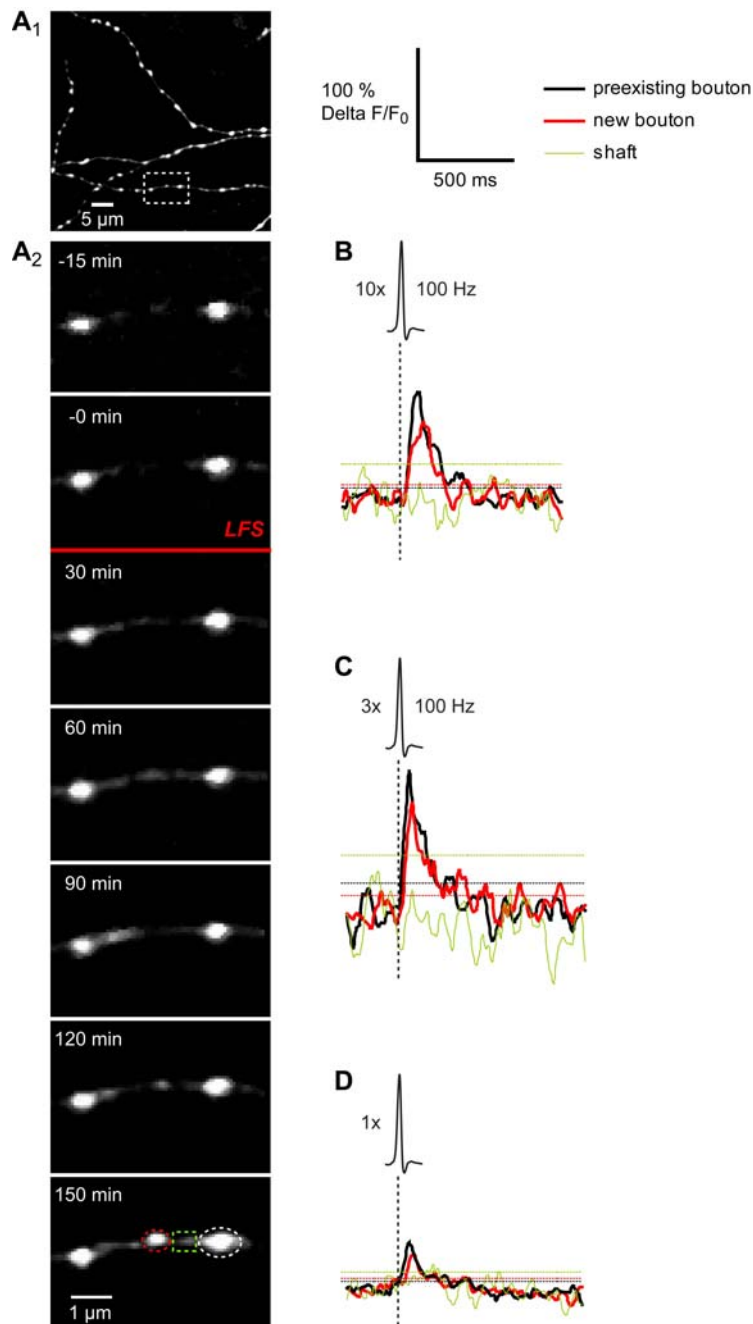


Figure 4.14 New boutons display Ca²⁺ responses. **A₁** Axon branches that experienced LFS. The white rectangle marks two preexisting boutons with the new bouton in the middle between them. **A₂** Time sequence of the region depicted in A₁ showing the appearance of a new bouton. ROIs chosen for analysis of Ca²⁺ responses are displayed in the last time point. **B** Traces show Ca²⁺ signals of the ROIs depicted in A in response to 10 APs (averages of three recordings). **C** Example of Ca²⁺ signals in preexisting and new boutons in response to 3 APs (averages of three recordings). **D** Example of Ca²⁺ signals in preexisting and new boutons in response to 1 AP (averages of seven recordings).

4.2.3 Reliability, spatial restriction and size of Ca²⁺ transients in newly grown boutons compared to preexisting boutons

In total, 75 boutons, 15 of them newly grown, were tested for Ca²⁺ transients, their spatial specificity and their sizes as a function of the number of evoked APs (Fig. 4.15). Out of 60 preexisting boutons, only five, i.e., less than 10 % did not show any Ca²⁺ transient in response to evoked APs (Fig. 4.15 A). Four of those were located on the same axon branch, indicating that the whole axon branch did not respond to activity. At the same time, six other boutons on three other axon branches of the same neuron did show Ca²⁺ transients in response to APs, showing that the neuron was active in general and sufficiently loaded with Ca²⁺ indicator. In all 15 newly grown boutons Ca²⁺ transients could be evoked independent of the number of APs (Fig. 4.15 A). On average, it took between 30 to 45 min from the first image of a new bouton until it was found and tested for Ca²⁺ transients. Out of 15 new boutons, 14 showed activity-triggered Ca²⁺ transients at the first time point tested. Only in a single case, a triggered Ca²⁺ transient could not be induced in the first trial, but was detectable when tested 20 min later. The fact that 100 % of the boutons were positive for AP-induced Ca²⁺ transients within 1 h of their first appearance suggests that the assembly of functional axon terminals may be a rapid process, and that VGCCs are inserted into the membrane of new boutons in less than 1 h. In an alternative scenario the new boutons are a result of having split off from previously existing boutons. These split products would be expected to have Ca²⁺ transients from the beginning. In any case, it is important to keep in mind that voltage-gated Ca²⁺ entry is just one of several steps necessary for activity-driven vesicular release of neurotransmitters.

Whether a Ca²⁺ transient was detectable in the shaft next to a bouton was dependent on the number of APs that were evoked. While a Ca²⁺ transient could be detected in the shaft after evoking 10 APs in about half of the preexisting boutons, it was only observed in about a fifth of the cases after 3 APs, and never after 1 AP (Fig. 4.15 A black and grey bars). This dependence on the number of APs is

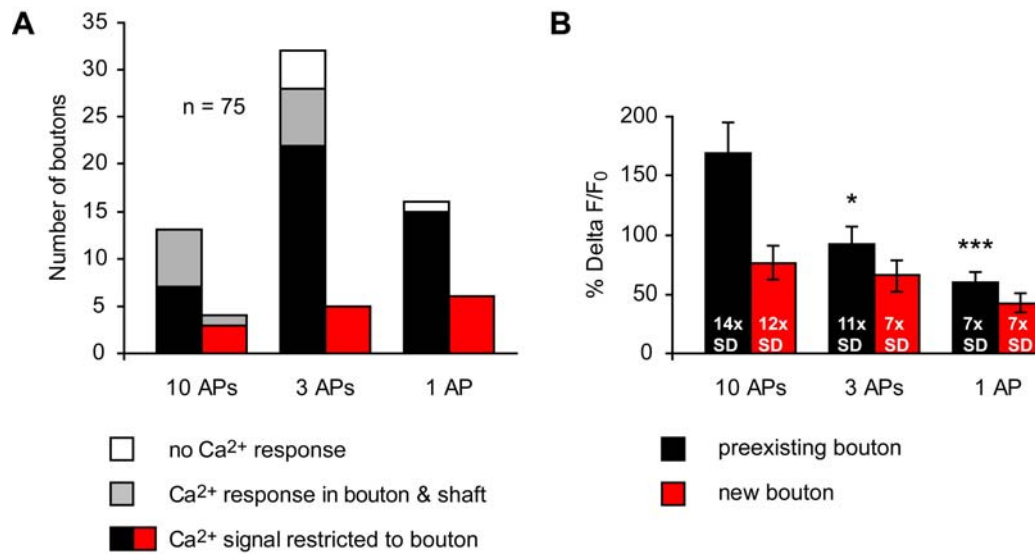


Figure 4.15 Reliability and amplitudes of Ca²⁺ responses. **A** Reliability of Ca²⁺ responses in boutons and occurrence in the axon shaft dependent on the number of APs for preexisting and new boutons. **B** Amplitude of Ca²⁺ responses depends on the number of APs for preexisting and new boutons. Numbers indicate the sizes of the amplitudes compared to the respective standard deviation (SD).

consistent with the idea that the more Ca²⁺ ions enter into boutons, the more will spread into neighboring shaft regions by passive diffusion. Conceivably, Ca²⁺ loads associated with a few APs can be absorbed by Ca²⁺ buffering mechanisms in and around the boutons, while larger loads may overcome the endogenous Ca²⁺ buffer and thus spill over into adjacent regions that otherwise would not experience a rise in Ca²⁺ concentration. For new boutons, a Ca²⁺ transient in the axon shaft was detected only once in response to 10 APs, never in any of the other cases (Fig. 4.15 A, red and grey bars). This is consistent with the observation that the Ca²⁺ transients in the new boutons were smaller in amplitude than in the preexisting boutons.

As expected, the amplitude of the Ca²⁺ transients was dependent on the number of action potentials for the preexisting boutons (Fig. 4.15 B). The signal amplitude significantly decreased with decreasing numbers of APs (10 APs: $170 \pm 25 \% \Delta F/F_0$, $n = 13$; 3 APs: $92 \pm 15 \% \Delta F/F_0$, $n = 27$; 1 AP: $60 \pm 9 \% \Delta F/F_0$,

$n = 20$; $p < 0.001$, single-factor ANOVA. The amplitude of the Ca^{2+} transients recorded from new boutons was not significantly different for the different numbers of evoked APs (10 APs: $76 \pm 15\% \Delta F/F_0$, $n = 4$; 3 APs: $65 \pm 13\% \Delta F/F_0$, $n = 5$; 1 AP: $43 \pm 8\% \Delta F/F_0$, $n = 6$; $p = 0.14$, single-factor ANOVA). However, there seems to be a trend for a positive correlation between the signal size and the number of APs. The preexisting and new boutons that received the same number of APs were also indistinguishable in the size of their Ca^{2+} transients. However, the Ca^{2+} transients in response to 10 APs were twice as large for preexisting boutons as compared to new boutons (preexisting boutons: $170 \pm 25\% \Delta F/F_0$, $n = 13$; new boutons: $76 \pm 15\% \Delta F/F_0$, $n = 4$), suggesting that the differences would become statistically significant if more experiments were included in the analysis. At this stage, no final conclusion can be drawn about whether low numbers of n or biological properties of new boutons prevent a clear correlation between signal size and number of APs.

4.2.4 Bouton turnover

The turnover in boutons caused by the induction of LTD in the Ca^{2+} imaging experiments was reassessed because the Ca^{2+} measurements brought about significant changes in the experimental conditions. First of all, Ca^{2+} indicators, which in effect buffer Ca^{2+} ions, are known to compromise the normal spatio-temporal intracellular Ca^{2+} dynamics, and thus may affect Ca^{2+} -dependent downstream signaling, including the structural plasticity, which was the focus of the study. Second, since the experiments were carried out in the whole-cell patch-clamp configuration for up to 7 h, proteins or ions critical for the expression of plasticity may have been diluted by the additional large volume of the patch pipette. Third, for practical reasons the axons in the Ca^{2+} imaging experiments did not receive the same periodic stimulation (apart from the APs to monitor Ca^{2+} transients and the LFS in the LTD experiments) as the axons in the previous experiments, which were stimulated every 15 sec. Thus, the bouton turnover of the

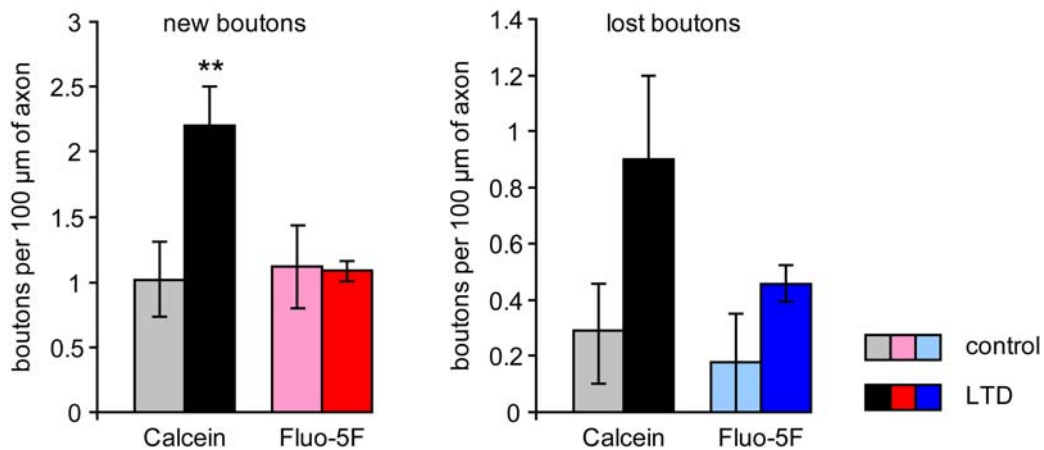


Figure 4.16 Comparison of bouton turnover between CA3 neurons patched and labeled with Fluo-5F and those bolus-loaded with Calcein red-orange AM. Left panel: Occurrence of new boutons under unstimulated control and LTD conditions for bolus-loaded (grey/black bars) and patched neurons (red bars). Right panel: Bouton loss under control and LTD conditions for bolus-loaded (grey/black bars) and patched neurons (blue bars).

Ca²⁺ imaging experiments was quantified under LTD and control conditions and compared to the no-stimulation condition of the structural plasticity experiments.

Unfortunately, but maybe not surprisingly, the effect of LTD induction on the turnover of presynaptic boutons was largely abolished under the conditions of the Ca²⁺ imaging experiments as compared with the clear LTD-induced structural effects observed under the original and more physiological experimental conditions. Specifically, the formation of new boutons was not enhanced in the Ca²⁺ imaging experiments, irrespective of whether LTD was induced or not (boutons gained per 100 μm; control (Calcein): 1.0 ± 0.3 ; $n = 14$ axons; control (Fluo-5F) 1.1 ± 0.3 ; $n = 3$ axons; LTD (Fluo-5F): 1.1 ± 0.1 ; $n = 19$ axons; $p = 0.89$ and $p = 0.83$, respectively; Fig. 4.16, left panel). Also the loss of boutons in the Fluo-5F labeled axons was not enhanced compared to the control condition of the Calcein-labeled axons, but tended to be enhanced compared to the control condition of the Fluo-5F-labeled axons (boutons lost per 100 μm; control (Calcein): 0.3 ± 0.2 ; $n = 14$ axons; control (Fluo-5F) 0.2 ± 0.2 ; $n = 3$ axons; LTD (Fluo-5F): 0.5 ± 0.1 ; $n = 19$ axons; $p = 0.20$ and $p = 0.06$, respectively; Fig. 4.16,

right panel). The fact that the enhanced bouton turnover effects could not be reproduced in neurons patched and labeled with a Ca^{2+} indicator suggests that either the patching itself or the Ca^{2+} buffering by the indicator impair structural plasticity. However, the difference between control and LTD conditions for the loss of boutons may come out clearer with increasing numbers of control experiments.

5 Discussion

Activity-driven plasticity of synaptic networks is thought to provide the basis for learning and memory. While the structural correlate of memory has remained elusive to date, many studies over the last decade have indicated that morphological changes at the level of single synapses play a key role in activity-dependent synaptic plasticity.

In my thesis, I examined in detail the structural changes associated with a classic model of cellular plasticity, namely LTD. I chose to explore the effects of synaptic depression on synaptic morphology, because previous reports from our laboratory and others had shown that LTD leads to prominent changes in dendritic spines on CA1 pyramidal neurons. In this study, I focused on possible effects of LTD on the presynaptic input fibers, which had not been studied in great detail so far. Moreover, because the Schaffer collaterals provide the presynaptic input onto the spines of the CA1 pyramidal neurons, presumably inducing their plasticity, I wanted to specifically study the interactions between connected pairs of boutons and spines that undergo morphological plasticity. To this end, I used dual-label two-photon time-lapse microscopy to monitor the effect of LTD induction on presynaptic boutons of Schaffer collaterals with or without contact to labeled dendritic spines of CA1 pyramidal neurons in hippocampal slice cultures.

A second line of work aimed at assessing the functional aspects of plastic presynaptic boutons, namely whether and when plastic boutons show voltage-gated entry of Ca^{2+} ions. The idea was to elucidate the functional consequences of the structural plasticity observed here. For this, I employed two-photon Ca^{2+} imaging in single presynaptic boutons, including preexisting and newly formed ones.

First, I demonstrated that LTD induction led to a significant remodeling of presynaptic boutons, which had remained unexamined in earlier studies that focused on postsynaptic structural dynamics. Moreover, it was shown that LTD induction reduced the number of boutons that are associated with dendritic spines, suggesting that some CA3-CA1 contacts are lost while overall synaptic strength decreased. This result might have been assumed from earlier studies in which LTD results in a loss of spines, but it is important to demonstrate that spine loss indeed results in contact break-up. Those data clearly show that the alternative scenario, a spine contact (or synapse, see below) turning into a shaft contact or synapse, does not occur or is at least very rare. Additionally, the data revealed that structural plasticity occurs mainly in smaller spines and boutons and their respective partners.

Second, it was established that Ca^{2+} transients can be reliably measured in single presynaptic boutons and that newly formed boutons show voltage-dependent Ca^{2+} transients right after their first morphological appearance. From those data it can be concluded that at least the initial condition for presynaptic functioning, AP-induced Ca^{2+} influx, is fulfilled. Furthermore, this rapid occurrence of voltage-dependent Ca^{2+} transients in new boutons suggests that the generation of functional new synaptic structures occurs fast and in a well-orchestrated manner.

5.1 LTD induces structural plasticity of presynaptic boutons

The present experiments show that the induction of LTD led to a pronounced increase (2-3 fold) in the turnover of presynaptic boutons. Functional LTD at the CA3-CA1 synapse has been shown to be expressed at the postsynaptic, but also at the presynaptic site of the synapse (Anwyl, 2006). Evidence for a presynaptic expression of LTD has been provided in studies showing persistent reduction in vesicular release (Zhang *et al.*, 2006), a change in paired-pulse ratio (Fitzjohn *et al.*, 2001; Faas *et al.*, 2002), a change in the coefficient of variation (Bolshakov

and Siegelbaum, 1994; Fitzjohn *et al.*, 2001), a decrease in frequency, but not amplitude of quantal excitatory postsynaptic currents (Oliet *et al.*, 1997), a decrease in the frequency, but not in the amplitude of miniature EPSCs (Bolshakov and Siegelbaum, 1994; Fitzjohn *et al.*, 2001), and a decreased rate of release (Zakharenko *et al.*, 2001). Those findings all point to a reduction in transmitter release. However, the underlying mechanisms are still unclear. Although suggested as one possible mechanism (Desmond and Levy, 1983), structural changes of presynaptic release sites following LTD induction have not yet been studied in great detail. The loss or shrinkage of a presynaptic release site would be expected to decrease synaptic transmission, because the pool of readily releasable vesicles (Dobrunz, 2002), as well as the amount of VGCCs to trigger release (Reid *et al.*, 1997) would decrease accordingly. Thus, structural changes of boutons could underlie the postulated decrease in synaptic transmission. Interestingly, the loss of presynaptic terminals observed in the present study built up over the course of several hours. This delay relative to the time point of LTD induction may reflect a more protracted morphological implementation of the rapidly expressed functional weakening of synapses; e.g. if the transmitter release of a synapse is down-regulated during LTD, the presynaptic site finally may be degraded completely if its release competence falls below a critical value.

About 11 % of boutons imaged during the experiment were affected, being either gained or lost. This fraction is substantially higher than the number of presynaptic remodeling events reported for theta-burst stimulation (TBS) (Nikonenko *et al.*, 2003). The discrepancy may reflect different expression mechanisms for LTD and (TBS-induced) LTP at Schaffer collateral/CA1 pyramidal neuron synapses. Alternatively, since great care was taken to optimize the present experiments such that the labeled axons were likely to have been activated during LTD induction, the chances to detect anatomical changes might have been better. The fraction reported here is comparable with the fraction reported for dynamic *en passant* boutons of mossy fibers in hippocampal slice cultures stimulated with a cAMP analog (De Paola *et al.*, 2003).

Under control conditions, a small net increase in the number of boutons was observed, which may reflect the developmental stage of the tissue with new boutons being continuously added. Surprisingly, the turnover was significantly more pronounced after LTD induction, contrasting with the net loss in connectivity of CA3 and CA1 pyramidal neurons. If the new boutons form synapses, it will be important to determine the identity of their postsynaptic partner. For instance, the new boutons could form synapses with inhibitory interneurons, which would contribute to an overall decrease in synaptic transmission from CA3 to CA1. Alternatively, the new boutons could have split off from existing boutons, as it has been observed previously by Krueger *et al.* (2003) (Fig. 5.1 A). On the one hand, splitting existing boutons in of itself may serve as a mechanism to reduce synaptic strength; on the other hand, the split products may become part of a dynamic pool of orphan presynaptic constituents that can be mobilized as a rapid expression mechanism of synaptic plasticity. This scenario is supported by the finding that high-frequency stimulation increases the fraction of dynamic boutons (De Paola *et al.*, 2003). In the present study, the temporal resolution of one image stack every 30 min is too slow to determine whether boutons form from existing boutons or are assembled *de novo*, although some suggestive examples of bouton trafficking have been observed (Fig.5.1 B). However, several studies have shown that boutons can form rapidly in different ways (Friedman *et al.*, 2000; Krueger *et al.*, 2003; Kim *et al.*, 2003). Those new boutons are immediately release-competent if they originate from existing boutons, independent of having a postsynaptic partner or not, and can be recruited to previously existing release sites (Krueger *et al.*, 2003). Friedman *et al.* (2000) have shown that newly formed boutons become release-competent within 30 min after the initial contact with a postsynaptic target, while clusters of the postsynaptic molecule SAP/PSD-95 and glutamate receptors were found on average only about 45 min after such boutons were first detected. Nikonenko *et al.* (2003) have found that an even shorter period, 30 min, was sufficient for triggering the formation of a postsynaptic density on a target cell. Moreover, depolarization-induced, Ca^{2+} -dependent vesicle release has been

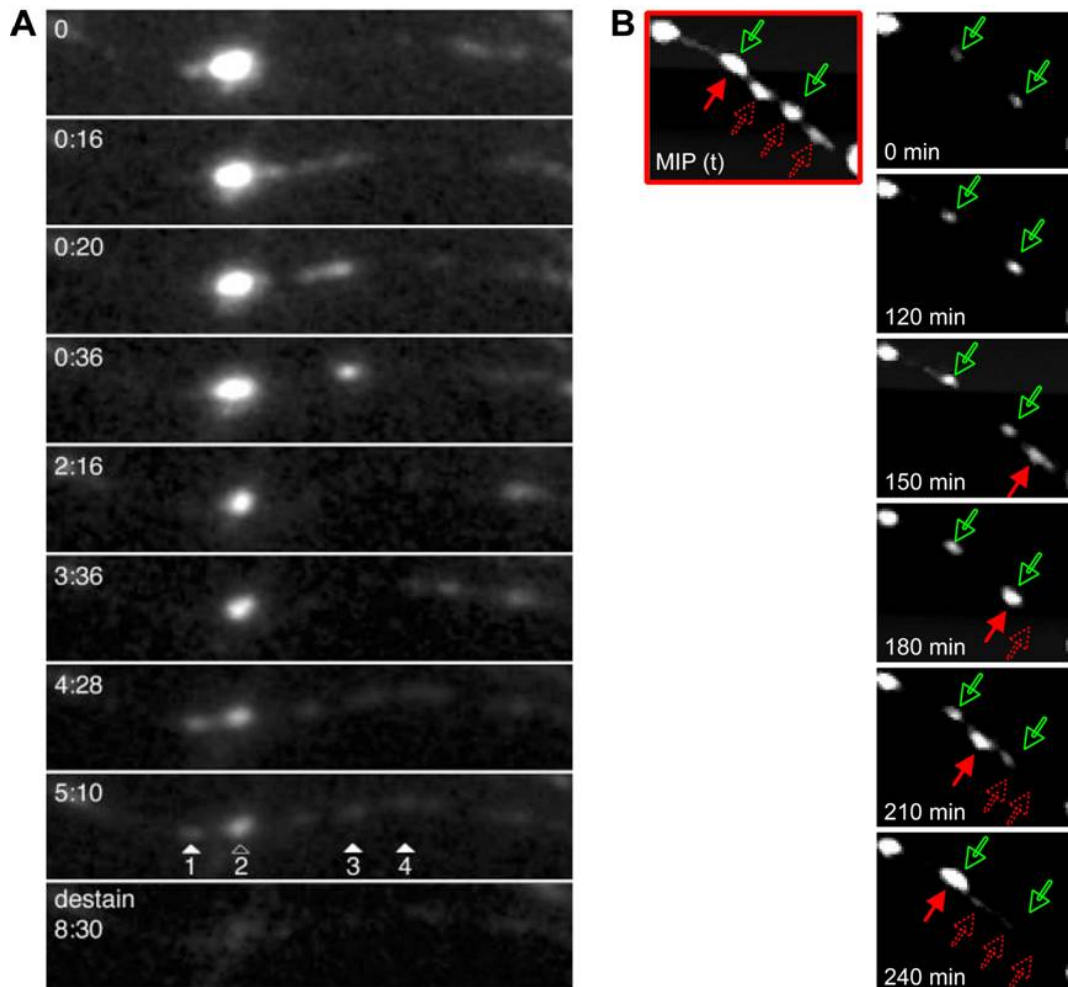


Figure 5.1 Trafficking of vesicle clusters respectively boutons along the axon. **A** Time-lapse images of FM1-43-labeled synaptic vesicle clusters splitting from an existing release site (open arrowheads) and moving to several locations adjacent to the established release site (filled arrowheads) in a dissociated neuronal culture. Modified from Krueger *et al.* (2003). **B** Left panel: Maximum intensity projection over time displaying the positions of stable boutons (green arrows), and the transient (open red arrows) and final (filled red arrow) positions of mobile boutons. Right panel: Time-lapse image series illustrating motile boutons (open red arrows), finally fusing with formerly stable boutons (open green arrows).

observed independent of cell-cell contact in axons of adult and developing neurons (Matteoli *et al.*, 1992; Kraszewski *et al.*, 1995), and functional release sites occurred within 1 h upon cell-cell contact (Ahmari *et al.*, 2000). Taken together, a functional new synapse can be formed within 1 to 2 h, with the bouton

preceding (Friedman *et al.*, 2000; Ahmari *et al.*, 2000). Thus, the new boutons observed here are very likely to form new synapses, even if boutons as split products served to reduce synaptic strength in the first place. However, two studies examining spine plasticity report that newly formed spines need many hours to become part of a functional synapse in a more mature preparation and *in vivo* (Knott *et al.*, 2006; Nägerl *et al.*, 2007). In any case, LTD induction appears to lead to a reorganization of the presynaptic machinery and most likely to a functional rewiring of the hippocampal network. The fact that bouton loss takes place in close proximity to existing boutons is particularly interesting in the light of several recent reports that neighboring presynaptic terminals can share proteins or even larger structural complexes (Krueger *et al.*, 2003; Darcy *et al.*, 2006; Tsurriel *et al.*, 2006) and that this can be done in an activity-dependent fashion (Waters and Smith, 2002; Vanden Berghe and Klingauf, 2006). Together with the finding that bouton addition and removal can both occur on the same axons, this is consistent with a model in which structural elements liberated at one site during bouton removal can be used at other sites where new boutons are built.

I observed that plastic boutons and spines, irrespective of whether they were gained or lost, were significantly smaller than stable structures. Although it is possible that the small sizes simply reflect the start of a long process of assembly (or the end of the disassembly process), it could also indicate that size is a key determinant for the ability of synaptic structures to undergo structural plasticity (Kopec and Malinow, 2006). This is in line with the work by Matsuzaki *et al.* (2004), which demonstrated that LTP-induced volume increases preferentially affect small spines. Given that bouton (Yeow and Peterson, 1991; Pierce and Mendell, 1993; Murthy *et al.*, 2001) and spine (Matsuzaki *et al.*, 2001; Noguchi *et al.*, 2005; Holtmaat *et al.*, 2006) sizes correlate with synaptic strength, the presented data suggest that structural plasticity preferentially affects weak synapses. Furthermore, a significant role of synapse size for plasticity is supported by the finding that the size of the structures also tended to be smaller if their associated partner underwent plasticity. In the context of LTD, this may suggest

that some of the depressed synapses became so weak, that synaptic transmission was entirely abolished. It seems a plausible scenario that these synapses were subsequently structurally degraded, either by disconnecting them from their synaptic partner, or by their complete removal.

5.2 LTD-induced reduction of contacts between Schaffer collaterals and CA1 pyramidal neurons

My experiments show that LTD induction led to a considerable loss of contacts between CA3 boutons and CA1 spines. Although LTD induction also increased the number of newly formed contacts between boutons and spines by 4 %, many more contacts were eliminated (11 %). If these contacts had been functional before they were lost, their removal may represent an important structural implementation for the weakening of CA3-CA1 synaptic transmission. The percent decrease in the field responses was about twice as large as the decrease in the number of contacts, suggesting that other non-structural LTD mechanisms, such as weakening of existing synapses without removing them, are also operational. For instance, the removal of AMPA receptors from the postsynaptic membrane has been shown to be one of the expression mechanisms underlying LTD at the CA3-CA1 synapse (Snyder *et al.*, 2001; Xiao *et al.*, 2001; Huang *et al.*, 2004; Nosyreva and Huber, 2005). However, since AMPA receptors are integrated into a tight protein network including matrix molecules across the synaptic cleft (Choquet and Triller, 2003), their removal may in some cases trigger a signaling cascade eventually leading to contact loss. Moreover, a discrepancy in the extent of structural and functional plasticity would be expected to the extent that not all labeled fibers were actually stimulated, diluting the structural effect. In any case, the relationship between the number of synapses and their combined strength is likely to be highly complex and therefore one would not expect to find a linear relationship between structural plasticity and changes in synaptic

transmission. Therefore, the presented findings are likely to have physiological relevance, especially if the structural changes occurred within defined synaptic pathways, considering that co-activation of just a few synapses can lead to action potential firing.

The fact that a spine contact being converted into a shaft contact was never observed corroborates the idea that spine retraction indeed abolishes synapses. Previous work, in which only the postsynaptic neurons were labeled, could not make such distinctions (Zhou *et al.*, 2004; Nägerl *et al.*, 2004). This interpretation is further supported by the observation that the loss of a spine was frequently associated with a volume decrease of the associated bouton.

5.2.1 Identity of contacts between boutons and spines

Although a physical contact between a bouton and a spine is necessary for a synaptic connection it is by no means sufficient. Nevertheless, several lines of evidence suggest that at least a significant fraction of contacts imaged over time represented actual synapses. First, the observation that spine loss caused a decrease in size of the corresponding bouton is indicative of a functional contact. Second, the observation that virtually all bouton-spine pairs made contact at the spine head is consistent with EM studies that show that synapses are typically formed at the head of the spine (Harris and Stevens, 1989) in a one-to-one relationship between CA1 spines and boutons of Schaffer collaterals (Harris and Stevens, 1989; Schikorski and Stevens, 1997). Third, the immunohistochemical data indicate that at least 89 % of the morphological varicosities along the axons represent functional presynaptic boutons. This is in line with previous reports showing that almost all boutons of mature neurons are functional (Yao *et al.*, 2006). The immunohistochemical data obtained from Gähwiler cultures are likely to represent a very conservative estimate of the actual protein distribution, because the plasma clot, in which the slices are embedded, hinders easy penetration of the antibodies. In addition, more than 95 % of all spines form synapses, at least in the neocortex (Arellano *et al.*, 2007).

The question of whether plastic boutons and spines had been or would have become parts of functional synapses awaits further study. Several experimental approaches could be adopted to address this question. However, most of those approaches would require considerable amount of technical development, which place them beyond the scope of my PhD project. Ca^{2+} imaging, FM-dye labeling, as well as post-hoc electron microscopy could provide experimental approaches suited to address synaptic features beyond light-microscopic morphology. A problem of all attempts to address whether removed structures had been previously functional is that all boutons and spines monitored during an experiment (hundreds) would have had to be tested for their function before only some of them changed. Furthermore, time-consuming offline analysis of the recorded image stacks was necessary to determine the contact sites of boutons and spines.

The Ca^{2+} imaging approach was used successfully for new boutons (see discussion in section 5.3). However, this approach needed to be performed in a set of experiments separate from the structural plasticity experiments, since the effect of a Ca^{2+} indicator (respectively Ca^{2+} buffer) on synaptic plasticity is unclear. In addition, the AM form of the used Ca^{2+} indicator did not work in a reliable manner (data not shown, and personal communication from S. Brenowitz), which makes it very hard to label the number of axons needed for the colocalization experiments with spines. The FM-dye labeling is known to be fraught with problems in the slice culture preparation, probably due to limited penetration through the plasma clot in which Gähwiler cultures are embedded. The EM approach has several limitations. First, only the synaptic ultrastructure of new boutons or spines could be assessed, because structures that disappeared do not leave any trace about their synaptic identity. Second, there is no possibility to label all axons needed with a light-convertible, EM-detectable dye.

However, there are possibilities to assess the functionality of synapses using genetically encoded fluorescent markers, e.g. for vesicle release. One approach currently pursued in our laboratory relies on virally transfecting slice cultures with synaptopHluorin, a construct consisting of a pH-sensitive GFP coupled to VAMP,

a protein integrated in the vesicle membrane facing the acidic lumen of the vesicle. The pH-sensitive GFP is non-fluorescent under acidic conditions, as it is in the vesicle lumen, and fluorescent under neutral conditions, given when the vesicle lumen faces extracellular space during release. Thus, an increase of fluorescence intensity upon evoked activity in a given bouton would prove this bouton being functional. Still, it remains unaddressed whether a spine in physical contact is indeed the associated postsynaptic target.

Finally, given that newly formed boutons (De Paola *et al.*, 2006) and spines in the sensory cortex (Knott *et al.*, 2006) as well as spines on CA1 pyramidal neurons (Nägerl *et al.*, 2007) can form synapses, it is likely that at least some of the new structures that were detected ultimately would have turned into functional synapses. Especially for newly formed boutons it has been shown that they become release-competent very rapidly (Matteoli *et al.*, 1992; Kraszewski *et al.*, 1995; Friedman *et al.*, 2000; Krueger *et al.*, 2003; Kim *et al.*, 2003). Although the synaptic network and its plasticity are probably different from the *in vivo* situation, there is a clear activity-dependent effect on structural plasticity, which is very likely relevant for the *in vivo* case as well.

5.3 New and preexisting boutons show activity-dependent Ca^{2+} transients

The data obtained in the second part of this thesis reveal that preexisting and newly formed boutons reliably show Ca^{2+} transients in response to APs. It has been demonstrated in a previous study that single APs and trains of APs reliably evoked Ca^{2+} transients in *en passant* boutons in axon collaterals of cortical layers 2/3, 4 and 5 (Koester and Sakmann, 2000). In the present study, 98 % (55 out of 60) of the preexisting boutons showed Ca^{2+} transients. Four of the five non-responding boutons were located on the same axon branch, while boutons on other branches of the same axon did respond. This suggests that branch point failures in AP propagation, resulting from a breakdown of the potential at one branch of an

axonal branch point (Luscher and Shiner, 1990), can occasionally occur, likely at the axon branch with the larger diameter (Grossman *et al.*, 1979). The single other bouton, that did not respond, was located in direct neighborhood to a responsive bouton, indicating that although APs passed this stretch of the axon, some boutons seem to lack VGCCs. Surprisingly, 100 % of the 15 new boutons detected in the present study showed Ca^{2+} transients, implying that all of those new boutons possess VGCCs, a prerequisite for transmitter release (Katz and Miledi, 1967; 1968). The Ca^{2+} dependence of neurotransmitter release is a fundamental property of chemical synapses. An AP induces the opening of VGCCs (Smith and Augustine, 1988; Reid *et al.*, 1997; Koester and Sakmann, 2000), and the resulting Ca^{2+} influx stimulates the exocytosis of neurotransmitter vesicles (Schneggenburger and Neher, 2005). Thus, an increase in intra-terminal Ca^{2+} concentration is the essential step preceding neurotransmission (DiGregorio and Vergara, 1997). All of the newly formed boutons observed here, fulfill this crucial prerequisite of Ca^{2+} influx.

While the size of the Ca^{2+} transients depended on the number of APs as it would be expected in preexisting boutons (Brenowitz and Regehr, 2007), the Ca^{2+} transients were not significantly different in respect to AP number in new boutons. However, there seems to be a trend for a positive correlation between the signal size and the number of APs. Possibly, the differences would become statistically significant if more experiments were included in the analysis. Alternatively, since the Ca^{2+} transients of new boutons in general tended to be small, this might reflect weak synaptic strength. This explanation would be in line with a previous report showing that the amplitude of presynaptic Ca^{2+} transients is strongly correlated with synaptic strength (Kirischuk and Grantyn, 2002). Interestingly, the amplitude of the Ca^{2+} transient of preexisting boutons decreased over time after induction of LTD. Since it was not tested how stably Ca^{2+} transients are maintained under control conditions, it is unclear whether the decrease is a specific effect of LTD induction or whether it reflects a run-down associated with the prolonged whole-cell configuration or photodamage due to the repeated imaging. However, it was

observed that one of two directly neighboring boutons maintained the same response amplitude while the other bouton showed decreased responses after LTD, which would argue against a general deleterious effect of the imaging. In any case, a decrease in the amplitude of AP-induced Ca^{2+} transients in the boutons after LTD induction would be expected to lead to a reduced release probability and thus the weakening of synaptic transmission.

5.3.1 The generation of Ca^{2+} transients in new boutons

New boutons rapidly showed Ca^{2+} transients, which were always detectable at the very first time point tested, usually between 30 and 45 min after a bouton had formed. This early presence of Ca^{2+} transients raises the question about the source of the Ca^{2+} ions. One possible concern is whether the Ca^{2+} transients originate from the new boutons themselves or whether the Ca^{2+} transient might have spread from neighboring preexisting boutons. Several lines of evidence argue against the latter scenario. First of all, a Ca^{2+} transient was rarely detected in the stretch of axon shaft between two neighboring boutons, even if the region of interest to measure the shaft intensity was placed close to the bouton. If a signal was detected in the axon shaft, it was clearly dependent on the amplitude of the signal in the boutons, indicating diffusional effects. However, even low-noise recordings of the axon shaft did not reveal any Ca^{2+} transients that were temporally coupled to triggered activity, indicating that the Ca^{2+} transients recorded in boutons are most likely sourced by local Ca^{2+} entry, and cannot be accounted for by diffusion from neighboring sites. Furthermore, it has been shown in a previous study, where Ca^{2+} transients were recorded at ribbon-structure terminals with several release sites, that evoked Ca^{2+} transients were always restricted to those release sites (Zenisek *et al.*, 2003), presumably by the action of the endogenous neuronal Ca^{2+} buffers (Schwaller *et al.*, 2002; Burnashev and Rozov, 2005). In conclusion, the Ca^{2+} transients observed in new boutons are likely to originate directly from the boutons themselves, indicating that VGCCs are present early on.

It remains to be discussed which Ca^{2+} channels are the source of the Ca^{2+} influx and how those channels are established in such a rapid manner in newly forming boutons. One possible way to form functional new boutons is the association of preassembled packets, as suggested by various previous studies (Friedman *et al.*, 2000; Ahmari *et al.*, 2000; Zhai *et al.*, 2001; Sabo and McAllister, 2003; Bresler *et al.*, 2004; Sabo *et al.*, 2006) for review see (Ziv and Garner, 2004; Zhen and Jin, 2004), and as discussed earlier in section 5.1. Since Friedman *et al.* (2000) found that new boutons become release-competent within 30 min, VGCCs would be assumed to be present at least at the same time, if not earlier, which is well in line with the time scale of Ca^{2+} transients described here.

Another possible scenario is that a few, sparsely distributed VGCCs are already present in the membrane of the axon shaft (Tippens *et al.*, 2008), which may be recruited to the sites where new boutons are formed. However, as far as the subcellular distribution of VGCCs is known, there is no evidence for continuous expression of VGCCs on the axon shaft. Until today, the following types of VGCC have been identified and localized on central neurons: L-type channels (Mikami *et al.*, 1989; Hui *et al.*, 1991), which are primarily expressed in the proximal dendrites and cell bodies of many types of central neurons (Hell *et al.*, 1993); P/Q-type channels (Mori *et al.*, 1991; Starr *et al.*, 1991), localized in nerve terminals of various central neurons and also at lower densities in some dendrites and cell bodies (Westenbroek *et al.*, 1995; Volsen *et al.*, 1995; Sakurai *et al.*, 1996; Day *et al.*, 1996; Craig *et al.*, 1998); N-type channels (Williams *et al.*, 1992; Dubel *et al.*, 1992), also found in nerve terminals and dendrites (Westenbroek *et al.*, 1992; Volsen *et al.*, 1995; Day *et al.*, 1996); R-type channels (Zhang *et al.*, 1993; Piedras-Renteria and Tsien, 1998), expressed in cell bodies and dendrites (Volsen *et al.*, 1995; Yokoyama *et al.*, 1995; Day *et al.*, 1996); and finally T-type channels (Perez-Reyes *et al.*, 1998; Williams *et al.*, 1999), located in cell bodies and dendrites; for review see (Catterall *et al.*, 2005). Therefore, only P/Q-type and N-type Ca^{2+} channels represent likely candidates being responsible for activity-dependent Ca^{2+} influx in new boutons. Although Ca^{2+} transients can be enhanced

by Ca^{2+} -induced Ca^{2+} release (Emptage *et al.*, 2001; Scott and Rusakov, 2006) from internal stores, such as smooth endoplasmic reticulum (sER) or mitochondria (Blaustein *et al.*, 1978; Henkart *et al.*, 1978) via ryanodine receptors (Sharp *et al.*, 1993), it is unlikely that sER serves as a primary source of voltage-dependent Ca^{2+} transients. In summary, P/Q-type and/or N-type VGCC are almost certainly inserted rapidly into the plasma membrane of new boutons, potentially even together with large parts of the release machinery. Although it can not be concluded from the data of this thesis that newly formed boutons are release-competent and functional as soon as they show activity-dependent Ca^{2+} transients, the data are consistent with the recent literature that suggests a rapid assembly of new, fully functional presynaptic terminals.

5.3.2 The significance of Ca^{2+} for LTD and structural plasticity

Surprisingly, the bouton turnover was not enhanced in the Ca^{2+} imaging experiments in which LTD was induced, neither compared to Ca^{2+} imaging experiments without LTD induction, nor compared to the no-stimulation control condition of the structural plasticity experiments. Since so far only three Ca^{2+} imaging control experiments were performed, the comparison of bouton turnover within the Ca^{2+} imaging experiments cannot be considered conclusive. However, in comparison with the structural plasticity experiments it seems certain that baseline bouton turnover in general is intact in the Ca^{2+} imaging experiments, while any additional activity-dependent changes appear to be impaired. Ca^{2+} has been shown to be an essential messenger in LTD (Mulkey and Malenka, 1992; Yang *et al.*, 1999; Cavazzini *et al.*, 2005). In particular, changes in paired-pulse ratio (Fitzjohn *et al.*, 2001; Faas *et al.*, 2002) and release probability (Bolshakov and Siegelbaum, 1994; Fitzjohn *et al.*, 2001) accompanying LTD indicate an important role for presynaptic Ca^{2+} levels. Thus, the Ca^{2+} indicator Fluo-5F may have significantly perturbed presynaptic Ca^{2+} levels and thus impaired the

induction of LTD, which is Ca^{2+} -dependent. In addition, dilution of factors essential for plasticity due to several hours of patch-clamping cannot be excluded.

While APs were definitely evoked at the single axon labeled in the Ca^{2+} imaging experiments, this cannot be assured for all labeled axons in the structural plasticity experiments. Thus, an alternative explanation for the divergence in bouton turnover might be that the plasticity-associated increase only affected unstimulated axons. This would be in line with a presynaptic structural effect of heterosynaptic LTD, as has been previously suggested by Desmond and Levy (1983). However, in both experiments homosynaptic and heterosynaptic plasticity cannot be distinguished, since recording from a second pathway that is independent of the activation of the first would have been required.

In summary, impairment of plasticity through the Ca^{2+} indicator or the patching is a likely explanation, while heterosynaptic presynaptic effects cannot be excluded. Necessary control experiments include to repeat the patch-clamp experiment without a Ca^{2+} indicator, and in addition to retract the pipette quickly after labeling and testing for evoked APs.

6 Conclusions & Outlook

Structural changes of synaptic connections are assumed to represent a morphological implementation of synaptic plasticity. The data presented here support this idea in that a decrease in synaptic transmission was accompanied by enhanced bouton turnover and a net loss of contacts between boutons and spines. Clearly, structural plasticity is a feature that is not specific to dendritic spines. In fact, presynaptic structural changes may even play a bigger role than spine changes given that the gain or loss of contacts was frequently due to bouton changes. Moreover, the finding that new boutons are rapidly capable of generating voltage-dependent Ca^{2+} transients suggests that LTD induction leads to a functional rewiring of the hippocampal network within a few hours. While this and previous studies of this laboratory and others consistently report morphological changes going along with synaptic plasticity, the molecular basis for those observations is largely unknown. Irrespective of its mode, the disconnection and the formation of synapses must entail complex molecular processes. Despite evidence for the assembly of the presynaptic site preceding the postsynaptic site, the sequence and coordination of events are still unclear. It will be important to determine the pathways involved in the communication across the synapse, which will be responsible for coordinating the assembly or disassembly of synapses. In particular, it will be exciting to examine the role of extracellular matrix molecules, (e.g. neurexin/neurologin, SynCam, cadherins) which are known to connect the pre- and postsynaptic site or even to signal across the synaptic cleft. Furthermore, it will be important to investigate how different forms of synaptic plasticity differentially affect the remodeling of synaptic contacts and thus, a neuronal network. Finally, it is necessary to transfer the findings to *in vivo* systems and explore their relevance for experience-dependent plasticity in the living animal.

Bibliography

- Ahmari, S. E., Buchanan, J., and Smith, S. J.** (2000). Assembly of presynaptic active zones from cytoplasmic transport packets. *Nat. Neurosci.* **3**, 445-451.
- Akaaboune, M., Culican, S. M., Turney, S. G., and Lichtman, J. W.** (1999). Rapid and reversible effects of activity on acetylcholine receptor density at the neuromuscular junction in vivo. *Science* **286**, 503-507.
- Alvarez, V. A. and Sabatini, B. L.** (2007). Anatomical and physiological plasticity of dendritic spines. *Annu. Rev. Neurosci.* **30**, 79-97.
- Amaral, D. G.** (1993). Emerging principles of intrinsic hippocampal organization. *Curr. Opin. Neurobiol.* **3**, 225-229.
- Anwyl, R.** (2006). Induction and expression mechanisms of postsynaptic NMDA receptor-independent homosynaptic long-term depression. *Prog. Neurobiol.* **78**, 17-37.
- Arellano, J. I., Espinosa, A., Fairen, A., Yuste, R., and Defelipe, J.** (2007). Non-synaptic dendritic spines in neocortex. *Neuroscience* **145**, 464-469.
- Artola, A., von Frijtag, J. C., Fermont, P. C., Gispen, W. H., Schrama, L. H., Kamal, A., and Spruijt, B. M.** (2006). Long-lasting modulation of the induction of LTD and LTP in rat hippocampal CA1 by behavioural stress and environmental enrichment. *Eur. J. Neurosci.* **23**, 261-272.
- Atwood, H. L. and Karunanithi, S.** (2002). Diversification of synaptic strength: presynaptic elements. *Nat. Rev. Neurosci.* **3**, 497-516.
- Bamji, S. X., Rico, B., Kimes, N., and Reichardt, L. F.** (2006). BDNF mobilizes synaptic vesicles and enhances synapse formation by disrupting cadherin-beta-catenin interactions. *J. Cell Biol.* **174**, 289-299.
- Barrionuevo, G., Schottler, F., and Lynch, G.** (1980). The effects of repetitive low frequency stimulation on control and "potentiated" synaptic responses in the hippocampus. *Life Sci.* **27**, 2385-2391.
- Bear, M. F. and Abraham, W. C.** (1996). Long-term depression in hippocampus. *Annu. Rev. Neurosci.* **19**, 437-462.
- Benson, D. L., Schnapp, L. M., Shapiro, L., and Huntley, G. W.** (2000). Making memories stick: cell-adhesion molecules in synaptic plasticity. *Trends Cell Biol.* **10**, 473-482.

- Biederer, T., Sara, Y., Mozhayeva, M., Atasoy, D., Liu, X., Kavalali, E. T., and Sudhof, T. C.** (2002). SynCAM, a synaptic adhesion molecule that drives synapse assembly. *Science* **297**, 1525-1531.
- Blaustein, M. P., Ratzlaff, R. W., Kendrick, N. C., and Schweitzer, E. S.** (1978). Calcium buffering in presynaptic nerve terminals. I. Evidence for involvement of a nonmitochondrial ATP-dependent sequestration mechanism. *J. Gen. Physiol* **72**, 15-41.
- Bliss, T. V. and Collingridge, G. L.** (1993). A synaptic model of memory: long-term potentiation in the hippocampus. *Nature* **361**, 31-39.
- Bliss, T. V., Lancaster, B., and Wheal, H. V.** (1983). Long-term potentiation in commissural and Schaffer projections to hippocampal CA1 cells: an in vivo study in the rat. *J. Physiol* **341**, 617-626.
- Bliss, T. V. and Lomo, T.** (1973). Long-lasting potentiation of synaptic transmission in the dentate area of the anaesthetized rabbit following stimulation of the perforant path. *J. Physiol* **232**, 331-356.
- Bolshakov, V. Y. and Siegelbaum, S. A.** (1994). Postsynaptic induction and presynaptic expression of hippocampal long-term depression. *Science* **264**, 1148-1152.
- Borgdorff, A. J. and Choquet, D.** (2002). Regulation of AMPA receptor lateral movements. *Nature* **417**, 649-653.
- Brenowitz, S. D. and Regehr, W. G.** (2007). Reliability and heterogeneity of calcium signaling at single presynaptic boutons of cerebellar granule cells. *J. Neurosci.* **27**, 7888-7898.
- Bresler, T., Shapira, M., Boeckers, T., Dresbach, T., Futter, M., Garner, C. C., Rosenblum, K., Gundelfinger, E. D., and Ziv, N. E.** (2004). Postsynaptic density assembly is fundamentally different from presynaptic active zone assembly. *J. Neurosci.* **24**, 1507-1520.
- Brose, N.** (1999). Synaptic cell adhesion proteins and synaptogenesis in the mammalian central nervous system. *Naturwissenschaften* **86**, 516-524.
- Buckby, L. E., Mummery, R., Crompton, M. R., Beesley, P. W., and Empson, R. M.** (2004). Comparison of neuroligin and synaptic marker protein expression in acute and cultured organotypic hippocampal slices from rat. *Brain Res. Dev. Brain Res.* **150**, 1-7.
- Burnashev, N. and Rozov, A.** (2005). Presynaptic Ca²⁺ dynamics, Ca²⁺ buffers and synaptic efficacy. *Cell Calcium* **37**, 489-495.
- Cai, Q., Pan, P. Y., and Sheng, Z. H.** (2007). Syntabulin-kinesin-1 family member 5B-mediated axonal transport contributes to activity-dependent presynaptic assembly. *J. Neurosci.* **27**, 7284-7296.

- Cajal, S. R.** El nuevo concepto de la histología de los centros nerviosos. *Rev. Ciencias Méd. Barcelona* (18), 361-541. 1892.
- Carroll, R. C., Lissin, D. V., von Zastrow, M., Nicoll, R. A., and Malenka, R. C.** (1999). Rapid redistribution of glutamate receptors contributes to long-term depression in hippocampal cultures. *Nat. Neurosci.* **2**, 454-460.
- Catterall, W. A., Perez-Reyes, E., Snutch, T. P., and Striessnig, J.** (2005). International Union of Pharmacology. XLVIII. Nomenclature and structure-function relationships of voltage-gated calcium channels. *Pharmacol. Rev.* **57**, 411-425.
- Cavazzini, M., Bliss, T., and Emptage, N.** (2005). Ca²⁺ and synaptic plasticity. *Cell Calcium* **38**, 355-367.
- Chi, P., Greengard, P., and Ryan, T. A.** (2003). Synaptic vesicle mobilization is regulated by distinct synapsin I phosphorylation pathways at different frequencies. *Neuron* **38**, 69-78.
- Choquet, D. and Triller, A.** (2003). The role of receptor diffusion in the organization of the postsynaptic membrane. *Nat. Rev. Neurosci.* **4**, 251-265.
- Craig, P. J., McAinsh, A. D., McCormack, A. L., Smith, W., Beattie, R. E., Priestley, J. V., Yip, J. L., Averill, S., Longbottom, E. R., and Volsen, S. G.** (1998). Distribution of the voltage-dependent calcium channel alpha(1A) subunit throughout the mature rat brain and its relationship to neurotransmitter pathways. *J. Comp Neurol.* **397**, 251-267.
- Dailey, M. E. and Smith, S. J.** (1996). The dynamics of dendritic structure in developing hippocampal slices. *J. Neurosci.* **16**, 2983-2994.
- Darcy, K. J., Staras, K., Collinson, L. M., and Goda, Y.** (2006). Constitutive sharing of recycling synaptic vesicles between presynaptic boutons. *Nat. Neurosci.* **9**, 315-321.
- Day, N. C., Shaw, P. J., McCormack, A. L., Craig, P. J., Smith, W., Beattie, R., Williams, T. L., Ellis, S. B., Ince, P. G., Harpold, M. M., Lodge, D., and Volsen, S. G.** (1996). Distribution of alpha 1A, alpha 1B and alpha 1E voltage-dependent calcium channel subunits in the human hippocampus and parahippocampal gyrus. *Neuroscience* **71**, 1013-1024.
- De Paola, V., Arber, S., and Caroni, P.** (2003). AMPA receptors regulate dynamic equilibrium of presynaptic terminals in mature hippocampal networks. *Nat. Neurosci.* **6**, 491-500.
- De Paola, V., Holtmaat, A., Knott, G., Song, S., Wilbrecht, L., Caroni, P., and Svoboda, K.** (2006). Cell type-specific structural plasticity of axonal branches and boutons in the adult neocortex. *Neuron* **49**, 861-875.

- De Simoni, A., Griesinger, C. B., and Edwards, F. A.** (2003). Development of rat CA1 neurones in acute versus organotypic slices: role of experience in synaptic morphology and activity. *J. Physiol* **550**, 135-147.
- Dean, C., Scholl, F. G., Choih, J., DeMaria, S., Berger, J., Isacoff, E., and Scheiffele, P.** (2003). Neurexin mediates the assembly of presynaptic terminals. *Nat. Neurosci.* **6**, 708-716.
- Debanne, D. and Thompson, S. M.** (1996). Associative long-term depression in the hippocampus in vitro. *Hippocampus* **6**, 9-16.
- Deng, J. and Dunaevsky, A.** (2005). Dynamics of dendritic spines and their afferent terminals: spines are more motile than presynaptic boutons. *Dev. Biol.* **277**, 366-377.
- Desmond, N. L. and Levy, W. B.** (1983). Synaptic correlates of associative potentiation/depression: an ultrastructural study in the hippocampus. *Brain Res.* **265**, 21-30.
- Diamond, D. M., Park, C. R., Campbell, A. M., and Woodson, J. C.** (2005). Competitive interactions between endogenous LTD and LTP in the hippocampus underlie the storage of emotional memories and stress-induced amnesia. *Hippocampus* **15**, 1006-1025.
- DiGregorio, D. A. and Vergara, J. L.** (1997). Localized detection of action potential-induced presynaptic calcium transients at a *Xenopus* neuromuscular junction. *J. Physiol* **505 (Pt 3)**, 585-592.
- Dobrunz, L. E.** (2002). Release probability is regulated by the size of the readily releasable vesicle pool at excitatory synapses in hippocampus. *Int. J. Dev. Neurosci.* **20**, 225-236.
- Doyere, V., Errington, M. L., Laroche, S., and Bliss, T. V.** (1996). Low-frequency trains of paired stimuli induce long-term depression in area CA1 but not in dentate gyrus of the intact rat. *Hippocampus* **6**, 52-57.
- Dubel, S. J., Starr, T. V., Hell, J., Ahlijanian, M. K., Enyeart, J. J., Catterall, W. A., and Snutch, T. P.** (1992). Molecular cloning of the alpha-1 subunit of an omega-conotoxin-sensitive calcium channel. *Proc. Natl. Acad. Sci. U. S. A* **89**, 5058-5062.
- Dudek, S. M. and Bear, M. F.** (1992). Homosynaptic long-term depression in area CA1 of hippocampus and effects of N-methyl-D-aspartate receptor blockade. *Proc. Natl. Acad. Sci. U. S. A* **89**, 4363-4367.
- Ehlers, M. D., Heine, M., Groc, L., Lee, M. C., and Choquet, D.** (2007). Diffusional trapping of GluR1 AMPA receptors by input-specific synaptic activity. *Neuron* **54**, 447-460.

- Emptage, N. J., Reid, C. A., and Fine, A.** (2001). Calcium stores in hippocampal synaptic boutons mediate short-term plasticity, store-operated Ca²⁺ entry, and spontaneous transmitter release. *Neuron* **29**, 197-208.
- Engert, F. and Bonhoeffer, T.** (1999). Dendritic spine changes associated with hippocampal long-term synaptic plasticity. *Nature* **399**, 66-70.
- Faas, G. C., Adwanikar, H., Gereau, R. W., and Saggau, P.** (2002). Modulation of presynaptic calcium transients by metabotropic glutamate receptor activation: a differential role in acute depression of synaptic transmission and long-term depression. *J. Neurosci.* **22**, 6885-6890.
- Fiala, J. C., Feinberg, M., Popov, V., and Harris, K. M.** (1998). Synaptogenesis via dendritic filopodia in developing hippocampal area CA1. *J. Neurosci.* **18**, 8900-8911.
- Fischer, M., Kaech, S., Wagner, U., Brinkhaus, H., and Matus, A.** (2000). Glutamate receptors regulate actin-based plasticity in dendritic spines. *Nat. Neurosci.* **3**, 887-894.
- Fitzjohn, S. M., Palmer, M. J., May, J. E., Neeson, A., Morris, S. A., and Collingridge, G. L.** (2001). A characterisation of long-term depression induced by metabotropic glutamate receptor activation in the rat hippocampus in vitro. *J. Physiol* **537**, 421-430.
- Friedman, H. V., Bresler, T., Garner, C. C., and Ziv, N. E.** (2000). Assembly of new individual excitatory synapses: time course and temporal order of synaptic molecule recruitment. *Neuron* **27**, 57-69.
- Froc, D. J., Chapman, C. A., Trepel, C., and Racine, R. J.** (2000). Long-term depression and depotentiation in the sensorimotor cortex of the freely moving rat. *J. Neurosci.* **20**, 438-445.
- Fukazawa, Y., Saitoh, Y., Ozawa, F., Ohta, Y., Mizuno, K., and Inokuchi, K.** (2003). Hippocampal LTP is accompanied by enhanced F-actin content within the dendritic spine that is essential for late LTP maintenance in vivo. *Neuron* **38**, 447-460.
- Fukunaga, K., Stoppini, L., Miyamoto, E., and Muller, D.** (1993). Long-term potentiation is associated with an increased activity of Ca²⁺/calmodulin-dependent protein kinase II. *J. Biol. Chem.* **268**, 7863-7867.
- Gähwiler, B. H.** (1981). Organotypic monolayer cultures of nervous tissue. *J. Neurosci. Methods* **4**, 329-342.
- Garcia, E. P., McPherson, P. S., Chilcote, T. J., Takei, K., and De Camilli, P.** (1995). rbSec1A and B colocalize with syntaxin 1 and SNAP-25 throughout the axon, but are not in a stable complex with syntaxin. *J. Cell Biol.* **129**, 105-120.

- Garner, C. C., Zhai, R. G., Gundelfinger, E. D., and Ziv, N. E.** (2002). Molecular mechanisms of CNS synaptogenesis. *Trends Neurosci.* **25**, 243-251.
- Gerdeman, G. L., Ronesi, J., and Lovinger, D. M.** (2002). Postsynaptic endocannabinoid release is critical to long-term depression in the striatum. *Nat. Neurosci.* **5**, 446-451.
- Goda, Y. and Davis, G. W.** (2003). Mechanisms of synapse assembly and disassembly. *Neuron* **40**, 243-264.
- Grossman, Y., Parnas, I., and Spira, M. E.** (1979). Differential conduction block in branches of a bifurcating axon. *J. Physiol* **295**, 283-305.
- Gruart, A., Munoz, M. D., and Delgado-Garcia, J. M.** (2006). Involvement of the CA3-CA1 synapse in the acquisition of associative learning in behaving mice. *J. Neurosci.* **26**, 1077-1087.
- Harris, K. M. and Stevens, J. K.** (1989). Dendritic spines of CA 1 pyramidal cells in the rat hippocampus: serial electron microscopy with reference to their biophysical characteristics. *J. Neurosci.* **9**, 2982-2997.
- Hedberg, T. G. and Stanton, P. K.** (1995). Long-term potentiation and depression of synaptic transmission in rat posterior cingulate cortex. *Brain Res.* **670**, 181-196.
- Hell, J. W., Westenbroek, R. E., Warner, C., Ahljianian, M. K., Prystay, W., Gilbert, M. M., Snutch, T. P., and Catterall, W. A.** (1993). Identification and differential subcellular localization of the neuronal class C and class D L-type calcium channel alpha 1 subunits. *J. Cell Biol.* **123**, 949-962.
- Henkart, M. P., Reese, T. S., and Brinley, F. J., Jr.** (1978). Endoplasmic reticulum sequesters calcium in the squid giant axon. *Science* **202**, 1300-1303.
- Heynen, A. J., Yoon, B. J., Liu, C. H., Chung, H. J., Haganir, R. L., and Bear, M. F.** (2003). Molecular mechanism for loss of visual cortical responsiveness following brief monocular deprivation. *Nat. Neurosci.* **6**, 854-862.
- Holtmaat, A., Wilbrecht, L., Knott, G. W., Welker, E., and Svoboda, K.** (2006). Experience-dependent and cell-type-specific spine growth in the neocortex. *Nature* **441**, 979-983.
- Holtmaat, A. J., Trachtenberg, J. T., Wilbrecht, L., Shepherd, G. M., Zhang, X., Knott, G. W., and Svoboda, K.** (2005). Transient and persistent dendritic spines in the neocortex in vivo. *Neuron* **45**, 279-291.
- Huang, C. C., You, J. L., Wu, M. Y., and Hsu, K. S.** (2004). Rap1-induced p38 mitogen-activated protein kinase activation facilitates AMPA receptor trafficking via the GDI.Rab5 complex. Potential role in (S)-3,5-dihydroxyphenylglycine-induced long term depression. *J. Biol. Chem.* **279**, 12286-12292.

- Huber, K. M., Kayser, M. S., and Bear, M. F.** (2000). Role for rapid dendritic protein synthesis in hippocampal mGluR-dependent long-term depression. *Science* **288**, 1254-1257.
- Huerta, P. T. and Lisman, J. E.** (1995). Bidirectional synaptic plasticity induced by a single burst during cholinergic theta oscillation in CA1 in vitro. *Neuron* **15**, 1053-1063.
- Hui, A., Ellinor, P. T., Krizanova, O., Wang, J. J., Diebold, R. J., and Schwartz, A.** (1991). Molecular cloning of multiple subtypes of a novel rat brain isoform of the alpha 1 subunit of the voltage-dependent calcium channel. *Neuron* **7**, 35-44.
- Jontes, J. D. and Smith, S. J.** (2000). Filopodia, spines, and the generation of synaptic diversity. *Neuron* **27**, 11-14.
- Katz, B. and Miledi, R.** (1967). A study of synaptic transmission in the absence of nerve impulses. *J. Physiol* **192**, 407-436.
- Katz, B. and Miledi, R.** (1968). The role of calcium in neuromuscular facilitation. *J. Physiol* **195**, 481-492.
- Katz, L. C. and Shatz, C. J.** (1996). Synaptic activity and the construction of cortical circuits. *Science* **274**, 1133-1138.
- Kemp, A. and Manahan-Vaughan, D.** (2004). Hippocampal long-term depression and long-term potentiation encode different aspects of novelty acquisition. *Proc. Natl. Acad. Sci. U. S. A* **101**, 8192-8197.
- Kemp, N. and Bashir, Z. I.** (2001). Long-term depression: a cascade of induction and expression mechanisms. *Prog. Neurobiol.* **65**, 339-365.
- Kesner, R. P. and Hopkins, R. O.** (2006). Mnemonic functions of the hippocampus: a comparison between animals and humans. *Biol. Psychol.* **73**, 3-18.
- Kim, J. H., Udo, H., Li, H. L., Youn, T. Y., Chen, M., Kandel, E. R., and Bailey, C. H.** (2003). Presynaptic activation of silent synapses and growth of new synapses contribute to intermediate and long-term facilitation in *Aplysia*. *Neuron* **40**, 151-165.
- Kirischuk, S. and Grantyn, R.** (2002). Inter-bouton variability of synaptic strength correlates with heterogeneity of presynaptic Ca(2+) signals. *J. Neurophysiol.* **88**, 2172-2176.
- Kirkwood, A. and Bear, M. F.** (1994). Homosynaptic long-term depression in the visual cortex. *J. Neurosci.* **14**, 3404-3412.
- Knott, G. W., Holtmaat, A., Wilbrecht, L., Welker, E., and Svoboda, K.** (2006). Spine growth precedes synapse formation in the adult neocortex in vivo. *Nat. Neurosci.* **9**, 1117-1124.

- Koester, H. J. and Sakmann, B.** (2000). Calcium dynamics associated with action potentials in single nerve terminals of pyramidal cells in layer 2/3 of the young rat neocortex. *J. Physiol* **529 Pt 3**, 625-646.
- Konur, S. and Yuste, R.** (2004). Imaging the motility of dendritic protrusions and axon terminals: roles in axon sampling and synaptic competition. *Mol. Cell Neurosci.* **27**, 427-440.
- Kopec, C. and Malinow, R.** (2006). Neuroscience. Matters of size. *Science* **314**, 1554-1555.
- Kopec, C. D., Li, B., Wei, W., Boehm, J., and Malinow, R.** (2006). Glutamate receptor exocytosis and spine enlargement during chemically induced long-term potentiation. *J. Neurosci.* **26**, 2000-2009.
- Kraszewski, K., Mundigl, O., Daniell, L., Verderio, C., Matteoli, M., and De Camilli, P.** (1995). Synaptic vesicle dynamics in living cultured hippocampal neurons visualized with CY3-conjugated antibodies directed against the luminal domain of synaptotagmin. *J. Neurosci.* **15**, 4328-4342.
- Krueger, S. and Fitzsimonds, R. M.** (2006). Remodeling the plasticity debate: the presynaptic locus revisited. *Physiology. (Bethesda.)* **21**, 346-351.
- Krueger, S. R., Kolar, A., and Fitzsimonds, R. M.** (2003). The presynaptic release apparatus is functional in the absence of dendritic contact and highly mobile within isolated axons. *Neuron* **40**, 945-957.
- Lang, C., Barco, A., Zablow, L., Kandel, E. R., Siegelbaum, S. A., and Zakharenko, S. S.** (2004). Transient expansion of synaptically connected dendritic spines upon induction of hippocampal long-term potentiation. *Proc. Natl. Acad. Sci. U. S. A* **101**, 16665-16670.
- Lemke, E. A. and Klingauf, J.** (2005). Single synaptic vesicle tracking in individual hippocampal boutons at rest and during synaptic activity. *J. Neurosci.* **25**, 11034-11044.
- Levy, W. B. and Steward, O.** (1979). Synapses as associative memory elements in the hippocampal formation. *Brain Res.* **175**, 233-245.
- Lisman, J., Schulman, H., and Cline, H.** (2002). The molecular basis of CaMKII function in synaptic and behavioural memory. *Nat. Rev. Neurosci.* **3**, 175-190.
- Lu, W., Man, H., Ju, W., Trimble, W. S., MacDonald, J. F., and Wang, Y. T.** (2001). Activation of synaptic NMDA receptors induces membrane insertion of new AMPA receptors and LTP in cultured hippocampal neurons. *Neuron* **29**, 243-254.
- Luscher, C., Xia, H., Beattie, E. C., Carroll, R. C., von Zastrow, M., Malenka, R. C., and Nicoll, R. A.** (1999). Role of AMPA receptor cycling in synaptic transmission and plasticity. *Neuron* **24**, 649-658.

- Luscher, H. R. and Shiner, J. S.** (1990). Computation of action potential propagation and presynaptic bouton activation in terminal arborizations of different geometries. *Biophys. J.* **58**, 1377-1388.
- Lynch, G. S., Dunwiddie, T., and Gribkoff, V.** (1977). Heterosynaptic depression: a postsynaptic correlate of long-term potentiation. *Nature* **266**, 737-739.
- Maguire, E. A., Gadian, D. G., Johnsrude, I. S., Good, C. D., Ashburner, J., Frackowiak, R. S., and Frith, C. D.** (2000). Navigation-related structural change in the hippocampi of taxi drivers. *Proc. Natl. Acad. Sci. U. S. A* **97**, 4398-4403.
- Majewska, A. K., Newton, J. R., and Sur, M.** (2006). Remodeling of synaptic structure in sensory cortical areas in vivo. *J. Neurosci.* **26**, 3021-3029.
- Maletic-Savatic, M., Malinow, R., and Svoboda, K.** (1999). Rapid dendritic morphogenesis in CA1 hippocampal dendrites induced by synaptic activity. *Science* **283**, 1923-1927.
- Malleret, G., Haditsch, U., Genoux, D., Jones, M. W., Bliss, T. V., Vanhose, A. M., Weitlauf, C., Kandel, E. R., Winder, D. G., and Mansuy, I. M.** (2001). Inducible and reversible enhancement of learning, memory, and long-term potentiation by genetic inhibition of calcineurin. *Cell* **104**, 675-686.
- Manahan-Vaughan, D.** (1997). Group 1 and 2 metabotropic glutamate receptors play differential roles in hippocampal long-term depression and long-term potentiation in freely moving rats. *J. Neurosci.* **17**, 3303-3311.
- Manahan-Vaughan, D. and Braunewell, K. H.** (1999). Novelty acquisition is associated with induction of hippocampal long-term depression. *Proc. Natl. Acad. Sci. U. S. A* **96**, 8739-8744.
- Martin, S. J., Grimwood, P. D., and Morris, R. G.** (2000). Synaptic plasticity and memory: an evaluation of the hypothesis. *Annu. Rev. Neurosci.* **23**, 649-711.
- Matsuo, N., Reijmers, L., and Mayford, M.** (2008). Spine-type-specific recruitment of newly synthesized AMPA receptors with learning. *Science* **319**, 1104-1107.
- Matsuzaki, M., Ellis-Davies, G. C., Nemoto, T., Miyashita, Y., Iino, M., and Kasai, H.** (2001). Dendritic spine geometry is critical for AMPA receptor expression in hippocampal CA1 pyramidal neurons. *Nat. Neurosci.* **4**, 1086-1092.
- Matsuzaki, M., Honkura, N., Ellis-Davies, G. C., and Kasai, H.** (2004). Structural basis of long-term potentiation in single dendritic spines. *Nature* **429**, 761-766.
- Matteoli, M., Takei, K., Perin, M. S., Sudhof, T. C., and De Camilli, P.** (1992). Exo-endocytotic recycling of synaptic vesicles in developing processes of cultured hippocampal neurons. *J. Cell Biol.* **117**, 849-861.
- McKernan, M. G. and Shinnick-Gallagher, P.** (1997). Fear conditioning induces a lasting potentiation of synaptic currents in vitro. *Nature* **390**, 607-611.

- Mikami, A., Imoto, K., Tanabe, T., Niidome, T., Mori, Y., Takeshima, H., Narumiya, S., and Numa, S.** (1989). Primary structure and functional expression of the cardiac dihydropyridine-sensitive calcium channel. *Nature* **340**, 230-233.
- Milner, B.** (1972). Disorders of learning and memory after temporal lobe lesions in man. *Clin. Neurosurg.* **19**, 421-446.
- Milner, B. and Penfield, W.** (1955). The effect of hippocampal lesions on recent memory. *Trans. Am. Neurol. Assoc.* 42-48.
- Moghaddam, B., Bolinao, M. L., Stein-Behrens, B., and Sapolsky, R.** (1994). Glucocorticoids mediate the stress-induced extracellular accumulation of glutamate. *Brain Res.* **655**, 251-254.
- Mori, Y., Friedrich, T., Kim, M. S., Mikami, A., Nakai, J., Ruth, P., Bosse, E., Hofmann, F., Flockerzi, V., Furuichi, T., and .** (1991). Primary structure and functional expression from complementary DNA of a brain calcium channel. *Nature* **350**, 398-402.
- Moser, E., Moser, M. B., and Andersen, P.** (1993). Spatial learning impairment parallels the magnitude of dorsal hippocampal lesions, but is hardly present following ventral lesions. *J. Neurosci.* **13**, 3916-3925.
- Mulkey, R. M., Herron, C. E., and Malenka, R. C.** (1993). An essential role for protein phosphatases in hippocampal long-term depression. *Science* **261**, 1051-1055.
- Mulkey, R. M. and Malenka, R. C.** (1992). Mechanisms underlying induction of homosynaptic long-term depression in area CA1 of the hippocampus. *Neuron* **9**, 967-975.
- Muller, D., Buchs, P. A., and Stoppini, L.** (1993). Time course of synaptic development in hippocampal organotypic cultures. *Brain Res. Dev. Brain Res.* **71**, 93-100.
- Murthy, V. N., Schikorski, T., Stevens, C. F., and Zhu, Y.** (2001). Inactivity produces increases in neurotransmitter release and synapse size. *Neuron* **32**, 673-682.
- Nägerl, U. V., Eberhorn, N., Cambridge, S. B., and Bonhoeffer, T.** (2004). Bidirectional activity-dependent morphological plasticity in hippocampal neurons. *Neuron* **44**, 759-767.
- Nägerl, U. V., Kostinger, G., Anderson, J. C., Martin, K. A., and Bonhoeffer, T.** (2007). Protracted synaptogenesis after activity-dependent spinogenesis in hippocampal neurons. *J. Neurosci.* **27**, 8149-8156.
- Neves, G., Cooke, S. F., and Bliss, T. V.** (2008). Synaptic plasticity, memory and the hippocampus: a neural network approach to causality. *Nat. Rev. Neurosci.* **9**, 65-75.
- Nikonenko, I., Jourdain, P., and Muller, D.** (2003). Presynaptic remodeling contributes to activity-dependent synaptogenesis. *J. Neurosci.* **23**, 8498-8505.

- Ninan, I., Liu, S., Rabinowitz, D., and Arancio, O.** (2006). Early presynaptic changes during plasticity in cultured hippocampal neurons. *EMBO J.*
- Noguchi, J., Matsuzaki, M., Ellis-Davies, G. C., and Kasai, H.** (2005). Spine-neck geometry determines NMDA receptor-dependent Ca²⁺ signaling in dendrites. *Neuron* **46**, 609-622.
- Nosyreva, E. D. and Huber, K. M.** (2005). Developmental switch in synaptic mechanisms of hippocampal metabotropic glutamate receptor-dependent long-term depression. *J. Neurosci.* **25**, 2992-3001.
- Okamoto, K., Nagai, T., Miyawaki, A., and Hayashi, Y.** (2004). Rapid and persistent modulation of actin dynamics regulates postsynaptic reorganization underlying bidirectional plasticity. *Nat. Neurosci.* **7**, 1104-1112.
- Oliet, S. H., Malenka, R. C., and Nicoll, R. A.** (1997). Two distinct forms of long-term depression coexist in CA1 hippocampal pyramidal cells. *Neuron* **18**, 969-982.
- Park, M., Salgado, J. M., Ostroff, L., Helton, T. D., Robinson, C. G., Harris, K. M., and Ehlers, M. D.** (2006). Plasticity-induced growth of dendritic spines by exocytic trafficking from recycling endosomes. *Neuron* **52**, 817-830.
- Perez-Reyes, E., Cribbs, L. L., Daud, A., Lacerda, A. E., Barclay, J., Williamson, M. P., Fox, M., Rees, M., and Lee, J. H.** (1998). Molecular characterization of a neuronal low-voltage-activated T-type calcium channel. *Nature* **391**, 896-900.
- Piedras-Renteria, E. S. and Tsien, R. W.** (1998). Antisense oligonucleotides against alpha1E reduce R-type calcium currents in cerebellar granule cells. *Proc. Natl. Acad. Sci. U. S. A* **95**, 7760-7765.
- Pierce, J. P. and Mendell, L. M.** (1993). Quantitative ultrastructure of Ia boutons in the ventral horn: scaling and positional relationships. *J. Neurosci.* **13**, 4748-4763.
- Prange, O. and Murphy, T. H.** (2001). Modular transport of postsynaptic density-95 clusters and association with stable spine precursors during early development of cortical neurons. *J. Neurosci.* **21**, 9325-9333.
- Rao, A., Harms, K. J., and Craig, A. M.** (2000). Neuroligation: building synapses around the neuroligin-neurexin link. *Nat. Neurosci.* **3**, 747-749.
- Reid, C. A., Clements, J. D., and Bekkers, J. M.** (1997). Nonuniform distribution of Ca²⁺ channel subtypes on presynaptic terminals of excitatory synapses in hippocampal cultures. *J. Neurosci.* **17**, 2738-2745.
- Rogan, M. T. and Ledoux, J. E.** (1995). LTP is accompanied by commensurate enhancement of auditory-evoked responses in a fear conditioning circuit. *Neuron* **15**, 127-136.

- Rogers, J. L., Hunsaker, M. R., and Kesner, R. P.** (2006). Effects of ventral and dorsal CA1 subregional lesions on trace fear conditioning. *Neurobiol. Learn. Mem.* **86**, 72-81.
- Rutishauser, U., Mamelak, A. N., and Schuman, E. M.** (2006). Single-trial learning of novel stimuli by individual neurons of the human hippocampus-amygdala complex. *Neuron* **49**, 805-813.
- Sabo, S. L., Gomes, R. A., and McAllister, A. K.** (2006). Formation of presynaptic terminals at predefined sites along axons. *J. Neurosci.* **26**, 10813-10825.
- Sabo, S. L. and McAllister, A. K.** (2003). Mobility and cycling of synaptic protein-containing vesicles in axonal growth cone filopodia. *Nat. Neurosci.* **6**, 1264-1269.
- Sakurai, T., Westenbroek, R. E., Rettig, J., Hell, J., and Catterall, W. A.** (1996). Biochemical properties and subcellular distribution of the BI and rbA isoforms of alpha 1A subunits of brain calcium channels. *J. Cell Biol.* **134**, 511-528.
- Scheiffele, P., Fan, J., Choih, J., Fetter, R., and Serafini, T.** (2000). Neuroligin expressed in nonneuronal cells triggers presynaptic development in contacting axons. *Cell* **101**, 657-669.
- Schikorski, T. and Stevens, C. F.** (1997). Quantitative ultrastructural analysis of hippocampal excitatory synapses. *J. Neurosci.* **17**, 5858-5867.
- Schneggenburger, R. and Neher, E.** (2005). Presynaptic calcium and control of vesicle fusion. *Curr. Opin. Neurobiol.* **15**, 266-274.
- Schwaller, B., Meyer, M., and Schiffmann, S.** (2002). 'New' functions for 'old' proteins: the role of the calcium-binding proteins calbindin D-28k, calretinin and parvalbumin, in cerebellar physiology. Studies with knockout mice. *Cerebellum.* **1**, 241-258.
- Scott, R. and Rusakov, D. A.** (2006). Main determinants of presynaptic Ca²⁺ dynamics at individual mossy fiber-CA3 pyramidal cell synapses. *J. Neurosci.* **26**, 7071-7081.
- Sharp, A. H., McPherson, P. S., Dawson, T. M., Aoki, C., Campbell, K. P., and Snyder, S. H.** (1993). Differential immunohistochemical localization of inositol 1,4,5-trisphosphate- and ryanodine-sensitive Ca²⁺ release channels in rat brain. *J. Neurosci.* **13**, 3051-3063.
- Shatz, C. J. and Stryker, M. P.** (1978). Ocular dominance in layer IV of the cat's visual cortex and the effects of monocular deprivation. *J. Physiol* **281**, 267-283.
- Smith, S. J. and Augustine, G. J.** (1988). Calcium ions, active zones and synaptic transmitter release. *Trends Neurosci.* **11**, 458-464.

- Snyder, E. M., Philpot, B. D., Huber, K. M., Dong, X., Fallon, J. R., and Bear, M. F.** (2001). Internalization of ionotropic glutamate receptors in response to mGluR activation. *Nat. Neurosci.* **4**, 1079-1085.
- Squire, L. R. and Zola-Morgan, S.** (1991). The medial temporal lobe memory system. *Science* **253**, 1380-1386.
- Staras, K.** (2007). Share and share alike: trading of presynaptic elements between central synapses. *Trends Neurosci.* **30**, 292-298.
- Starr, T. V., Prystay, W., and Snutch, T. P.** (1991). Primary structure of a calcium channel that is highly expressed in the rat cerebellum. *Proc. Natl. Acad. Sci. U. S. A* **88**, 5621-5625.
- Stettler, D. D., Yamahachi, H., Li, W., Denk, W., and Gilbert, C. D.** (2006). Axons and synaptic boutons are highly dynamic in adult visual cortex. *Neuron* **49**, 877-887.
- Stoppini, L., Buchs, P. A., and Muller, D.** (1991). A simple method for organotypic cultures of nervous tissue. *J. Neurosci. Methods* **37**, 173-182.
- Tada, T. and Sheng, M.** (2006). Molecular mechanisms of dendritic spine morphogenesis. *Curr. Opin. Neurobiol.* **16**, 95-101.
- Takita, M., Izaki, Y., Jay, T. M., Kaneko, H., and Suzuki, S. S.** (1999). Induction of stable long-term depression in vivo in the hippocampal-prefrontal cortex pathway. *Eur. J. Neurosci.* **11**, 4145-4148.
- Tashiro, A., Dunaevsky, A., Blazeski, R., Mason, C. A., and Yuste, R.** (2003). Bidirectional regulation of hippocampal mossy fiber filopodial motility by kainate receptors: a two-step model of synaptogenesis. *Neuron* **38**, 773-784.
- Thiagarajan, T. C., Lindskog, M., and Tsien, R. W.** (2005). Adaptation to synaptic inactivity in hippocampal neurons. *Neuron* **47**, 725-737.
- Thiels, E., Norman, E. D., Barrionuevo, G., and Klann, E.** (1998). Transient and persistent increases in protein phosphatase activity during long-term depression in the adult hippocampus in vivo. *Neuroscience* **86**, 1023-1029.
- Thomas, M. J., Beurrier, C., Bonci, A., and Malenka, R. C.** (2001). Long-term depression in the nucleus accumbens: a neural correlate of behavioral sensitization to cocaine. *Nat. Neurosci.* **4**, 1217-1223.
- Tippens, A. L., Pare, J. F., Langwieser, N., Moosmang, S., Milner, T. A., Smith, Y., and Lee, A.** (2008). Ultrastructural evidence for pre- and postsynaptic localization of Cav1.2 L-type Ca²⁺ channels in the rat hippocampus. *J. Comp Neurol.* **506**, 569-583.
- Toni, N., Buchs, P. A., Nikonenko, I., Bron, C. R., and Muller, D.** (1999). LTP promotes formation of multiple spine synapses between a single axon terminal and a dendrite. *Nature* **402**, 421-425.

- Trachtenberg, J. T., Chen, B. E., Knott, G. W., Feng, G., Sanes, J. R., Welker, E., and Svoboda, K.** (2002). Long-term in vivo imaging of experience-dependent synaptic plasticity in adult cortex. *Nature* **420**, 788-794.
- Tsuriel, S., Geva, R., Zamorano, P., Dresbach, T., Boeckers, T., Gundelfinger, E. D., Garner, C. C., and Ziv, N. E.** (2006). Local sharing as a predominant determinant of synaptic matrix molecular dynamics. *PLoS. Biol.* **4**, e271.
- Tsvetkov, E., Carlezon, W. A., Benes, F. M., Kandel, E. R., and Bolshakov, V. Y.** (2002). Fear conditioning occludes LTP-induced presynaptic enhancement of synaptic transmission in the cortical pathway to the lateral amygdala. *Neuron* **34**, 289-300.
- Turrigiano, G. G. and Nelson, S. B.** (2004). Homeostatic plasticity in the developing nervous system. *Nat. Rev. Neurosci.* **5**, 97-107.
- Tyler, W. J., Zhang, X. L., Hartman, K., Winterer, J., Muller, W., Stanton, P. K., and Pozzo-Miller, L.** (2006). BDNF increases release probability and the size of a rapidly recycling vesicle pool within rat hippocampal excitatory synapses. *J. Physiol* **574**, 787-803.
- Umeda, T., Ebihara, T., and Okabe, S.** (2005). Simultaneous observation of stably associated presynaptic varicosities and postsynaptic spines: morphological alterations of CA3-CA1 synapses in hippocampal slice cultures. *Mol. Cell Neurosci.* **28**, 264-274.
- Vanden Berghe, P. and Klingauf, J.** (2006). Synaptic vesicles in rat hippocampal boutons recycle to different pools in a use-dependent fashion. *J. Physiol* **572**, 707-720.
- Volsen, S. G., Day, N. C., McCormack, A. L., Smith, W., Craig, P. J., Beattie, R., Ince, P. G., Shaw, P. J., Ellis, S. B., Gillespie, A., and .** (1995). The expression of neuronal voltage-dependent calcium channels in human cerebellum. *Brain Res. Mol. Brain Res.* **34**, 271-282.
- Washbourne, P., Bennett, J. E., and McAllister, A. K.** (2002). Rapid recruitment of NMDA receptor transport packets to nascent synapses. *Nat. Neurosci.* **5**, 751-759.
- Waters, J. and Smith, S. J.** (2002). Vesicle pool partitioning influences presynaptic diversity and weighting in rat hippocampal synapses. *J. Physiol* **541**, 811-823.
- Westenbroek, R. E., Hell, J. W., Warner, C., Dubel, S. J., Snutch, T. P., and Catterall, W. A.** (1992). Biochemical properties and subcellular distribution of an N-type calcium channel alpha 1 subunit. *Neuron* **9**, 1099-1115.
- Westenbroek, R. E., Sakurai, T., Elliott, E. M., Hell, J. W., Starr, T. V., Snutch, T. P., and Catterall, W. A.** (1995). Immunochemical identification and subcellular distribution of the alpha 1A subunits of brain calcium channels. *J. Neurosci.* **15**, 6403-6418.

- Whitlock, J. R., Heynen, A. J., Shuler, M. G., and Bear, M. F.** (2006). Learning induces long-term potentiation in the hippocampus. *Science* **313**, 1093-1097.
- Wickens, J. R. and Abraham, W. C.** (1991). The involvement of L-type calcium channels in heterosynaptic long-term depression in the hippocampus. *Neurosci. Lett.* **130**, 128-132.
- Williams, M. E., Brust, P. F., Feldman, D. H., Patthi, S., Simerson, S., Maroufi, A., McCue, A. F., Velicelebi, G., Ellis, S. B., and Harpold, M. M.** (1992). Structure and functional expression of an omega-conotoxin-sensitive human N-type calcium channel. *Science* **257**, 389-395.
- Williams, M. E., Washburn, M. S., Hans, M., Urrutia, A., Brust, P. F., Prodanovich, P., Harpold, M. M., and Stauderman, K. A.** (1999). Structure and functional characterization of a novel human low-voltage activated calcium channel. *J. Neurochem.* **72**, 791-799.
- Xiao, M. Y., Zhou, Q., and Nicoll, R. A.** (2001). Metabotropic glutamate receptor activation causes a rapid redistribution of AMPA receptors. *Neuropharmacology* **41**, 664-671.
- Xu, L., Anwyl, R., and Rowan, M. J.** (1997). Behavioural stress facilitates the induction of long-term depression in the hippocampus. *Nature* **387**, 497-500.
- Yang, C. H., Huang, C. C., and Hsu, K. S.** (2005). Behavioral stress enhances hippocampal CA1 long-term depression through the blockade of the glutamate uptake. *J. Neurosci.* **25**, 4288-4293.
- Yang, S. N., Tang, Y. G., and Zucker, R. S.** (1999). Selective induction of LTP and LTD by postsynaptic $[Ca^{2+}]_i$ elevation. *J. Neurophysiol.* **81**, 781-787.
- Yao, J., Qi, J., and Chen, G.** (2006). Actin-dependent activation of presynaptic silent synapses contributes to long-term synaptic plasticity in developing hippocampal neurons. *J. Neurosci.* **26**, 8137-8147.
- Yeow, M. B. and Peterson, E. H.** (1991). Active zone organization and vesicle content scale with bouton size at a vertebrate central synapse. *J. Comp Neurol.* **307**, 475-486.
- Yokoyama, C. T., Westenbroek, R. E., Hell, J. W., Soong, T. W., Snutch, T. P., and Catterall, W. A.** (1995). Biochemical properties and subcellular distribution of the neuronal class E calcium channel alpha 1 subunit. *J. Neurosci.* **15**, 6419-6432.
- Yuste, R. and Bonhoeffer, T.** (2001). Morphological changes in dendritic spines associated with long-term synaptic plasticity. *Annu. Rev. Neurosci.* **24**, 1071-1089.
- Yuste, R. and Bonhoeffer, T.** (2004). Genesis of dendritic spines: insights from ultrastructural and imaging studies. *Nat. Rev. Neurosci.* **5**, 24-34.

- Zakharenko, S. S., Patterson, S. L., Dragatsis, I., Zeitlin, S. O., Siegelbaum, S. A., Kandel, E. R., and Morozov, A.** (2003). Presynaptic BDNF required for a presynaptic but not postsynaptic component of LTP at hippocampal CA1-CA3 synapses. *Neuron* **39**, 975-990.
- Zakharenko, S. S., Zablow, L., and Siegelbaum, S. A.** (2001). Visualization of changes in presynaptic function during long-term synaptic plasticity. *Nat. Neurosci.* **4**, 711-717.
- Zenisek, D., Davila, V., Wan, L., and Almers, W.** (2003). Imaging calcium entry sites and ribbon structures in two presynaptic cells. *J. Neurosci.* **23**, 2538-2548.
- Zhai, R. G., Vardinon-Friedman, H., Cases-Langhoff, C., Becker, B., Gundelfinger, E. D., Ziv, N. E., and Garner, C. C.** (2001). Assembling the presynaptic active zone: a characterization of an active one precursor vesicle. *Neuron* **29**, 131-143.
- Zhang, J. F., Randall, A. D., Ellinor, P. T., Horne, W. A., Sather, W. A., Tanabe, T., Schwarz, T. L., and Tsien, R. W.** (1993). Distinctive pharmacology and kinetics of cloned neuronal Ca²⁺ channels and their possible counterparts in mammalian CNS neurons. *Neuropharmacology* **32**, 1075-1088.
- Zhang, X. L., Zhou, Z. Y., Winterer, J., Muller, W., and Stanton, P. K.** (2006). NMDA-dependent, but not group I metabotropic glutamate receptor-dependent, long-term depression at Schaffer collateral-CA1 synapses is associated with long-term reduction of release from the rapidly recycling presynaptic vesicle pool. *J. Neurosci.* **26**, 10270-10280.
- Zhen, M. and Jin, Y.** (2004). Presynaptic terminal differentiation: transport and assembly. *Curr. Opin. Neurobiol.* **14**, 280-287.
- Zhou, Q., Homma, K. J., and Poo, M. M.** (2004). Shrinkage of dendritic spines associated with long-term depression of hippocampal synapses. *Neuron* **44**, 749-757.
- Ziakopoulos, Z., Tillett, C. W., Brown, M. W., and Bashir, Z. I.** (1999). Input- and layer-dependent synaptic plasticity in the rat perirhinal cortex in vitro. *Neuroscience* **92**, 459-472.
- Ziv, N. E. and Garner, C. C.** (2004). Cellular and molecular mechanisms of presynaptic assembly. *Nat. Rev. Neurosci.* **5**, 385-399.

Acknowledgements

First of all, I would like to thank Dr. Valentin Nägerl for the supervision of my thesis and for introducing me to the fascinating world of two-photon imaging. I am very grateful for the enthusiasm he shared for my project and tried to learn from his unlimited optimism and creativity.

I am very grateful to Prof. Tobias Bonhoeffer for giving me the opportunity to do my PhD in his department. I deeply appreciate that he always took the time for discussions and advice, despite his busy schedule.

I am very thankful to Prof. Gerd Schuller for reviewing this thesis.

Thanks a lot to Dr. Corette Wierenga and Dr. Valentin Stein for their scientific support and helpful discussions as members of my thesis committee. I am especially grateful to Corette for her everyday help and encouragement.

Many thanks to Dr. Rosalina Fonseca who took the time to introduce me to the department, the two-photon setup and slice labeling during my first and her last month in this lab.

I really enjoyed working in the Bonhoeffer department. Thanks a lot to all of you who helped with many big and little things, thank you for all the fun, for sharing the Blocksberg office, my worries, the sunshine-and-muffin breaks and conference trips with me, and for a spontaneous trip to Sardegna!

I would like to thank the Boehringer Ingelheim Fonds for their generous funding of the major part of my thesis. I also enjoyed all the inspiring seminars and the joyful and cooperative atmosphere within the BIF community.

I am very grateful to Prof. Susanne Schmid and Prof. Dai Stephens for sparking my scientific interest and promoting me in the early stages of my scientific training.

Special thanks go to Miriam Mann and Susana Gomis-Rüth, in particular for the non-scientific support. You added a lot of sunshine and balance to my time here.

I would like to thank my family for being incredibly caring, supportive and understanding; I will always feel at home with you.

With all my heart I would like to thank Holger. With your cheerful and balanced nature, you are the best companion I can imagine.

Curriculum vitae

Personal data

Name Nadine Becker
Born 02.04.1980 in Düren, Germany

Education

Since 03/2005 PhD thesis with Prof. Tobias Bonhoeffer and Dr. Valentin Nägerl at the Max Planck Institute of Neurobiology, Martinsried

12/2004 Diploma in Biology (grade 1.0)

02/2004 – 11/2004 Diploma thesis with PD Dr. Susanne Schmid, Department of Animal Physiology, University of Tübingen (grade 1.0)

10/2003 – 12/2003 Studies of Psychology, University of Sussex, UK, Practical project with Prof. David N. Stephens, Department of Experimental Psychology

10/1999 – 12/2004 Studies of Biology, Eberhard-Karls-Universität Tübingen

06/1999 Abitur (grade 1.7)

Teaching

10/2000 – 07/2001 Course tutor; zoological courses I and II

04/2004 – 07/2004 Course tutor; animal physiology course

08/2004 and 02/2005 Course tutor; special training: “Patch-clamp recordings in acute slice preparations of rat brains“

Grants

2003 ERASMUS scholarship for studies at the University of Sussex, Brighton, UK

2004 Travel grant of the Reinhold-und-Maria-Teufel-Stiftung for participation in the 6th Meeting of the German Neuroscience Society

2005 - 2008 PhD scholarship of the Boehringer Ingelheim Foundation

2007 Scholarship of the DAAD (Deutscher Akademischer Austauschdienst) for participation in the *European synapse summer school* in Bordeaux

Publications

Research articles

Becker, N., Wierenga, J. C., Fonseca, R., Bonhoeffer, T., Nägerl, U.V.; LTD induction causes morphological changes of presynaptic boutons and reduces their contacts with spines. *Under revision*.

Wierenga, J. C., Becker, N., Bonhoeffer, T.; Formation of GABAergic synapses occurs largely without the involvement of protrusions. *Under revision*.

Mead, A.N., Zamanillo, D. Becker, N., Stephens, D.N. (2007); AMPA-receptor subunits are involved in the control over behavior by cocaine-paired cues, *Neuropsychopharmacology*, 32 (2), 343-353.

Weinl, C., Becker, N., Loeschinger, J. (2005); Responses of temporal retinal growth cones to ephrinA5-coated beads. *J Neurobiol.* 62 (2), 219-230.

Conference contributions (Posters)

Becker, N., Wierenga, J. C., Fonseca, R., Bonhoeffer, T., Nägerl, U.V. (2007); Activity-dependent pre- and postsynaptic structural plasticity at the CA3-CA1 synapse. *Abstracts of the 36th Annual Meeting of the Society for Neuroscience*.

Becker, N., Fonseca, R., Wierenga, J. C., Bonhoeffer, T., Nägerl, U.V. (2007); Hippocampal LTD enhances bouton turnover and removes synaptic connections. *Neurizons, Interdisciplinary Meeting of the Neurosciences, Göttingen*.

Becker, N., Fonseca, R., Wierenga, J. C., Bonhoeffer, T., Nägerl, U.V. (2007); Imaging structural plasticity of hippocampal CA3-CA1 synapses. *Abstracts of the 7th Meeting of the German Neuroscience Society, Suppl. to Neuroforum 1/07, XIII*.

Becker, N., Fonseca, R., Bonhoeffer, T., Nägerl, U.V. (2005); Simultaneous imaging of presynaptic boutons and postsynaptic spines in hippocampal neurons. *Abstracts of the 35th Annual Meeting of the Society for Neuroscience*.

Schmid, S., Plappert, C., Pilz, P., Becker, N., Hölscher, C., Fendt, M. (2005); Role of metabotropic glutamate receptors in fear conditioning in vivo and in synaptic transmission and plasticity in the lateral amygdala *in vitro*. *Satellite symposium "Molecular and cellular cognition meeting", 35th Annual Meeting of the Society for Neuroscience*

Becker, N., van der Putten, H., Schnitzler, H.U., Schmid, S. (2005); LTP and the role of mGluR8 in the lateral amygdala. *Abstracts of the 6th Meeting of the German Neuroscience Society, Suppl. to Neuroforum 1/05, XI*.

Others

Becker, N. (2006); Structural and functional plasticity of single hippocampal synapses. *B.I.F. FUTURA* 21 (1), 19-20.